

ADSORPTION OF ACETALDEHYDE VAPOUR IN LOW CONCENTRATION
IN AIR WITH FIXED-BEDS OF CHARCOAL

by

19
410 5940

HEUNGWOO CHUN

B. S., University of Southern California, 1969

B. S., Seoul National University, 1965

A MASTER'S THESIS

submitted in partial fulfillment of the requirement
for the degree

MASTER OF SCIENCE

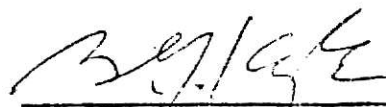
Department of Chemical Engineering

KANSAS STATE UNIVERSITY

Manhattan, Kansas

1974

Approved by



Major Professor

**THIS BOOK
CONTAINS
NUMEROUS PAGES
WITH THE ORIGINAL
PRINTING BEING
SKEWED
DIFFERENTLY FROM
THE TOP OF THE
PAGE TO THE
BOTTOM.**

**THIS IS AS RECEIVED
FROM THE
CUSTOMER.**

LD
2668
T4
1974
C58
C.2
Document

ii

TABLE OF CONTENTS

	PAGE
I. INTRODUCTION -----	1
I-1. Theory -----	3
1. Equilibrium Isotherm -----	3
2. Classification of Isotherms -----	8
3. Rate Processes -----	10
4. Fixed-Bed Operations -----	18
II. EXPERIMENTAL EQUIPMENT AND TECHNIQUE -----	30
III. RESULTS AND DISCUSSION -----	40
III-1. General Observations -----	40
(a) Mid-point Time and Break-Time versus Residence Time -----	40
(b) Effect of Bed Lengths -----	42
(c) Effect of Superficial Velocity -----	42
(d) Effect of Charcoal Particle Size -----	44
III-2. Modeling Study -----	47
(a) Particle-phase Diffusion Model -----	49
(b) Pore Diffusion Model -----	57
(c) External Diffusion Model -----	66
(d) Reaction Kinetics Model -----	74
III-3. Charcoal Capacity -----	82
(a) Capacity from Experimental Breakthrough Curve -----	82
(b) Capacity from Equilibrium Tests -----	85
(c) Capacity from Modeling Study -----	92
IV. CONCLUSIONS AND APPLICATIONS TO DESIGN -----	93

	PAGE
NOMENCLATURE	95
ACKNOWLEDGMENTS	99
BIBLIOGRAPHY	100
APPENDIX	104
A-1. Verification of Constant $(\partial Z_v / \partial V)_x$ for Constant-Pattern Limit	105
A-2. Experimental Breakthrough Curves and Modeling Breakthrough Curves	106
A-3. Calculation of Bed Capacity from the Breakthrough Curve	120
A-4. The Sample Calculations of Modeling Break-Time	124
A-5. Static Equilibrium Measurement Error Analysis	128

CHAPTER I

INTRODUCTION

Odorous substances, even in low concentration in air, cause unpleasant smells and are sometimes hazardous to human health. For example, acetaldehyde has an aromatic odor, but is harmful to living things even at low concentrations. Therefore, control of odors has been one of the basic factors in air conditioning for a long time. The standard method suggested as a means of control is the use of activated charcoal, a substance which has the ability to trap or adsorb many of the organic compounds which produce odors in air.

Activated charcoal as an odor removal substance has certain potential advantages over other materials used for odor removal. These advantages include:

- (1) Charcoal adds no odor of its own into the air.
- (2) Charcoal has a high surface area which results in a high capacity for adsorption.
- (3) Activated charcoal is effective in adsorbing a wide variety of organic odorants, even in a humid atmosphere.
- (4) Charcoal is dust free and available in a wide variety of shapes and sizes making it easy to install and replace.

However, one limitation to the effective application of activated charcoal for odor removal has been the lack of quantitative data concerning the effective capacity and

adsorption kinetics of activated charcoal for gaseous atmospheric contaminants in the low parts per million range under dynamic conditions at ambient temperature. Providing such data is the purpose of this work.

The work will consist of three parts:

- (1) Construction of equipment and development of suitable experimental techniques to obtain reliable breakthrough data with fixed-beds of charcoal.
- (2) Obtaining breakthrough data for fixed-beds of Pittsburgh PCB charcoal fed with an influent stream containing 28 parts per million of acetaldehyde vapour in air. The effect of charcoal particle size, bed length, and fluid velocity on the breakthrough behavior will be investigated.
- (3) Analysis of these data to acquire thermodynamic and kinetic knowledge of adsorption at low adsorbate concentration with emphasis upon the development of a design procedure.

I-1. THEORY

1. Equilibrium Isotherm

A gas or vapour has the tendency to be collected on the surface of a solid, when brought into contact with the solid. This phenomenon is known as adsorption. In this case, the solid that takes up the gas or vapour is called the adsorbent and the gas or vapour attached to the surface of the solid is called the adsorbate. The amount of gas or vapour adsorbed per gram of solid, y , depends on the equilibrium pressure, p , the temperature, T , and the nature of the gas or vapour and of the solid. This relationship can be stated mathematically

$$y = f(p, T, \text{gas, solid}) \text{ -----(I-1)}$$

For a pure gas or vapour adsorbed on a given solid and at a fixed temperature, this statement can be simplified to

$$y = f(p)_{T, \text{gas, solid}} \text{ -----(I-2)}$$

The above statement is called the equilibrium adsorption isotherm which relates the amount adsorbed to the pressure while the temperature is kept constant. This relationship also can be explained by the Phase Rule. The Phase Rule as stated by Ross and Oliver for systems with interfaces (36) is

$$\begin{aligned} \text{Number of phases} + \text{Degrees of freedom} &= \text{Number of} \\ \text{components} + \text{Number of interfaces} + 2 &\text{ ----(I-3)} \end{aligned}$$

When a gas is in contact with a solid, it is a two-component system of two bulk phases. And if we visualize an ideal solid

having only one type of interface and take sorption into account, the phase rule that applies is equation (I-3) with one interface. With three phases and two components, the degrees of freedom is two. Therefore for a specific gas and solid, the variables are p , T , and y . And if the temperature of the system and the pressure in the gas phase are fixed, y is fixed, or if only the temperature is fixed, y is a function of p only. This equilibrium isotherm relationship is the most widely used method of representing adsorption equilibrium data.

In 1915, Polanyi (30, 31, 32, 33) and Langmuir (23, 24, 25) each proposed entirely independent, but different, theories of adsorption. Langmuir believed that adsorption was a chemical process and the adsorbed layer was unimolecular, and Polanyi believed that adsorption was a physical process and the adsorbed layer was multimolecular. Both treatments were successful in many cases, and both have their limitations. The Polanyi theory is applied to physical adsorption only, and the Langmuir theory is applied with suitable assumptions to both chemical and physical adsorption.

According to Langmuir, the rate of adsorption is proportional to (a) the number of molecules which strike a unit surface per unit time, (b) the fraction of the number of striking molecules that remain on the surface long enough for an exchange of kinetic energy to take place, and (c) the fraction of the unit surface not occupied by adsorbed molecules. And the rate of desorption is proportional to the

fraction of the total number of adsorbed molecules that have enough energy to escape the attractive forces of the surface. At equilibrium, the rate of adsorption is equal to the rate of desorption. Following this derivation, the Langmuir isotherm equation is

$$v_a = \frac{v_m b_L p}{1 + b_L p} \text{ ----- (I-4)}$$

Where p is the pressure exerted by the adsorbate, v_a is the volume adsorbed at p , v_m is the volume adsorbed when the solid surface is covered with a complete unimolecular layer and b_L is a proportionality constant.

In 1934, Zeldowitsch (50) derived his semitheoretical isotherm equation from the Langmuir equation:

$$v_a = k p^{1/n} \text{ ----- (I-5)}$$

where k and n ($n > 1$) are constants. This equation is generally known as the Freundlich isotherm equation. This equation has a tenuous theoretical basis, but is still widely used by many investigators, particularly in industrial practice.

The logarithmic form of Freundlich equation can be expressed as a straight line on log-log coordinates. From this straight line the constants can be calculated and the applicable range can be extended even to small surface coverage. The Langmuir equation, when applicable, is also capable of fitting experimental data from zero to saturation

pressure. At low pressure (small surface coverage), the $b_L p$ term in the denominator of Langmuir equation (I-4) can be neglected in comparison with 1 and the equation reduces to

$$v_a = v_m b_L p \text{ ----- (I-6a)}$$

or

$$v_a = k' p \text{ ----- (I-6b)}$$

where k' is a constant. This linear isotherm is known as Henry's Law and the region where the linear isotherm is obeyed is called the Henry's Law region. This type of linear isotherm has been found experimentally by many investigators (6,10, 22, 29, 46).

Markham and Benton (27) considered the adsorption from a binary gas mixture based on identical assumptions with those of Langmuir. The equations they derived are

$$v_{a1} = \frac{v_{m1} b_{L1} p_1}{1 + b_{L1} p_1 + b_{L2} p_2} \text{ ----- (I-7a)}$$

and

$$v_{a2} = \frac{v_{m2} b_{L2} p_2}{1 + b_{L1} p_1 + b_{L2} p_2} \text{ ----- (I-7b)}$$

Where, v_{a1} = the volume of gas 1 adsorbed at equilibrium partial pressure p_1 ,

v_{a2} = the volume of gas 2 adsorbed at equilibrium partial pressure p_2 ,

v_{m1} = the volume of gas 1 necessary to cover the entire surface with unimolecular adsorbed layer,
 v_{m2} = the volume of gas 2 necessary to cover the entire surface with unimolecular adsorbed layer.

The above equations predict that one gas always decreases the adsorption of the other. If $b_{L1}P_1$ and $b_{L2}P_2$ are negligible compared to 1 in the denominator, these equations simplify to Henry's Law. If $b_{L2}P_2$ term is negligible compared to 1 and the $b_{L1}P_1$ term is comparable to 1, the equations become

$$v_{a1} = \frac{v_{m1} b_{L1} P_1}{1 + b_{L1} P_1} \text{-----(I-8a)}$$

and

$$v_{a2} = \frac{v_{m2} b_{L2} P_2}{1 + b_{L1} P_1} \text{-----(I-8b)}$$

In this case, gas 1 will be adsorbed as though gas 2 were not present, but the adsorption of gas 2 will be diminished strongly by gas 1. This happens in the adsorption of organic vapours by charcoal in the presence of air. Air is displaced from the surface of the adsorbent by organic vapour and the adsorption of organic vapour remains unaffected by the presence of air. This usually is applicable even if the partial pressure of the organic vapour is much smaller than that of air. Therefore, when we replace v_{m1} by v_m , b_{L1} by b_L , P_1 by p and v_{a1} by v_a , equation (I-8a) is identical to the single component Langmuir equation (I-4).

2. Classification of Isotherms.

Three major classes of isotherms can be characterized by their different effects on fixed-bed behavior. The shapes of these distribution isotherms are important in determining the conditions of fixed-bed operation. These three types of isotherms are:

- (a) Favorable isotherm
- (b) Linear isotherm
- (c) Unfavorable isotherm

DeVault (8) first identified favorable equilibrium as that for which the isotherm is convex upward, and unfavorable equilibrium as that for which the curve is concave upward. The linear isotherm is an intermediate case (see Figure (I-1)).

The slope of a favorable isotherm is, therefore, a decreasing function, while the slope of an unfavorable isotherm is an increasing function of the concentration in the fluid phase. In fixed-bed adsorption, favorable equilibrium leads to relatively sharp concentration gradients in the direction of flow, while unfavorable equilibrium leads to more diffuse boundaries.

The adsorbate affinity of most solids tends to decrease with increasing adsorbate concentration, hence most isotherms are convex or favorable. Linear behavior is often, but not always, approached at low concentrations.

**THIS BOOK
CONTAINS
NUMEROUS PAGES
WITH DIAGRAMS
THAT ARE CROOKED
COMPARED TO THE
REST OF THE
INFORMATION ON
THE PAGE.**

**THIS IS AS
RECEIVED FROM
CUSTOMER.**

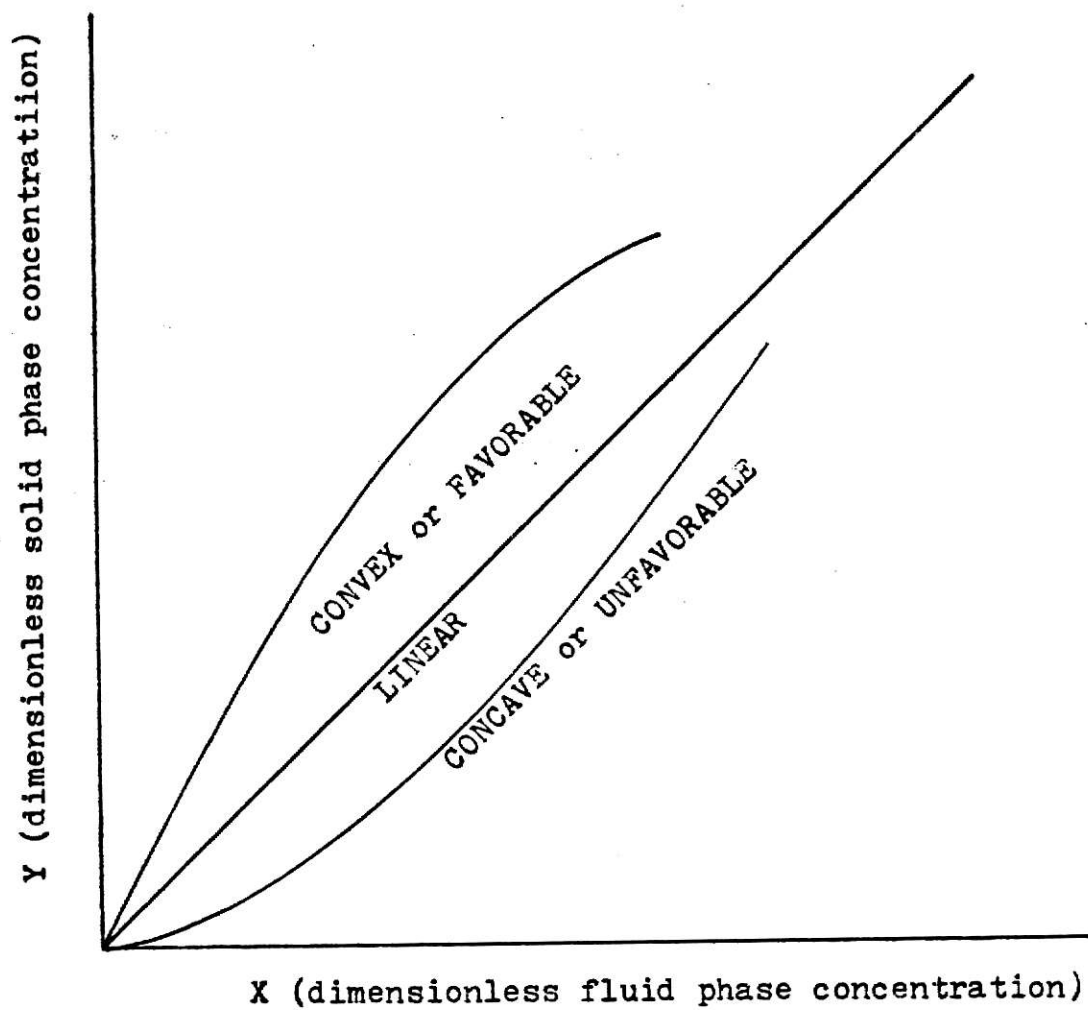


Fig.(I-1) Three Types of Isotherms

3. Rate Processes.

The effective rate of adsorption of a gaseous component from a stream flowing through a fixed-bed of porous adsorbent particles is determined by one or more of several different steps.

Individual steps in the transport mechanism are:

- (1) Diffusion in the solid phase (Solid-phase internal diffusion, Particle diffusion)
- (2) Fluid-phase external diffusion (Film diffusion).
- (3) Fluid-phase pore diffusion (Fluid-phase internal diffusion).
- (4) Adsorption at the phase boundaries.
- (5) Axial or radial dispersion in the packed-bed of adsorbent.

Any of the above steps may restrict the rate of mass transport in a certain region of operating conditions.

Solid-phase Diffusion

Diffusion by a concentration gradient within the individual adsorbent particles, after the adsorbate is adsorbed on the solid, is called particle-phase, sorbent-phase, or internal diffusion. This diffusion includes diffusion through a homogeneous, permeable non-porous solid and diffusion in a mobile, adsorbed phase covering the pore surface of a porous solid whose crystalline portion is

impermeable.

The rate of internal diffusion for a perfect spherical particle is expressed by

$$D_p \left(\frac{\partial^2 Y_r}{\partial r^2} + \frac{2}{r} \frac{\partial Y_r}{\partial r} \right) = \frac{\partial Y_r}{\partial t} \text{-----(I-9)}$$

Where, D_p is the particle-phase diffusivity, Y_r is the dimensionless solid-phase concentration at any internal radius r , and t is time. Glueckauf and Coates (13, 14) assumed that the amount entering or leaving the sphere is proportional to the difference between the existing mean concentration and that obtained at the surface of the particle. From this assumption, the rate of mass transfer was approximated by

$$\left(\frac{dY}{dt} \right)_{\text{particle}} = \frac{k_p a_p}{D e} (Y^* - Y) \text{-----(I-10)}$$

Where Y is the dimensionless concentration of the solid averaged over the entire particle, Y^* is the value that is in equilibrium with the instantaneous fluid-phase concentration outside the particle, k_p is the particle phase mass-transfer coefficient, a_p is the outer surface area of the adsorbent particle per unit volume of fixed-bed, D is distribution ratio, e is external void fraction of the packed bed, and t is time. The product term, $k_p a_p$, can be expressed as the equation

$$k_p a_p = \frac{60 D_p D e}{d_p^2} \text{-----(I-11)}$$

Fluid-phase Effects

A. Pore Diffusion

As indicated in Figure (I-2), the adsorbate may enter into a particle of adsorbent directly from the exterior fluid-phase through the fluid-phase in the pores. In the case where the amount of material held in the pores is negligible compared with that held by the solid, the diffusion rate is given by a relation analogous to equation (I-9),

$$\frac{\partial Y_r}{\partial t} = \frac{D_{\text{pore}}(1 - e)}{D e} \left\{ \frac{\partial^2 X_r}{\partial r^2} + \frac{2}{r} \left(\frac{\partial X_r}{\partial r} \right) \right\} \text{ ---- (I-12)}$$

This equation has been solved analytically for only a few cases (9, 34). Through the work of Wheeler (44), the pore diffusivity can be expressed as

$$D_{\text{pore}} = \frac{D_f x_p}{2} \left[1 - \text{Exp} \left\{ - \frac{4 \bar{r}_p}{3 D_f} \left(\frac{8 R_g T}{M} \right)^{0.5} \right\} \right] \text{ ---- (I-13)}$$

where x_p is the internal porosity of the particle, \bar{r}_p is the average pore radius, and $(8 R_g T / M)^{0.5}$ is the molecular velocity group based on the gas constant, absolute temperature, and mean molecular weight of fluid.

If a linear driving potential is used, the rate equation is approximated by (13)

$$\left(\frac{dY}{dt} \right)_{\text{particle}} = \frac{k_{\text{pore}} a_p (X - X^*)}{D e} \text{ ---- (I-14)}$$

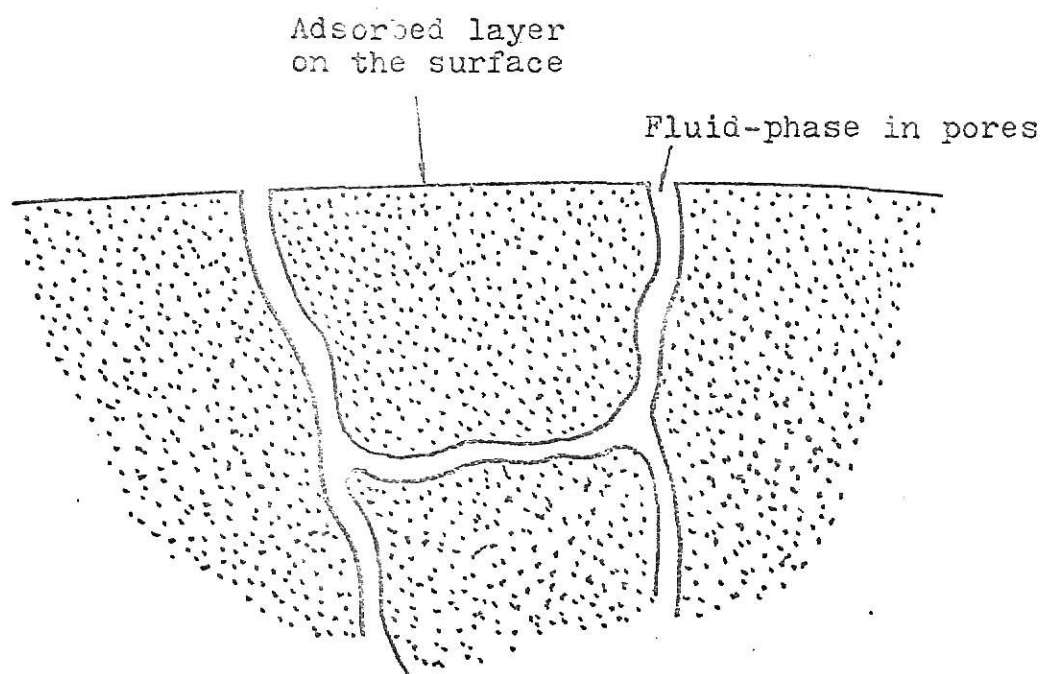


Fig.(I-2) Diffusion Path within Adsorbent Particle

Where X is the dimensionless concentration of the fluid-phase and X^* is the dimensionless concentration of the fluid-phase in equilibrium with the solid phase concentration. Hiester et al. (19) expressed the product term $k_{\text{pore}} a_p$ of equation (I-14) as

$$k_{\text{pore}} a_p = \frac{60 D_{\text{pore}}}{d_p^2} (1 - e) \text{-----} \text{(I-15)}$$

where d_p is the effective diameter of a spherical particle.

B. External Diffusion.

The rate of diffusion of adsorbate between the bulk of the flowing fluid and the outer surface of the granules of adsorbent is controlled by the molecular diffusivity and also, in turbulent flow, by the eddy diffusivity which controls the effective thickness of the residual laminar layer.

The rate of adsorbate transfer is given by the equation:

$$\left(\frac{dY}{dt} \right)_{\text{particle}} = \frac{k_f a_p}{D e} (X - X^*) \text{-----} \text{(I-16)}$$

where k_f is the fluid-phase mass-transfer coefficient.

Wilke and Hougen (47) evaluated the mass-transfer coefficient for packed-bed operations and offered the following correlation

$$k_f a_f = \frac{10.9 F(1 - e)}{d_{pSB}} \left[\frac{D_f}{d_p (F/S)} \right]^{0.51} \left(\frac{D_f \rho_f}{\mu} \right)^{0.16} \text{-----} \text{(I-17)}$$

Where B is the logarithmic mean of $(1 - Y)$ and Y (usually B is near unity). Y is the mole fraction of the diffusing component in the entire phase, F/S is superficial velocity (volumetric flow rate of fluid F per unit area S of the fixed-bed cross section), D_f is fluid phase diffusivity, ρ_f is fluid phase density and μ is viscosity.

Adsorption at the Phase Boundaries.

An attempt has been made to obtain the relation when adsorption on the surface is the rate controlling step for the case where the adsorption is reversible and the adsorbed gas exerts a back pressure. For such conditions the rate of adsorption of a single component obeying the Langmuir isotherm is (41)

$$\left(\frac{dv}{dt}\right)_{\text{particle}} = k_i \left[p(v_m - v) - \frac{v}{b_L} \right] \text{----- (I-18)}$$

Where k_i is the coefficient of the adsorption rate, v_m is the volume adsorbed when the solid surface is covered with a complete unimolecular layer. Equation (I-18) can be expressed in terms of dimensionless variables from the definitions

$$X = p/p_o$$

$$Y = v/v_o^*$$

where v_o^* is the volume adsorbed in equilibrium with the inlet concentration, p_o , and is given by the Langmuir equation

$$\frac{v_o^*}{v_m} = \frac{b_L p_o}{1 + b_L p_o}$$

By substituting above values in the equation (I-18), the equation can be written as

$$\left(\frac{dY}{dt}\right)_{\text{particle}} = k_i p_o \left[X \left(\frac{1 + b_L p_o}{b_L p_o} - Y \right) - \frac{Y}{b_L p_o} \right] \text{---(I-19)}$$

Equation (I-19) can be further simplified by introducing the separation factor R

$$R = \frac{1}{1 + b_L p_o} \quad \text{or} \quad b_L p_o = \frac{1 - R}{R} \text{-----(I-20)}$$

Substitute $b_L p_o$ value into the equation (I-19)

$$\left(\frac{dY}{dt}\right)_{\text{particle}} = \frac{k_i p_o}{1 - R} [X(1 - Y) - RY(1 - X)] \text{-----(I-21)}$$

or by introducing a new time variable t_R

$$t_R = \frac{k_F t}{D e} \quad \text{with} \quad k_F = \frac{k_i p_o D e}{1 - R}$$

equation (I-21) can be written as

$$\left(\frac{dY}{dt_R}\right)_{\text{particle}} = X(1 - Y) - RY(1 - X) \text{-----(I-22)}$$

The rate of adsorption can also be expressed in terms of solid and fluid phase driving forces, from equations (I-10) and (I-16)

$$\left(\frac{dY}{dt}\right)_{\text{particle}} = \frac{k_p a_p}{D e} (Y^* - Y) = \frac{k_f a_p}{D e} (X - X^*) \text{---(I-23)}$$

X^* and Y^* terms can be eliminated by using the definition of the separation factor R

$$X^* = \frac{RY}{1 + (R - 1)Y} \quad \text{and} \quad Y^* = \frac{X}{R + (1 - R)X}$$

Then summation of numerators and denominators of equation (I-23) leads to

$$\left(\frac{dY}{dt}\right)_{\text{particle}} = \frac{\frac{X}{R + (1 - R)X} - Y + X - \frac{RY}{1 + (R - 1)Y}}{D e \left(\frac{1}{k_p a_p} + \frac{1}{k_f a_p} \right)}$$

or by using the new time variable t_R

$$\left(\frac{dY}{dt_R}\right)_{\text{particle}} = \frac{\frac{1}{k_F}}{\frac{1}{k_p a_p} + \frac{1}{k_f a_p}} \left[\frac{(1+R) [(X-RY)-2XY(1-R)]}{[R+(1-R)X][1+(R-1)Y]} + \frac{(1-R) [X^2+RY^2-XY(X-Y)(1-R)]}{[R+(1-R)X][1+(R-1)Y]} \right] \text{----- (I-24)}$$

Equating equation (I-22) and equation (I-24) and rearrangement leads to the usual reciprocal form for resistances in series, but modified by a correction term b

$$\frac{b}{k_F} = \frac{1}{k_p a_p} + \frac{1}{k_f a_p} \text{----- (I-25)}$$

where

$$b = \frac{(1+R) [(X-RY)-2XY(1-R)] + (1-R) [X^2+RY^2-XY(X-Y)(1-R)]}{[R+(1-R)X][1+(R-1)Y][X(1-Y)-RY(1-X)]}$$

As the equation shows, b is a function of X , Y , and R , but has been found to depend mainly on R (19). Therefore for a given system (constant R), the correction factor b may be regarded as a constant.

Adsorption at the solid surface is usually found to be extremely rapid except in isolated cases of activated adsorption, and the resistance due to this step will generally be negligible. However, this mechanism finds wide usage because with the correction term b the rate expression is equivalent to that written for combined particle-phase and fluid-phase resistances.

4. Fixed-Bed Operations.

In fixed-bed operations, the fluid which contains adsorbate is flowing through the bed of granular adsorbent. When it is doing so, adsorbate originally present in the fluid tends to be adsorbed by the adsorbent until the entire bed becomes saturated with adsorbate. And at the same time, the adsorbate concentration of the outgoing fluid is increasing until it reaches the feed stream concentration. This change in effluent concentration with time is called the "breakthrough curve". Therefore the main object of a mathematical analysis of fixed-bed adsorption is an expression for the dependence of the effluent concentration on time.

Mass Balance Relation

Consider a fluid stream containing adsorbate flowing through a bed of adsorbent, as shown in Figure (I-3). Each layer of the adsorbent removes a portion of the adsorbate from the flowing stream, hence the concentration of adsorbate drops from an influent value of C_0 to an effluent value of C_e . And a cross section of infinitesimal thickness, dH , will reduce the concentration from C to $C+dC$ (dC is negative in this case). Therefore, from the principle of conservation of mass it follows that

$$\begin{aligned} \text{Amount of adsorbate entering} &= \text{Amount of adsorbate picked} \\ &\quad \text{up by adsorbent} + \text{Amount of adsorbate leaving} \\ &\quad + \text{Accumulation of adsorbate within the void space} \\ &\quad \text{-----} \end{aligned} \quad \text{(I-26)}$$

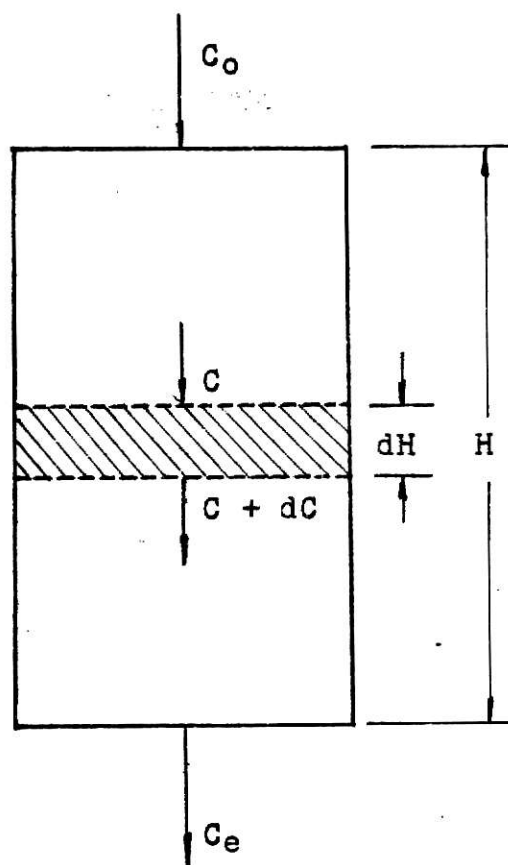


Fig.(I-3) Flow of Fluid through a Fixed-Bed of Adsorbent.

and, amount of adsorbate entering = CdV -----(I-27)

amount of adsorbate picked up by adsorbent

$$= \rho_b(\partial q/\partial t)dvd t \text{ -----(I-28)}$$

amount of adsorbate leaving = $(C + dC)dV$ -----(I-29)

amount of adsorbate accumulated within the void space

$$= e(dC/dt)dvd t \text{ -----(I-30)}$$

where, C = concentration of adsorbate in the fluid phase

q = concentration of adsorbate in the particle phase

v = volume of fixed-bed

V = volume of fluid entering fixed-bed

t = time

ρ_b = bulk density of solid particles in fixed-bed

The mathematical expression of the material balance can now be written

$$CdV = (C + dC)dV + \rho_b \frac{\partial q}{\partial t} dvdt + e\left(\frac{dC}{dt}\right)dvdt$$

the above equation simplifies to

$$dCdV + \rho_b \frac{\partial q}{\partial t} dvdt + e\left(\frac{dC}{dt}\right)dvdt = 0$$

Dividing by $dvdV$ gives

$$-\left(\frac{\partial C}{\partial v}\right)_V = \rho_b \left(\frac{\partial q}{\partial V}\right)_v + e\left(\frac{\partial C}{\partial V}\right)_v \text{ -----(I-31)}$$

Since C is a function of v and V , it can also be expressed as a function of v and $V - ve$:

$$C = f(v, V - ve) \text{ -----(I-32)}$$

by a fundamental property of partial derivatives,

$$dC = \left(\frac{\partial C}{\partial v}\right)_{V-ve} dv + \left[\frac{\partial C}{\partial (V-ve)}\right]_v d(V-ve) \text{ --- (I-33)}$$

and

$$\left(\frac{\partial C}{\partial v}\right)_V = \left(\frac{\partial C}{\partial v}\right)_{V-ve} - e\left(\frac{\partial C}{\partial (V-ve)}\right)_v \text{ ----- (I-34)}$$

or

$$-\left(\frac{\partial C}{\partial v}\right)_V = e\left(\frac{\partial C}{\partial V}\right)_v - \left(\frac{\partial C}{\partial v}\right)_{V-ve} \text{ ----- (I-35)}$$

Here equation (I-31) and equation (I-35) can be equated and simplified to

$$-\left(\frac{\partial C}{\partial v}\right)_{V-ve} = \rho_b\left(\frac{\partial q}{\partial V}\right)_v \text{ ----- (I-36)}$$

Now let

$$X = C/C_0$$

$$Y = q/q_0$$

and define a dimensionless through-put parameter

$$Z = \frac{C_0(V - ve)}{q_0 \rho_b v} = \frac{V - ve}{veD}$$

then equation (I-36) becomes

$$-\left(\frac{\partial X}{\partial v}\right)_{Zv} = \left(\frac{\partial Y}{\partial Zv}\right)_v \text{ ----- (I-37)}$$

This is the material balance partial differential equation for a fixed-bed.

Where, X = dimensionless fluid-phase concentration,

Y = dimensionless solid-phase concentration,

$V-ve$ = amount of fluid that has flowed through

fixed-bed of volume v ,

C_0 = initial concentration of adsorbate in fluid-phase,

q_0 = saturation concentration of adsorbate in solid-phase in equilibrium with C_0 .

Constant-Pattern Limit (Favorable Equilibrium)

It is an experimental fact that break-through curves sometimes retain a constant shape, regardless of bed length. This is because of a constant rate of movement of all parts of the exchange zone. It means that $(\partial Z_v / \partial v)_X$ is constant (see appendix (A-1) for the verification). Therefore, from the material balance equation (I-37), we can write

$$-\left(\frac{\partial X}{\partial v}\right)_{Z_v} = \left(\frac{\partial X}{\partial Z_v}\right)_v \left(\frac{\partial Y}{\partial X}\right)_v \text{ ----- (I-38)}$$

Rearrangement gives

$$\left(\frac{dY}{dX}\right)_v = - \frac{(\partial X / \partial v)_{Z_v}}{(\partial X / \partial Z_v)_v} = \left(\frac{\partial Z_v}{\partial v}\right)_X = \text{const.} \text{ -- (I-39)}$$

and

$$Y = (\text{const.}) X + C_1 \text{ ----- (I-40)}$$

where C_1 is a constant.

Since X and Y have the same limits,

$$X = Y \text{ ----- (I-41)}$$

and also

$$dX = dY \text{ ----- (I-42)}$$

Equation (I-41) and equation (I-42) are the continuity conditions for the constant-pattern case.

The constant-pattern case was first identified and discussed by Bohart and Adams (4), Wicke (45), and Sillen (37).

Breakthrough equations will be developed below for several rate controlling mechanisms.

A. Particle-phase Diffusion.

The derivation for this model begins with the rate approximated by the linear driving force relation

$$\left(\frac{dY}{dt}\right)_{\text{particle}} = \frac{k_p a_p}{De} (Y^* - Y) \text{ ----- (I-10)}$$

The term $Y^* - Y$ can be expressed in terms of X and a constant separation factor R

$$Y^* = \frac{X}{R + (1 - R)X} \text{ ----- (I-43)}$$

and

$$Y^* - Y = \frac{X}{R + (1 - R)X} - Y \text{ ----- (I-44)}$$

Since for constant-pattern limit case, $X = Y$

The $Y^* - Y$ term can be expressed as

$$Y^* - Y = \frac{X}{R + (1 - R)X} - X = \frac{X(1 - X)(1 - R)}{R + (1 - R)X} \text{ -- (I-45)}$$

Substitute this value into equation (I-10)

$$\left(\frac{dY}{dt}\right)_{\text{particle}} = \frac{k_p a_p}{De} \frac{X(1 - X)(1 - R)}{R + (1 - R)X} \text{ ---- (I-46)}$$

or because $dY = dX$ for constant-pattern limit case

$$\left(\frac{dX}{dt}\right)_{\text{particle}} = \frac{k_p a_p}{De} \frac{X(1 - X)(1 - R)}{R + (1 - R)X} \text{ ---- (I-47)}$$

By separation of variables

$$\frac{R + (1 - R)X}{X(1 - X)(1 - R)} dX = \frac{k_p a_p}{De} dt = \frac{k_p a_p v}{F} \frac{dt}{Dve/F}$$

$$= N_p dZ \text{ ----- (I-48)}$$

where

$$N_p = \frac{k_p a_p v}{F} \quad \text{and} \quad Z = \frac{t}{Dev/F}$$

Integration of equation (I-48)

$$\int_{X=1}^X \frac{R + (1 - R)X}{(1 - R)X(1 - X)} dX = N_p \int_1^Z dZ \text{ ----- (I-49)}$$

along with the material balance condition

$$\int_{Z=0}^{X=1} (1 - X) dZ = 1$$

gives

$$\frac{R}{1 - R} \ln X - \frac{1}{1 - R} \ln (1 - X) = N_p (Z - 1) + \alpha_p \text{ --- (I-50)}$$

where α_p represents the sum of constant terms. This relation was first derived by Glueckauf and Coates (13).

B. Pore Diffusion.

If the amount of adsorbate held in the pores of the solid particle is negligible compared with that held by the solid, the rate of diffusion into a uniformly porous, spherical particle is assumed to be given by Fick's second law, and from equation (I-12)

$$\frac{\partial Y_r}{\partial t} = \frac{D_{pore}(1 - e)}{r^2 D e} \frac{\partial}{\partial r} \left(r^2 \frac{\partial X_r}{\partial r} \right) \text{ ----- (I-51)}$$

And the mean solid concentration value Y , averaged over the particle is

$$Y = \frac{3}{r_s^3} \int_0^{r_s} Y_r r^2 dr \text{ -----(I-52)}$$

where r_s is the particle radius. Differentiating equation (I-52) with respect to time and r gives

$$\frac{\partial}{\partial r} \left(\frac{\partial Y}{\partial t} \right) = \frac{\partial Y_r}{\partial t} \frac{3 r^2}{r_s^3} \text{ -----(I-53)}$$

Combination of equations (I-51) and (I-53) leads to

$$\frac{D_{\text{pore}}(1 - e)}{D e r^2} \frac{\partial}{\partial r} \left(r^2 \frac{\partial X_r}{\partial r} \right) = \frac{r_s^3}{3r^2} \frac{\partial}{\partial r} \left(\frac{\partial Y}{\partial t} \right) \text{ --- (I-54)}$$

or

$$\frac{\partial Y}{\partial t} = \frac{3 D_{\text{pore}}(1 - e)}{D e r_s^3} r^2 \frac{\partial X_r}{\partial r} \text{ -----(I-55)}$$

When $R = 0$ (irreversible case), equation (I-51) is simplified by the assumption that the concentration wave penetrating into the particle fully saturates each spherical-shell element before proceeding. If the saturation region has penetrated to a shell of radius r_i , then $\partial Y_r / \partial t$ is zero for $r_i < r < r_s$, infinite at $r = r_i$, and zero for $r < r_i$; while Y_r is unity for $r_i < r < r_s$ and zero for $r < r_i$. Therefore, integration of equation (I-52) over r , gives

$$Y = \frac{3}{r_s^3} \int_{r_i}^{r_s} Y_r r^2 dr = \frac{r_s^3 - r_i^3}{r_s^3} \text{ -----(I-56)}$$

Since the derivative $\partial Y_r / \partial t$ is zero for $r_i < r < r_s$, equation (I-51) becomes

$$\frac{\partial}{\partial r} \left(r^2 \frac{\partial X_r}{\partial r} \right) = 0 \text{ -----(I-57)}$$

or

$$r^2 \frac{\partial X_r}{\partial r} = \text{const.} = g \text{ ----- (I-58)}$$

By integration between the limits of r_i and r_s with X_r equal to 0 and X_s respectively. X_s is the fluid-phase concentration outside the particle and can be replaced by X

$$g = \frac{X}{1/r_i - 1/r_s} \text{ ----- (I-59)}$$

or

$$r^2 \frac{\partial X_r}{\partial r} = \frac{X r_i r_s}{r_s - r_i} \text{ ----- (I-60)}$$

and from differentiation of equation (I-56)

$$\frac{\partial Y}{\partial t} = -3 \frac{r_i^2}{r_s^3} \frac{\partial r_i}{\partial t} \text{ ----- (I-61)}$$

from equations (I-55), (I-60), and (I-61)

$$- \frac{3 r_i^2}{r_s^3} \frac{\partial r_i}{\partial t} = \frac{3 D_{\text{pore}}(1 - e)}{D e r_s^3} \frac{X r_i r_s}{r_s - r_i} \text{ ----- (I-62)}$$

For the constant-pattern limit $X = Y$ and $dX = dY$, therefore from equation (I-56)

$$X = \frac{r_s^3 - r_i^3}{r_s^3} \text{ ----- (I-63)}$$

($r_i < r < r_s$)

Then

$$-\frac{3 r_i^2}{r_s^3} \frac{\partial r_i}{\partial t} = \frac{3 D_{\text{pore}}(1-e)}{D e r_s^3} \frac{r_s^3 - r_i^3}{r_s^3} \frac{r_i r_s}{r_s - r_i} \text{------(I-64)}$$

and

$$\frac{dr_i}{dt} = - \frac{D_{\text{pore}}(1-e)}{D e r_s^2} \frac{r_s^3 - r_i^3}{r_i(r_s - r_i)} \text{------(I-65)}$$

Since

$$k_{\text{pore}} a_p = \frac{60 D_{\text{pore}}(1-e)}{d_p^2}$$

$$N_{\text{pore}} = \frac{k_{\text{pore}} a_p v}{F}$$

Equation (I-65) becomes

$$\frac{dr_i}{dt} = - \frac{N_{\text{pore}}}{15 D e / F} \frac{r_s^2 + r_s r_i + r_i^2}{r_i} \text{------(I-66)}$$

Integration of equation (I-66) can be followed by numerical evaluation of X. The result fits the empirical relation

$$X = 0.557 [N_{\text{pore}}(Z - 1) + 1.15] - 0.0774 [N_{\text{pore}}(Z - 1) + 1.15]^2 \text{------(I-67)}$$

This derivation is due to Vermeulen (41).

C. External Diffusion

When external diffusion is the rate controlling mechanism, the rate expression is

$$\left(\frac{dY}{dt} \right)_{\text{particle}} = \frac{k_f a_p}{D e} (X - X^*) \text{------(I-16)}$$

For the constant pattern limit, $X = Y$ and $dX = dY$

and for a constant separation factor, R

$$X^* = \frac{RY}{1 + (R - 1)Y}$$

with the above substitutions, equation (I-16) becomes

$$\frac{1 + (R - 1)X}{(R - 1)X(X - 1)} dX = N_f dz \quad \text{-----(I-68)}$$

where

$$N_f = \frac{k_f a_p v}{F}$$

By integration

$$\begin{aligned} & \int_{X@Z=1}^X \left[\frac{1}{(1 - R)X(1 - X)} - \frac{1}{(1 - X)} \right] dX \\ &= N_f \int_1^Z dz \end{aligned}$$

then

$$\frac{1}{1 - R} \ln X - \frac{R}{1 - R} \ln (1 - X) = N_f (Z - 1) + Q_f \quad \text{-----(I-69)}$$

where Q_f is the sum of constant terms. Equation (I-69) is Michaels' result (28).

D. Reaction Kinetics.

From equation (I-22)

$$\left(\frac{dY}{dt_R} \right)_{\text{particle}} = X(1 - Y) - RY(1 - X) \quad \text{-----(I-22)}$$

with

$$t_R = \frac{k_F t}{D e} \qquad k_F = \frac{k_i p_o D e}{1 - R}$$

Rearrangement gives

$$\frac{dY}{dt} = \frac{k_F v/F}{D e v/F} X(1 - Y) - RY(1 - X) \text{ -----(I-70)}$$

with

$$N_R = \frac{k_F v}{F}$$

and

$$Z = \frac{t}{D e v/F}$$

equation (I-70), for constant pattern limit, becomes

$$\frac{dX}{dt} = N_R(1 - R)X(1 - X)dZ \text{ -----(I-71)}$$

Rearrangement and integration between the usual limits gives

$$\frac{1}{1 - R} \ln \frac{X}{1 - X} = N_R(Z - 1) \text{ -----(I-72)}$$

or

$$X = \frac{1}{1 + e^{-u}} \text{ -----(I-73)}$$

where $u = (1 - R)N_R(Z - 1)$

This result was first derived by Sillen and Ekedahl (37).

All of these four models (particle-phase diffusion, pore diffusion, external diffusion, and reaction kinetics) derived above will be tested against the experimental breakthrough data to find whether they can be successfully used for design purposes.

CHAPTER II

EXPERIMENTAL EQUIPMENT AND TECHNIQUE

There were three major aspects of this experimental investigation:

- (1) Generation of gas mixtures: It was necessary to be able to generate a known and reproducible gas mixture containing extremely low concentrations of adsorbable vapours.
- (2) Adsorption: The gas mixture of constant composition was passed through a fixed-bed of activated charcoal at a constant flow rate.
- (3) Analysis: The ability to analyse a gas stream containing adsorbate in the parts per million range with a gas chromatograph was necessary in order to monitor influent and effluent streams.

A diagram of the entire experimental apparatus is shown on Figure (II-1) and a detailed discussion of the apparatus and techniques follows.

Mixtures of acetaldehyde and air in the parts per million range were generated through the use of a diffusion cell. The diffusion cell essentially consisted of a long capillary tube connecting a reservoir to a mixing chamber. The function of the reservoir is to prevent a rapid change in liquid level in the capillary tube and to allow operation over a long

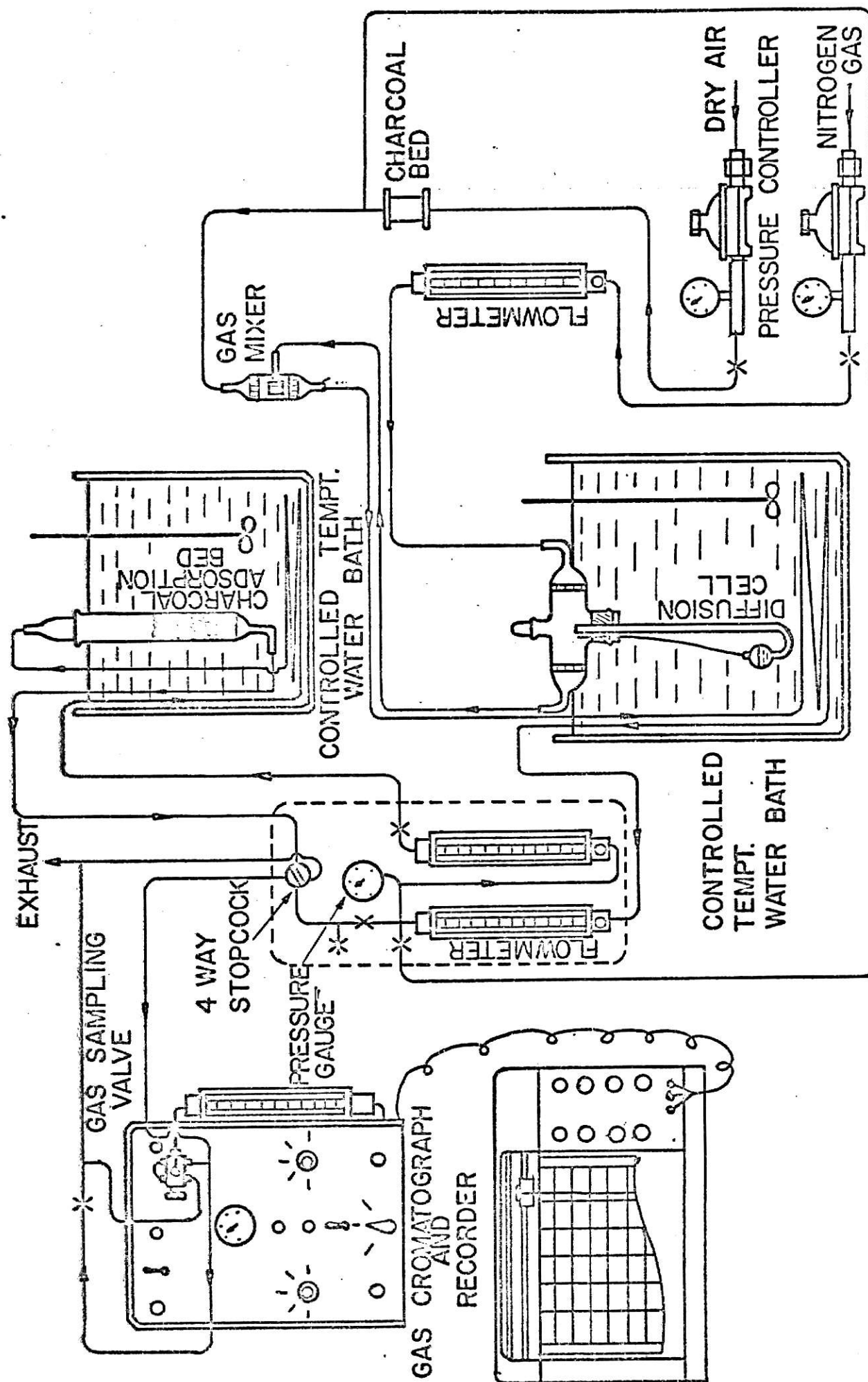


FIG. (II-1) EXPERIMENTAL ADSORPTION SYSTEM

period of time. The drawing of the diffusion cell assembly is shown on Figure (II-2).

The diffusion process involves essentially the diffusion of molecules from the liquid-gas interface in the capillary to the upper end of the capillary tube and mixing with nitrogen gas flowing through the mixing chamber. The driving force is the concentration gradient of the vapour between interface and chamber. The rate of diffusion is also governed by the temperature of the liquid. This temperature defines the partial pressure of the vapour above the liquid. The rate of diffusion is expressed by the equation:

$$r_d = \frac{2.303 D_m M P A}{R_g L T} \log \frac{P}{P - p} \text{ -----(II-1)}$$

Where, r_d = rate of diffusion of vapour out of the diffusion tube, gm/sec.

D_m = molecular diffusion coefficient of the vapour into the nitrogen gas, cm^2/sec .

M = molecular weight of vapour

P = total pressure in the diffusion cell, atm.

p = partial pressure at a temperature T of the vapour, atm.

A = cross-sectional area of the diffusion tube, cm^2

R_g = gas law constant, liter atm/mole $^{\circ}\text{K}$

T = temperature, $^{\circ}\text{K}$

L = length of diffusion path, cm

From this equation, the desired concentration can be regulated

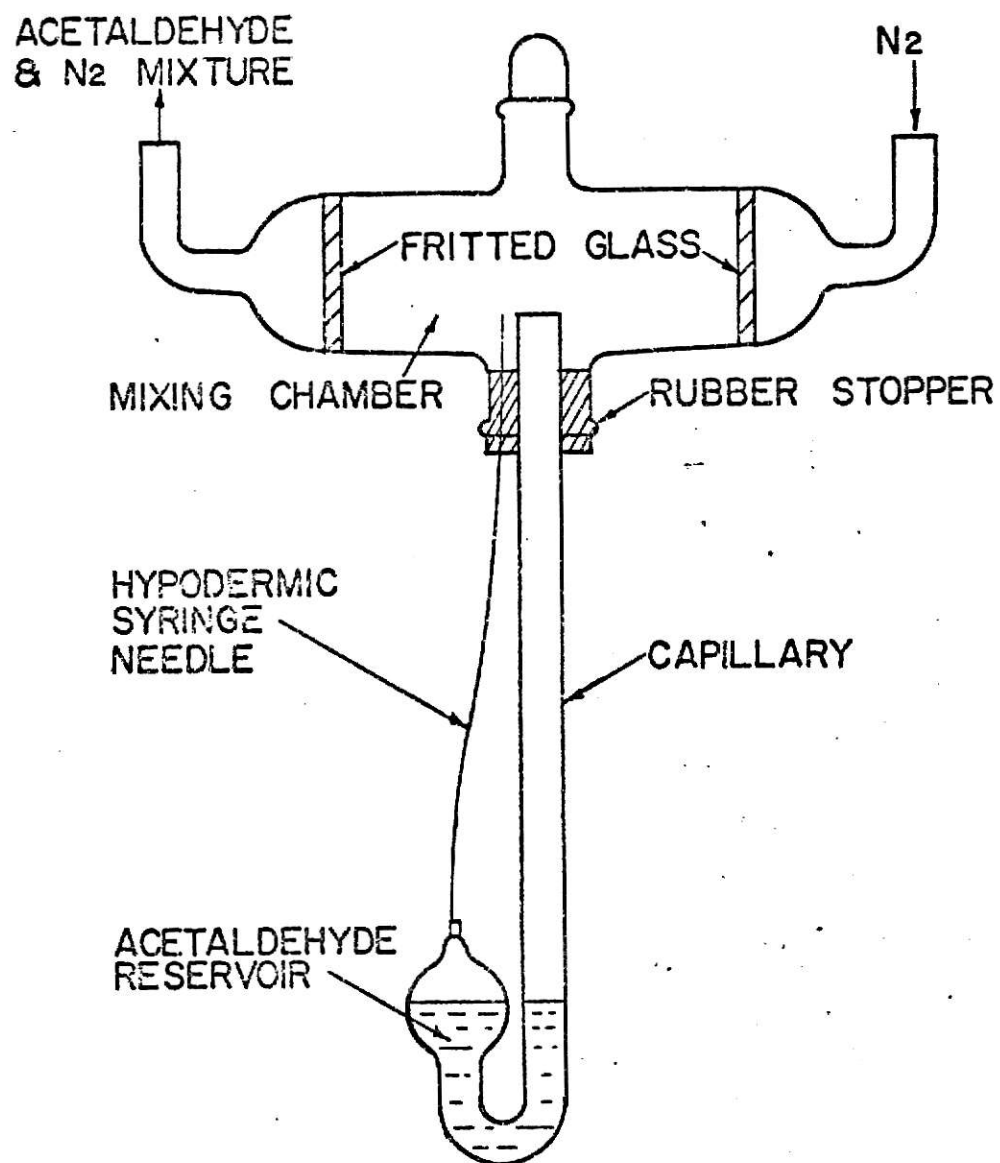


FIG.(II-2) DIFFUSION TUBE

by gas flow, temperature, and diameter or length of the capillary tube. This diffusion tube application has been described by Altshuller and Cohen (1).

To establish the diffusion rate experimentally, a diffusion tube without reservoir was used. The diffusion rate was determined by measuring the change in liquid height inside the capillary tube over a measured time interval. The level change, measured by means of a cathetometer, was converted to a volume by means of a previously established calibration. This calibration was made by partial filling of the capillary with a known weight of mercury and measurement of the mercury column height with the cathetometer. From the volume of liquid evaporated per unit time, the diffusion rate was determined from the known density of acetaldehyde.

When this diffusion tube was operated, it was noticed that the diffusion rate was not constant over a long period time, but decreased with time. The probable cause of this behavior was believed to be air oxidation of acetaldehyde with accumulation of reaction products at the gas-liquid interface. To test this hypothesis, the diffusion cell was operated with a nitrogen flow instead of an air flow past the upper end of the diffusion tube. The result of this test was a constant diffusion rate over several days of operation.

Because nitrogen gas was used, it was necessary to mix the nitrogen-acetaldehyde mixture from the diffusion cell with air to form the influent stream to the charcoal bed.

The reason for the mixing was that the original purpose of this experiment was to test the adsorption of acetaldehyde in air. A specially designed mixer fabricated from glass, as shown on Figure (II-3), was used for this mixing purpose. The gas leaving the mixer was passed through several feet of tubing before entering the charcoal bed in order to obtain thorough mixing. This tubing was placed in the constant temperature bath so as to obtain the desired gas temperature.

The influent gas stream flowed through two flowmeters. The first flowmeter was used to control the flow rate through the mixer and thereby produce the desired acetaldehyde concentration while the second was used to control the flow to the charcoal bed. A diagram of the charcoal bed, fabricated from glass, is shown on Figure (II-4). Beds of different diameters in the range of 16 to 25 mm and lengths of 8 to 46 cm range were used.

After leaving the charcoal bed the gas stream flowed through the measuring system which consisted of a gas sample valve connected to a Varian Aerograph Model 600D gas chromatograph. This allowed the acetaldehyde concentration in the effluent and influent gas to be monitored at various times as a chromatographic peak height which could be converted to concentration of acetaldehyde from a calibration curve. The calibration curve was constructed by recording the chromatographic peak heights for a number of different

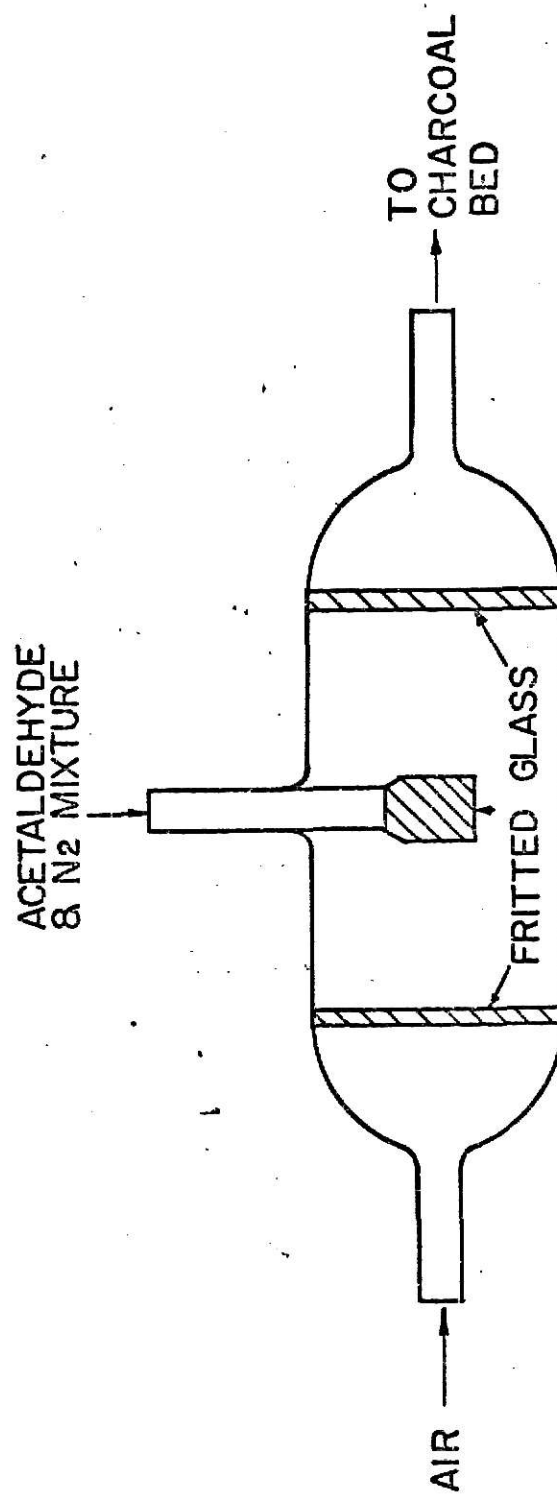


FIG. (II-3) GAS MIXER

TO GAS CHROMATOGRAPH

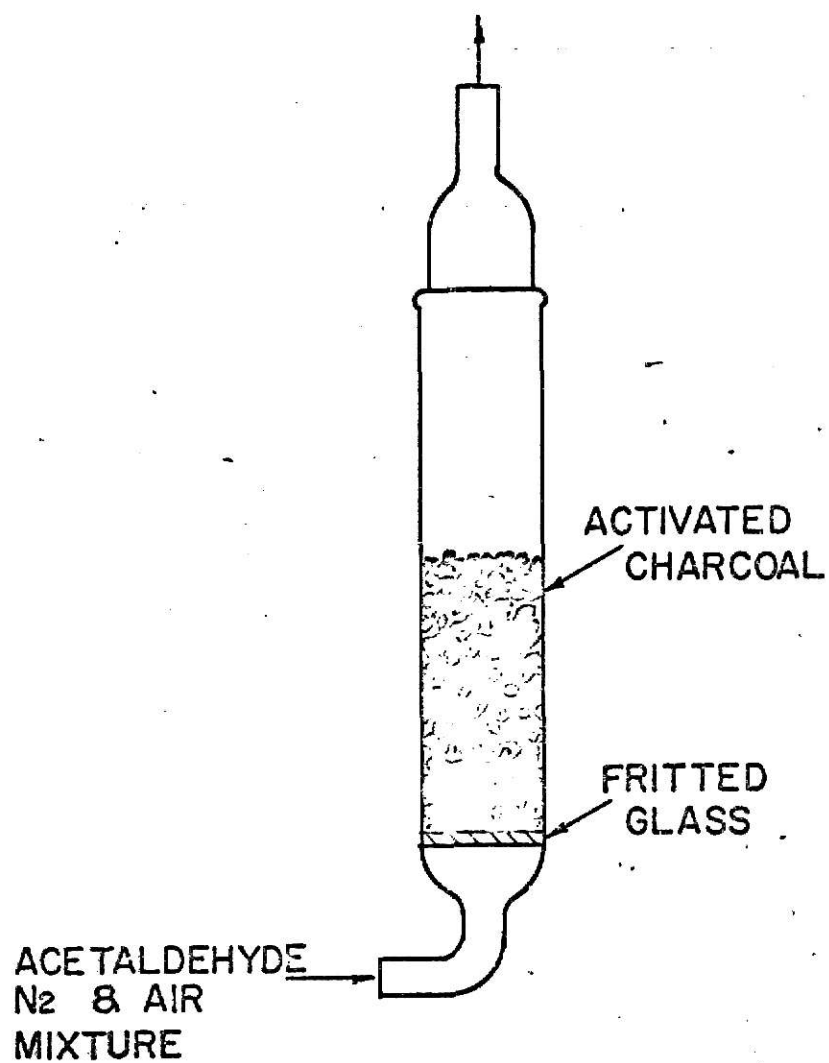


FIG.(II-4) CHARCOAL BED

known acetaldehyde diffusion rates using the calibrated diffusion tube. The calibration curve of acetaldehyde concentration up to 60 ppm is shown on Figure (A-2) in the appendix.

Thus a "breakthrough curve" could be obtained at a given flow rate and influent concentration by determining the effluent concentration at various times.

Static Equilibrium Test

It is possible to determine adsorption equilibrium data by measuring known quantities of charcoal and acetaldehyde into a container of known volume and determining the equilibrium gas phase composition by chromatographic analysis. Claphan, Junker, and Tobias (7) used this method to obtain equilibrium data for the adsorption of organic vapours in the parts per million range in air on charcoal.

For this purpose, a 3,000 ml flask was connected to the previously described gas mixture generating system outlet and a gas mixture of the desired acetaldehyde concentration was passed through the flask. The acetaldehyde concentration was controlled by regulating the flow rate through the diffusion tube and the concentration was monitored continuously by the gas chromatograph to obtain a known concentration of gas in the flask. A known weight of charcoal was then added and the flask was set in a constant temperature chamber. The concentration inside the flask was checked periodically by taking samples from the flask with a hyperdermic syringe and injecting them into the gas chromato-

graph. These analysis were performed at 5 to 10 day intervals until the concentration change during any period became negligible. This final concentration was considered as an equilibrium concentration with the charcoal. From a mass balance calculation, the amount of acetaldehyde adsorbed on charcoal in equilibrium with the final acetaldehyde concentration in the gas phase was obtained. Several different conditions of this experiment were used so that the adsorption isotherm curve could be constructed.

CHAPTER III

RESULTS AND DISCUSSION

By applying the techniques discussed in chapter II breakthrough data were obtained at 30 °C for fixed-beds of Pittsburgh PCB charcoal fed with a constant influent concentration of 28 ppm of acetaldehyde in air. The effect of bed length, superficial velocity, and charcoal particle size was studied. The ranges of these variables were: 8 to 46 cm bed length, 10, 12, 14 mesh charcoal particle size, and 8.4 to 39.5 cm/sec superficial velocity. Barneby (2) states that the customary superficial velocity used in commercial fixed-bed adsorption operation is 35 to 75 ft/min. (18 to 38 cm/sec).

In this chapter, some general and empirical observations are presented; this is followed by a modeling study of the breakthrough data. Finally, the static equilibrium data obtained by the technique described in chapter II are analysed and compared with charcoal capacities obtained from the breakthrough data and the modeling study.

III-1. General Observations.

(a) Mid-point time and Break-time versus Residence time.

From the experimentally obtained breakthrough curves, which are shown on Figures (A-1) to (A-13) in appendix, the mid-point time and break-time can be obtained. The mid-point and break-time are the times required for the effluent

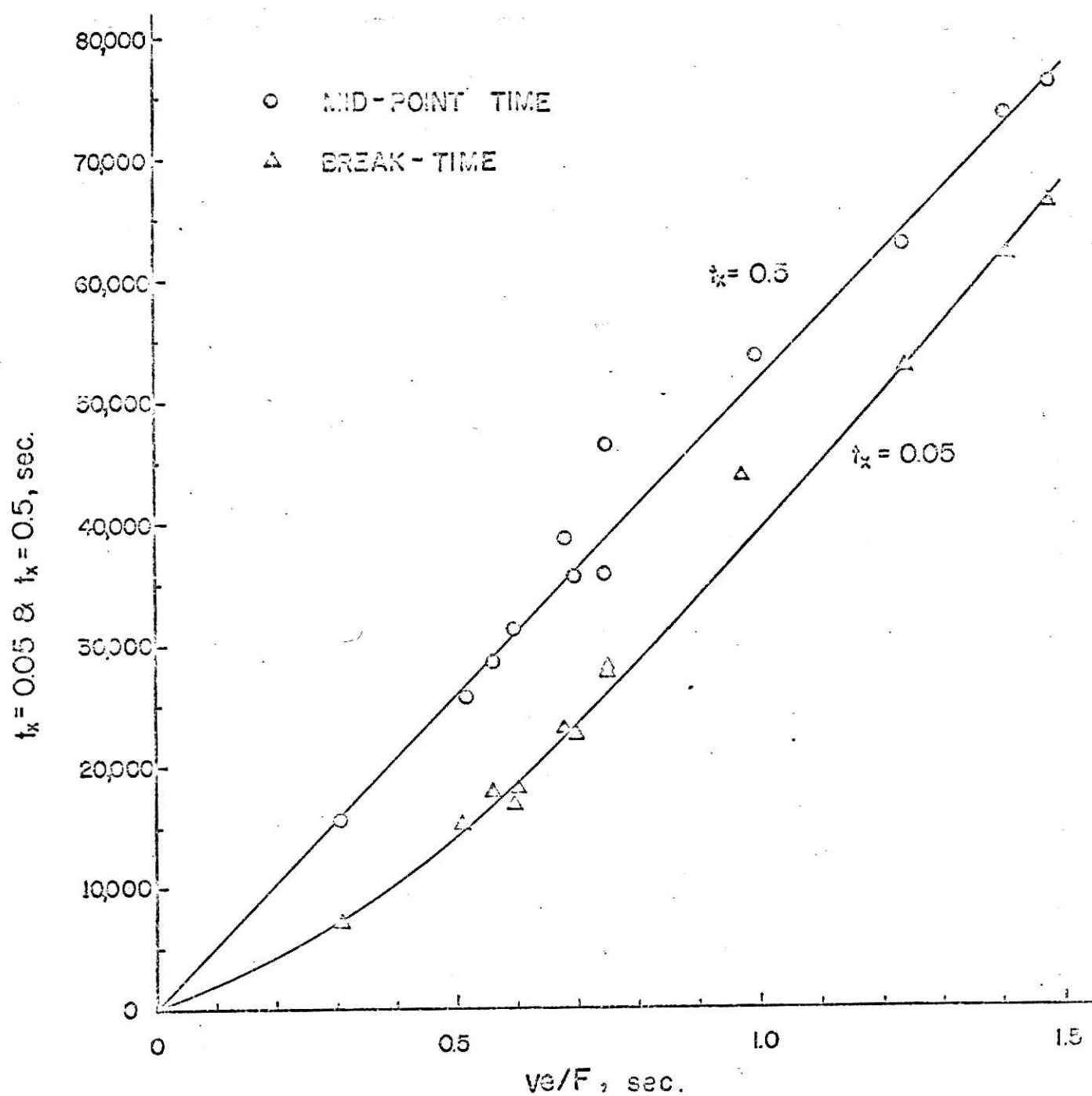


FIG.(III-1) BREAK-TIME AND MID-POINT TIME RELATED TO RESIDENCE TIME, ve/F .

concentration to reach to 50 % and 5 % of the influent concentration respectively. As shown on Figure (III-1), the mid-point time is almost linearly proportional to the mean residence time (v_e/F), and the break-time also increases with the mean residence time.

(b) Effect of bed lengths.

In an effort to determine the effect of bed length on the breakthrough curve, four tests were made with the same superficial velocity (16.4 cm/sec) and same charcoal size (14 mesh), but different bed lengths. The comparison of these tests (APC-19, APC-20, APC-21, and APC-29) is shown on Figure (III-2) where the time scales have been shifted to make all the breakthrough curves match at 4 ppm. From Figure (III-2), it is seen that the breakthrough curves match fairly well in the lower range except for APC-19, and it seems like that the lower part of these breakthrough curves do not depend on bed length. With this result, it will be appropriate to apply the constant pattern limit for modeling study. The constant pattern limit requires that the breakthrough curves retain a constant shape, regardless of the bed length.

(c) Effect of superficial velocity.

Four tests have been conducted using 18 inch deep beds of Pittsburgh FCB 14 mesh charcoal fed with an influent stream containing 28 parts per million of acetaldehyde in air. These tests (APC-29, APC-30, APC-31, and APC-32) were made with

ILLEGIBLE DOCUMENT

**THE FOLLOWING
DOCUMENT(S) IS OF
POOR LEGIBILITY IN
THE ORIGINAL**

**THIS IS THE BEST
COPY AVAILABLE**

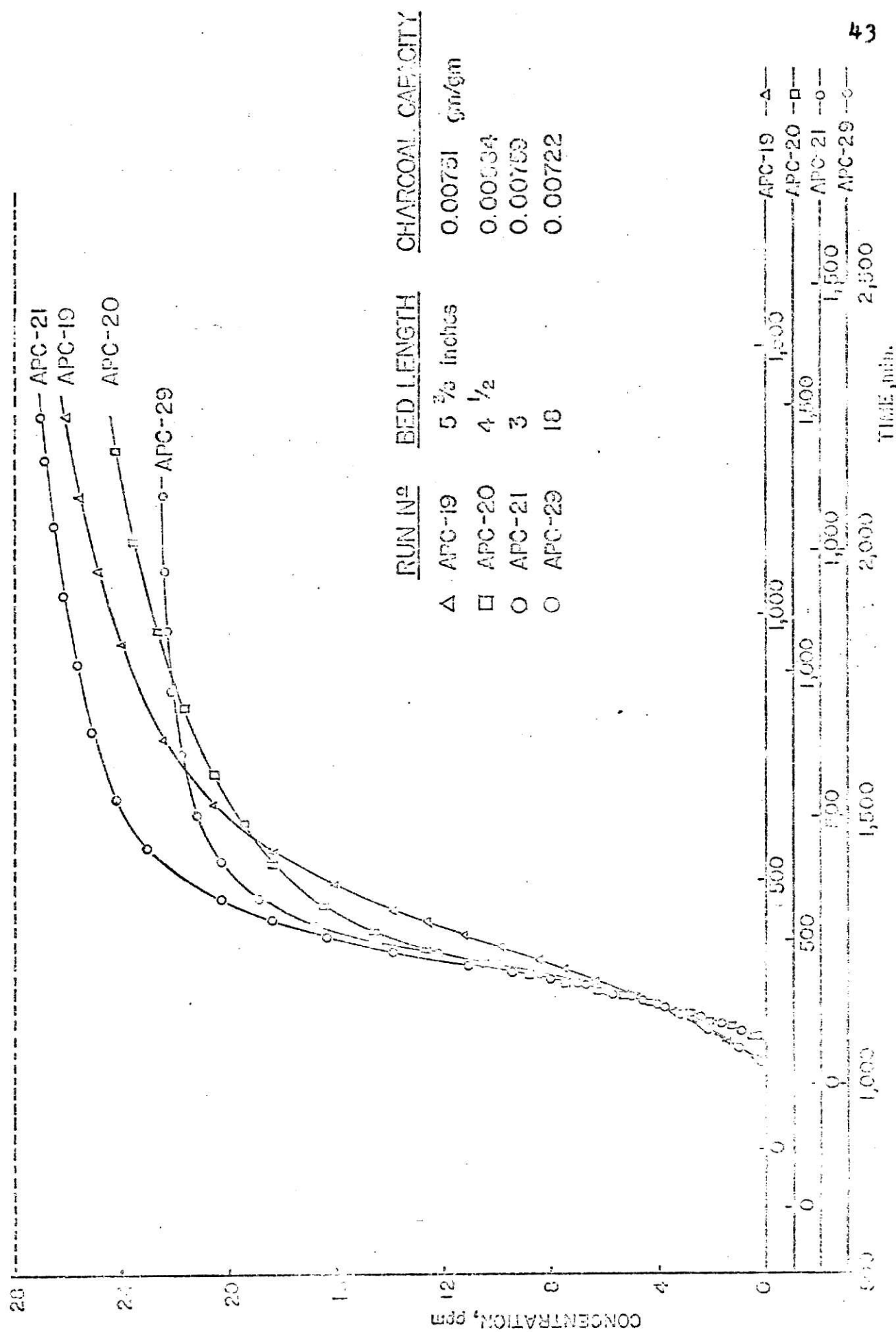


FIGURE 1. COLLECTION OF BREAKTHROUGH DATA FOR DIFFERENT BED LENGTH

... IN THE PLOT SURFACE, VELOCITY OF 16.4 cm/sec

superficial fluid velocities of 16.4, 25.0, 35.0, and 30 cm/sec respectively. The breakthrough curves for these four tests are plotted on Figure (III-3) where the time scales have been shifted so as to make the curves match at an effluent concentration of 4 ppm. It is seen from Figure (III-3) that the curves superimpose quite well in the range 0 to 14 ppm. Therefore, it can be said that the shape of the lower half of the breakthrough curve does not strongly depend on fluid velocity in the range of 16.4 to 35 cm/sec superficial velocity.

(d) Effect of charcoal particle size.

Tests were also made with 10 and 12 mesh charcoal. For these tests, the bed diameters were selected so that the ratio of bed diameter to particle diameter would be at least 8 to 1. The influent flow rate was adjusted to obtain a superficial velocity of 16.4 cm/sec with an influent concentration of 28 ppm of acetaldehyde in air. The resulting breakthrough curves for charcoals of different size are shown on Figure (III-4) along with the breakthrough curve for 14 mesh charcoal with the same superficial velocity and bed height (APC-29). It appears that the breakthrough curves become slightly sharper as the particle size decreases. It also appears from the charcoal capacities of 0.0058, 0.0061, and 0.0072 gm/(gm charcoal) for 10 mesh, 12 mesh, and 14 mesh charcoal respectively that the effective charcoal capacity seems to decrease as the particle size increases, but there is little statistical significance between the capacities of 10 and 12 mesh charcoal.

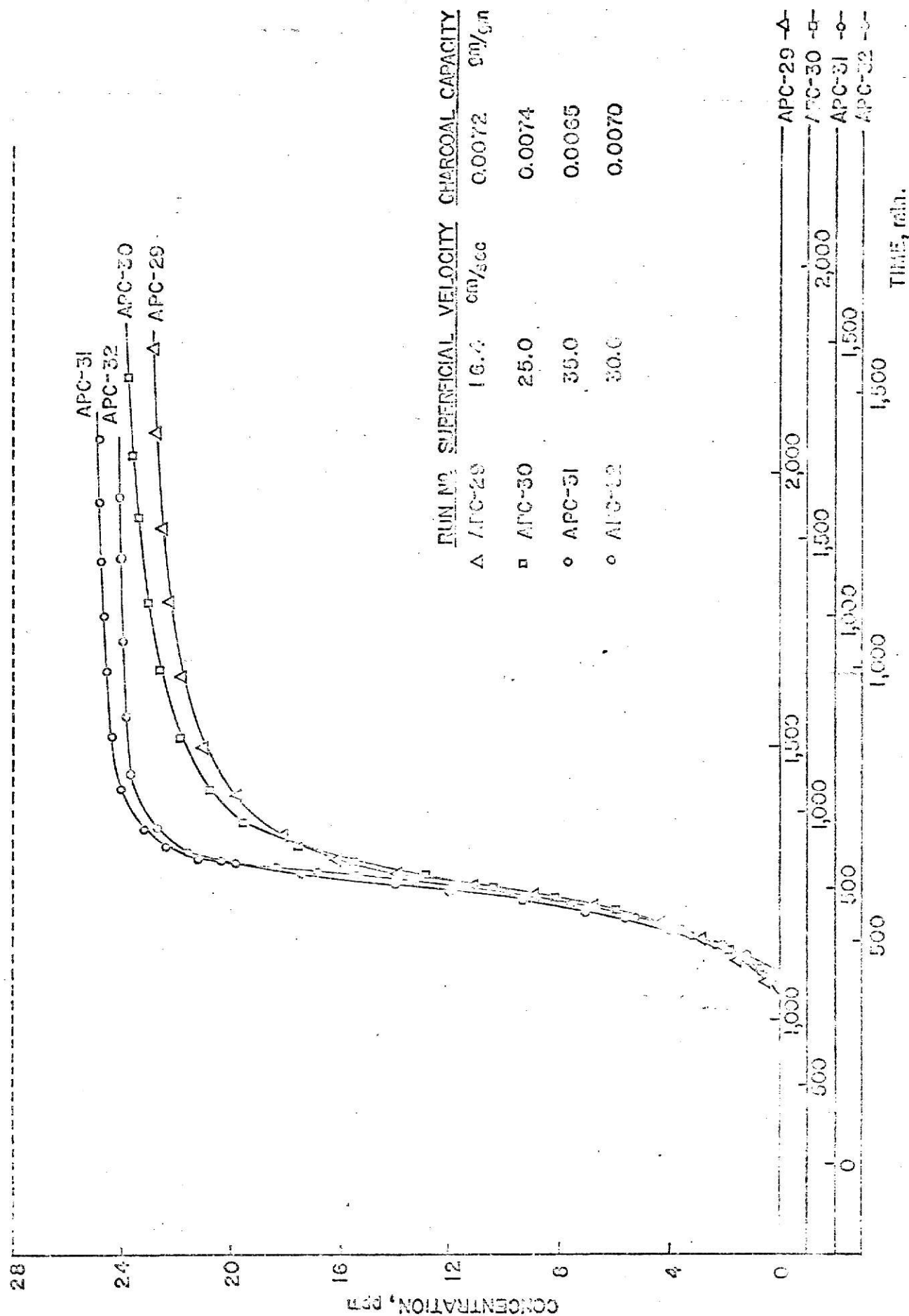


FIG. (III-3). COMPARISON OF BREAKTHROUGH DATA FOR DIFFERENT SUPERFICIAL

VELOCITIES AND DIFFERENT CHARCOAL CAPACITIES

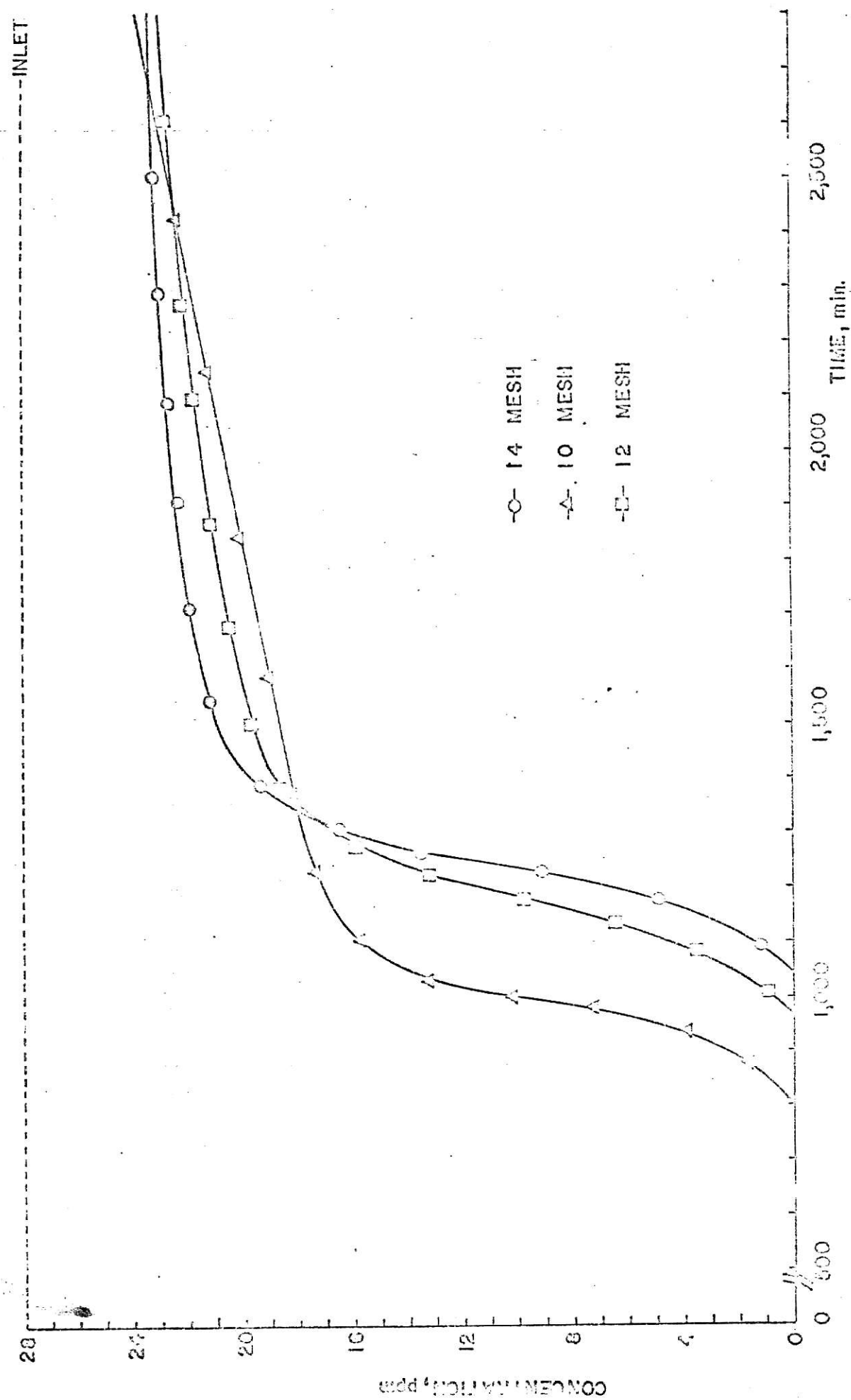


FIG.(III-4). COMPARISON OF BREAKTHROUGH DATA FOR DIFFERENT SIZE OF CHARCOAL AT SAME BED DEPTH OF 18" AND SAME SUPERFICIAL VELOCITY OF 16.4 cm/sec

III-2. Modeling Study.

The objective of the modeling study is to establish the rate mechanism and to determine the dependence of the parameters in the rate expression upon the system variables so that the design of adsorption systems for odor removal can be accomplished. By fitting a selected model breakthrough equation to the experimental breakthrough curve, the evaluation of the model parameters is possible. The validity of a given model is then determined by its ability to fit the experimental breakthrough curve and also by whether the experimentally determined model parameters are realistic. With design as our prime objective, we want fairly simple models whose parameters have physical significance and can be readily estimated. Four such models (solid diffusion model, pore diffusion model, external diffusion model, and reaction kinetics model) were tested.

These models have two parameters: the number of mass transfer units and the effective distribution ratio. The distribution ratio is defined (19) as

$$D = \frac{q_o W}{C_o v_e} \text{ -----(III-1)}$$

where q_o is the solid phase concentration in equilibrium with the gas phase concentration C_o , and W is bed weight. The distribution ratios calculated from this equation and capacities determined from the breakthrough curves show values ranging 73,523 to 124,670 instead of an expected constant value. These calculated values of D are shown in Table (III-1).

Table (III-1) Calculated Values of Void Fraction and Distribution Ratios.

Run No.	W gm	bed dia. mm	bed length cm	e	D
APC-14	5.2	16	8.16	0.649	73,523
APC-18	6.1	16	10.16	0.649	73,523
APC-19	8.3	16	13.82	0.649	73,523
APC-20	6.8	16	11.33	0.649	73,523
APC-21	4.54	16	7.56	0.649	73,523
APC-22	7.56	16	12.59	0.649	73,523
APC-26	16.5	16	20.32	0.525	123,071
APC-29	37.5	16	45.72	0.520	124,670
APC-30	37.5	16	45.72	0.520	124,670
APC-31	37.5	16	45.72	0.520	124,670
APC-32	37.5	16	45.72	0.520	124,670
APC-38	102	25	45.72	0.465	114,564
APC-39	58	19	45.72	0.474	115,571

Avg. = 99,463

The reason for this inconsistency is because of the different values of the void fraction, e , of the fixed-beds. The e values are different for the different bed dimensions because of uneven packing of the charcoal in the bed. Also e is observed to decrease with increasing bed diameter which indicates that wall effects may be important. Furthermore, when the average value of the distribution ratio (99,436) was used in the model equations, it was found that the resulting one-parameter model gave a poor fit to the experimental breakthrough data. Therefore, the distribution ratio was treated as a free parameter so that the resulting two-parameter model equations could better fit the experimental breakthrough curve. These "two-parameter" model equations do not fit the entire experimental breakthrough curves, but do a reasonably good job fitting the first half of the curves.

(a) Particle-phase diffusion model.

The particle-phase diffusion model is expressed as equation (I-50) for favorable equilibrium and a constant separation factor. The equation is

$$\frac{R}{1-R} \ln X - \frac{1}{1-R} \ln(1-X) = N_p(Z-1) + \alpha_p \text{ --- (I-50)}$$

For our system R is 0.28 as calculated from the equilibrium isotherm (see section III-3) and α_p is 1.076 for this R value. The α_p value was obtained from Figure (A-16) in appendix. The equation then becomes

$$0.389 \ln X - 1.389 \ln(1-X) - 1.076 = N_p(Z-1) \text{ -- (III-2)}$$

with

$$Z = \frac{t}{D_{ep} ve/F}$$

Where Z is the through-put parameter, D_{ep} is the effective distribution ratio, and N_p is the number of mass transfer units, which Hiester et al. (19) has defined as

$$N_p = \frac{k_p a_p v}{F} = \left(\frac{k_p a_p}{e} \right) \frac{ve}{F} \text{ ----- (III-3)}$$

The N_p and D_{ep} values were calculated by the least square curve fitting method applied to the first half of the experimental breakthrough curves. These parameters are shown on Figures (III-5) and (III-6). As Figure (III-5) shows, the effective distribution ratio can be considered constant, as expected, and has an average value of 57,865 with standard deviation of 5,293.5 which means that D_{ep} is less variable than the charcoal capacity data (see section III-2).

From equation (III-3), because k_p is not expected to depend upon fluid velocity, N_p should be linearly proportional to residence time, ve/F , as shown on Figure (III-5) as the dotted line. But the data appear to fit the solid curve slightly better and the model equation using the N_p values obtained from this straight line did not fit the experimental breakthrough data as well as those obtained from the solid curve.

From the model equation with these smoothed N_p and D_{ep} values, the break-times were calculated for all of the runs

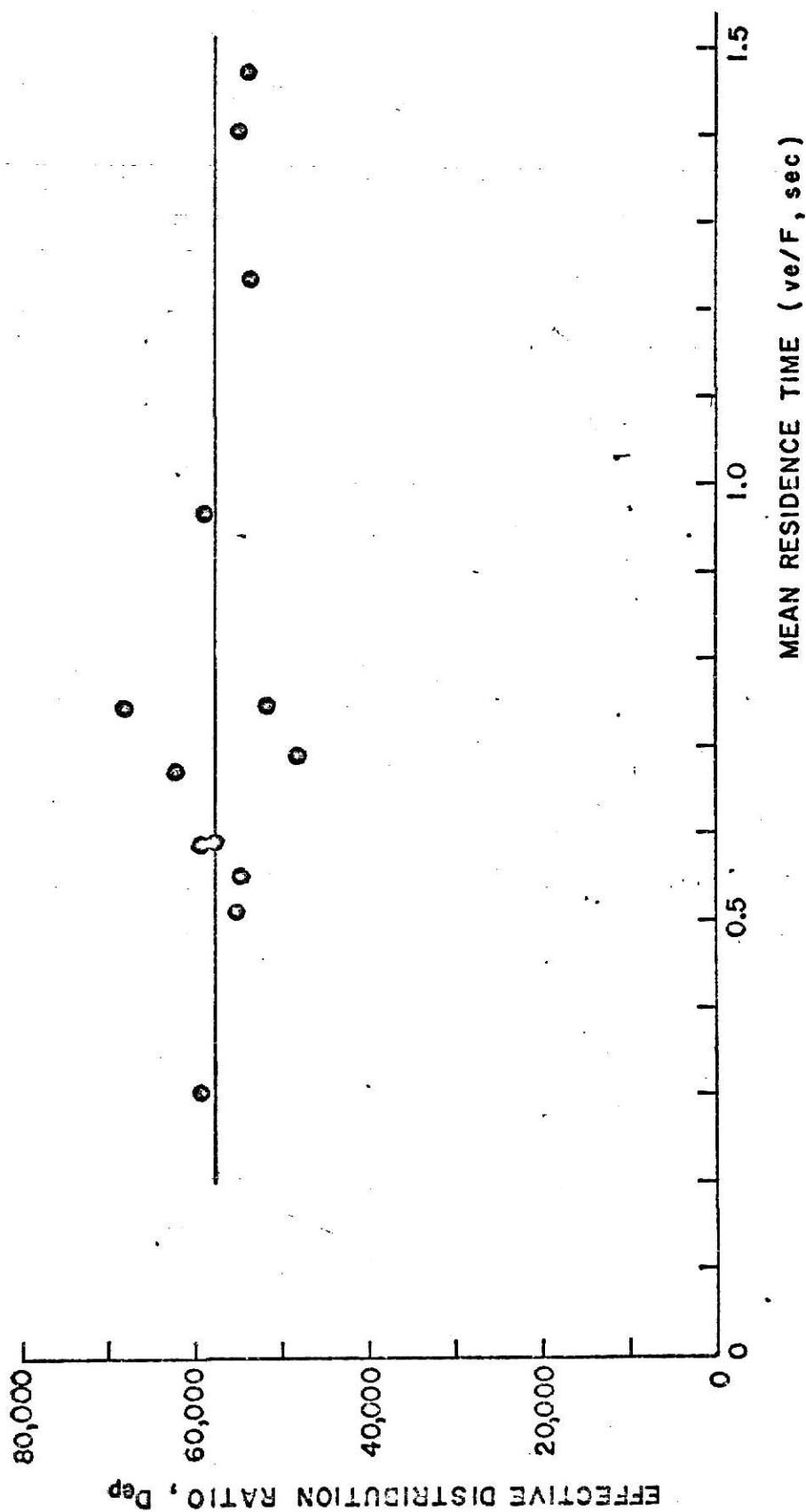


FIG.(III-5). RELATION BETWEEN MEAN RESIDENCE TIME AND EFFECTIVE DISTRIBUTION RATIO FOR PARTICLE-PHASE DIFFUSION MODEL. AVERAGE VALUE OF $D_{ep}=57,865$

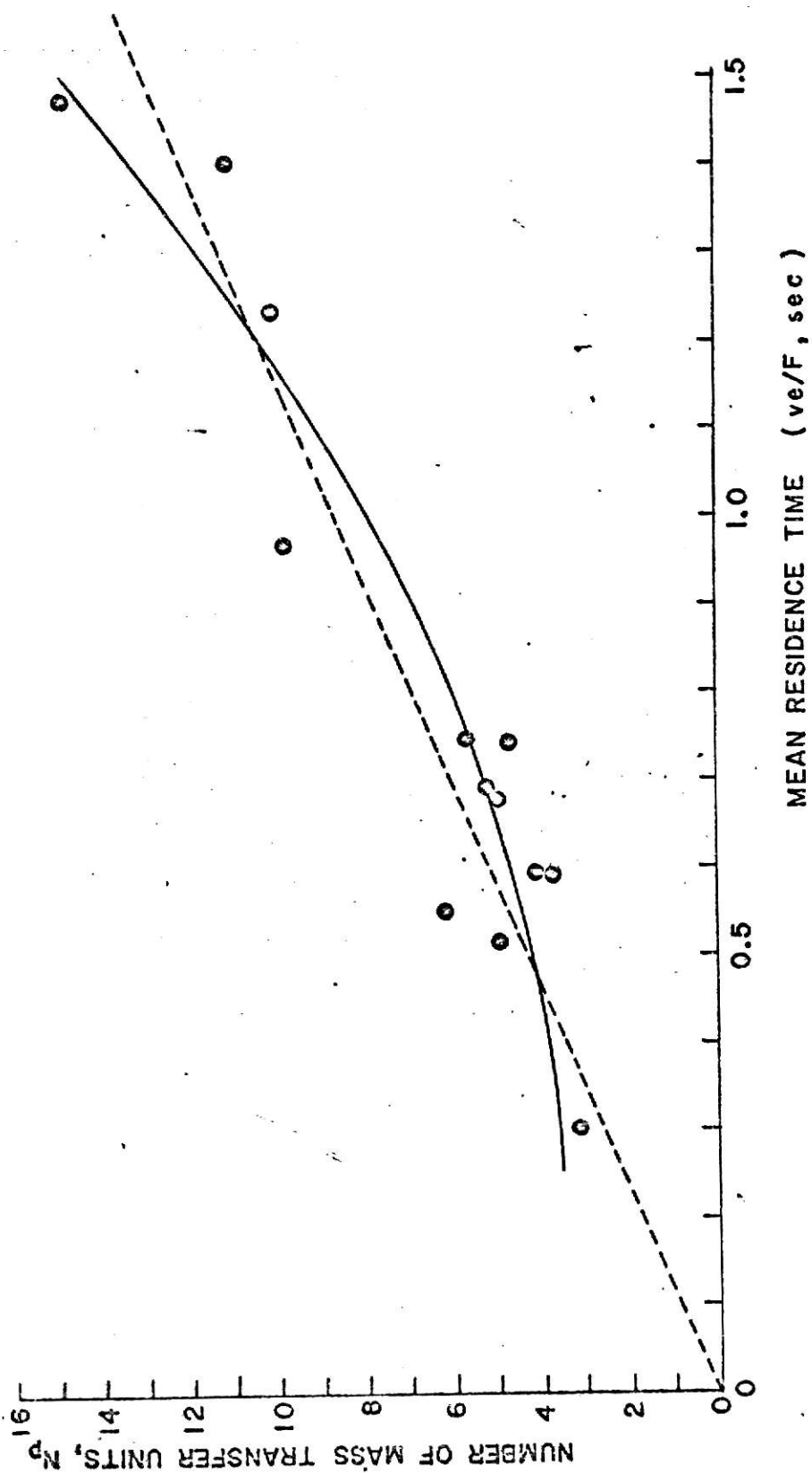


FIG. (III-6). NUMBER OF MASS TRANSFER UNITS VERSUS RESIDENCE TIME FOR PARTICLE-PHASE DIFFUSION MODEL

and the complete results are shown on Tables (III-2) and (III-3). Also, comparison of the model equations with the experimental breakthrough curves are shown on Figures (A-1) to (A-13) in appendix. The sample calculation of break-time is also shown in appendix (A-4). This model fits the breakthrough curve well up to 60 % of effluent concentration and with smoothed parameters reproduces the break-time within ± 10 % accuracy. On Figure (III-7), calculated break-times are compared with experimental values.

Table (III-2). Parameters Obtained from Model Equation
for Particle-phase Diffusion Model

Run No.	ve/F sec	Effective Dist- ribution Ratio Dep	Number of Mass Transfer Units N _p
APC-14	0.677	62,386	5.00
APC-18	0.595	57,990	4.00
APC-19	0.592	59,179	3.60
APC-20	0.515	54,441	4.80
APC-21	0.303	59,020	3.00
APC-22	0.747	68,341	4.60
APC-26	0.556	54,002	6.30
APC-29	1.471	53,159	15.00
APC-30	0.966	58,127	10.00
APC-31	0.691	47,780	5.25
APC-32	0.745	51,179	5.98
APC-38	1.239	52,872	10.00
APC-39	1.401	54,577	11.00

Table (III-3). Calculated Break-time and Estimation Error based on the Smoothed parameters for Particle-phase Diffusion Model.

Run No.	Smoothed Model Parameters		Break-time		Error* %
	Dep	N _p	Calculated sec	Experimental sec	
APC-14	57,865	5.0	23,637	23,400	+ 1.01
APC-18	57,865	4.4	18,911	18,300	+ 3.34
APC-19	57,865	4.4	18,817	16,800	+ 6.91
APC-20	57,865	4.0	15,027	15,300	- 1.78
APC-21	57,865	3.5	7,597	7,200	+ 5.54
APC-22	57,865	5.4	27,351	28,800	- 5.04
APC-26	57,865	4.2	16,982	18,000	- 5.66
APC-29	57,865	14.4	73,395	66,600	+ 10.20
APC-30	57,865	7.9	41,866	44,280	- 5.45
APC-31	57,865	5.0	24,126	22,500	+ 7.23
APC-32	57,865	5.4	27,278	28,080	- 2.86
APC-38	57,865	10.9	58,652	53,100	+ 10.46
APC-39	57,865	13.2	68,890	62,400	+ 10.40

*

$$\text{Error \%} = \frac{t_{x=0.05}(\text{Modeling}) - t_{x=0.05}(\text{Experimental})}{t_{x=0.05}(\text{Experimental})} \times 100$$

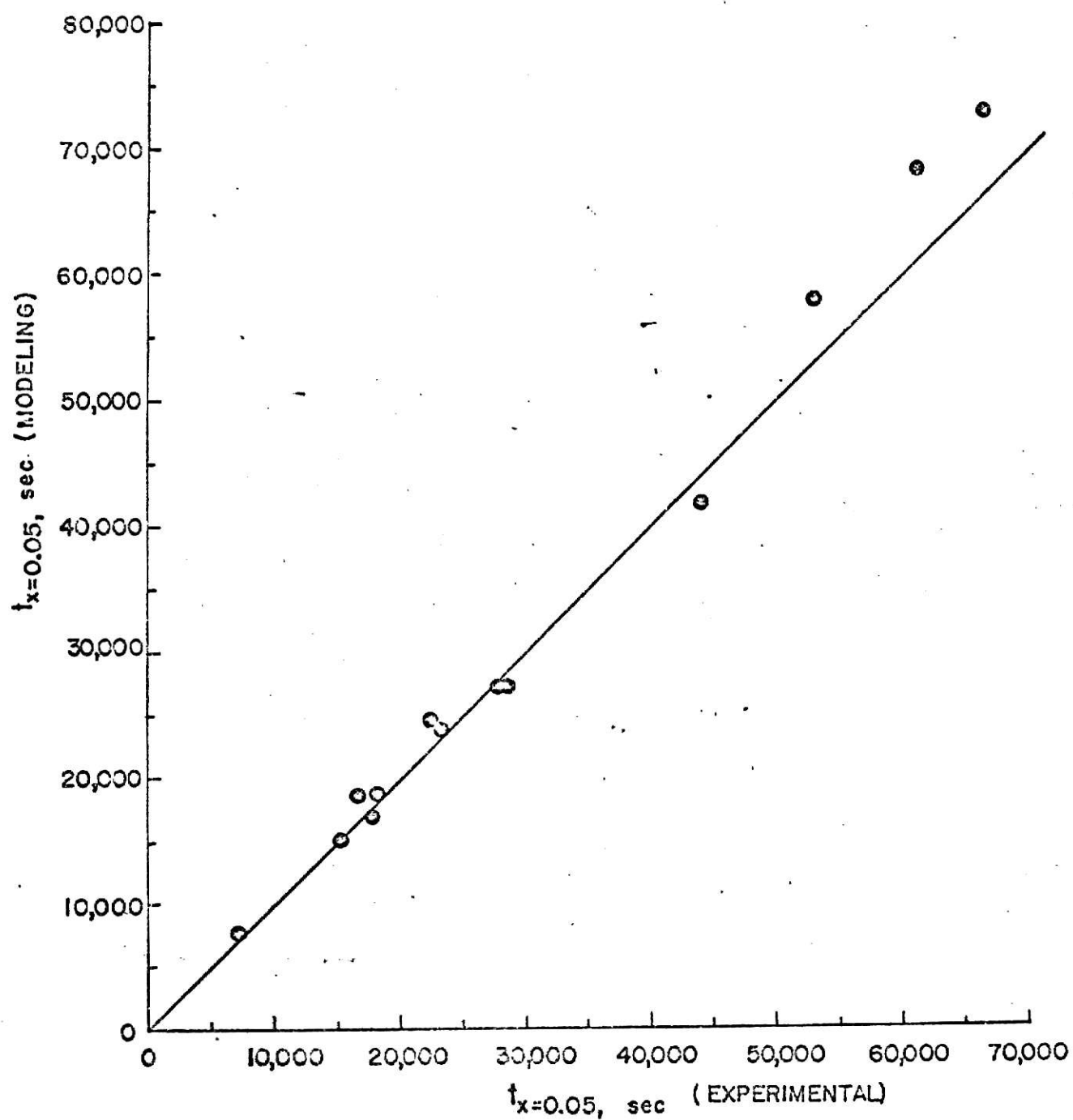


FIG.(III-7). COMPARISON OF PARTICLE-PHASE MODELING BREAK-TIMES WITH EXPERIMENTAL VALUES

(b) Pore Diffusion Model.

The pore diffusion problem for favorable equilibrium ($0 < R < 1$) has not been solved analytically except for $R = 0$. Therefore only the pore diffusion model equation (I-67) for this irreversible case ($R = 0$) can be applied to the experimental data. The equation is

$$X = 0.557 [N_{\text{pore}}(Z - 1) + 1.15] - 0.0774 [N_{\text{pore}}(Z - 1) + 1.15]^2 \text{ ----- (I-67)}$$

with

$$Z = \frac{t}{D_{\text{epore}} v_e / F}$$

Where D_{epore} is the effective distribution ratio and N_{pore} is the number of mass transfer units for pore diffusion which can be expressed as

$$N_{\text{pore}} = \frac{k_{\text{pore}} a_p v}{F} = \left(\frac{k_{\text{pore}} a_p}{e} \right) \frac{v_e}{F} \text{ ----- (III-4)}$$

The N_{pore} and D_{epore} values were calculated by a least square method applied to the first half of the experimental breakthrough curves. The D_{epore} is constant at 53,210 as shown on Figure (III-8) with standard deviation of 4,856.6 which shows less variation than the charcoal capacity data (see section III-2).

The value of k_{pore} is expected to be independent of F and v , therefore N_{pore} should be linearly proportional to v_e/F as shown on Figure (III-9) as the dotted line. However,

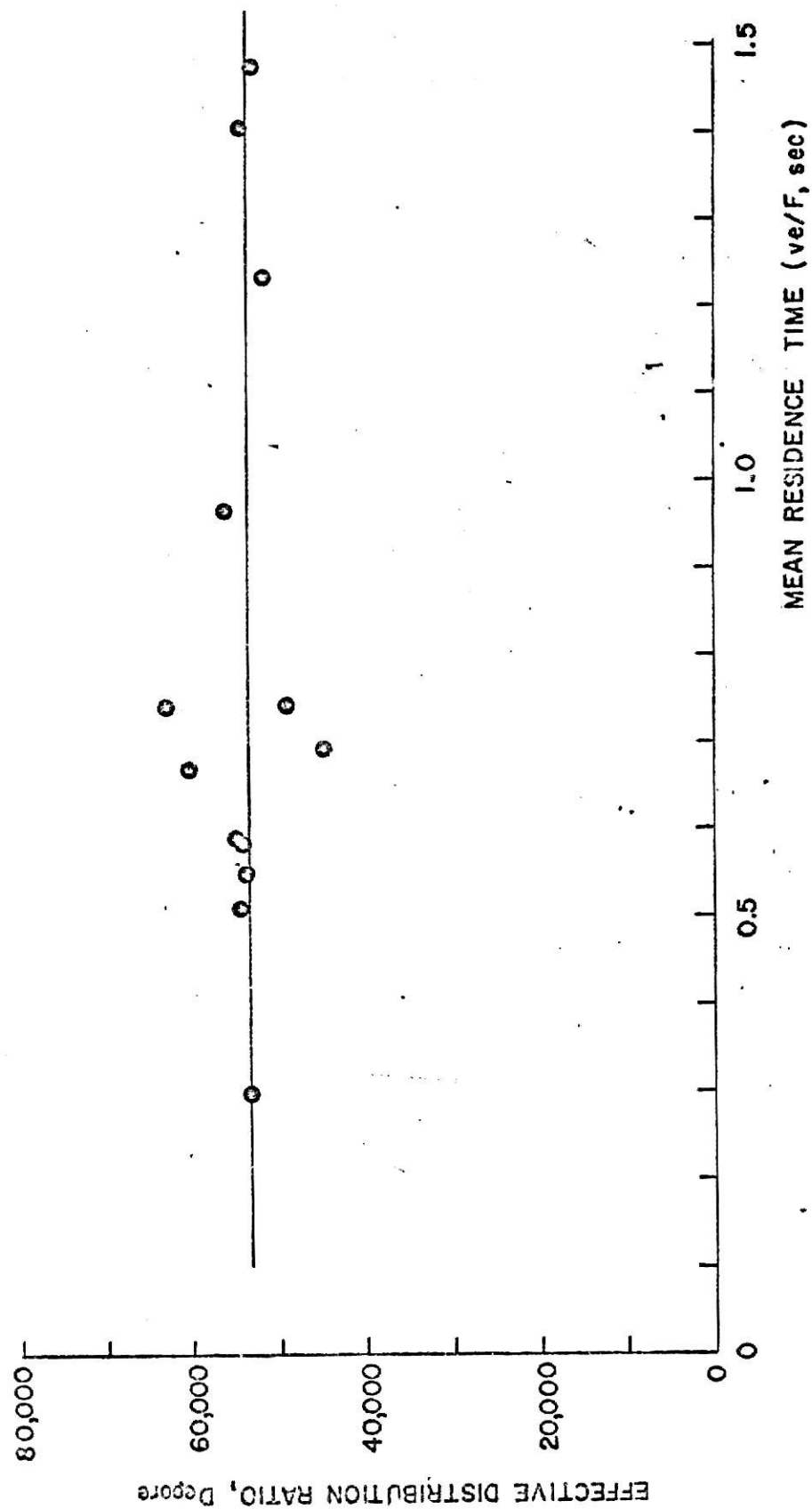


FIG.(III-8). RELATION BETWEEN MEAN RESIDENCE TIME AND EFFECTIVE
DISTRIBUTION RATIO FOR PORE DIFFUSION MODEL
AVERAGE VALUE OF $Depore = 53,210$

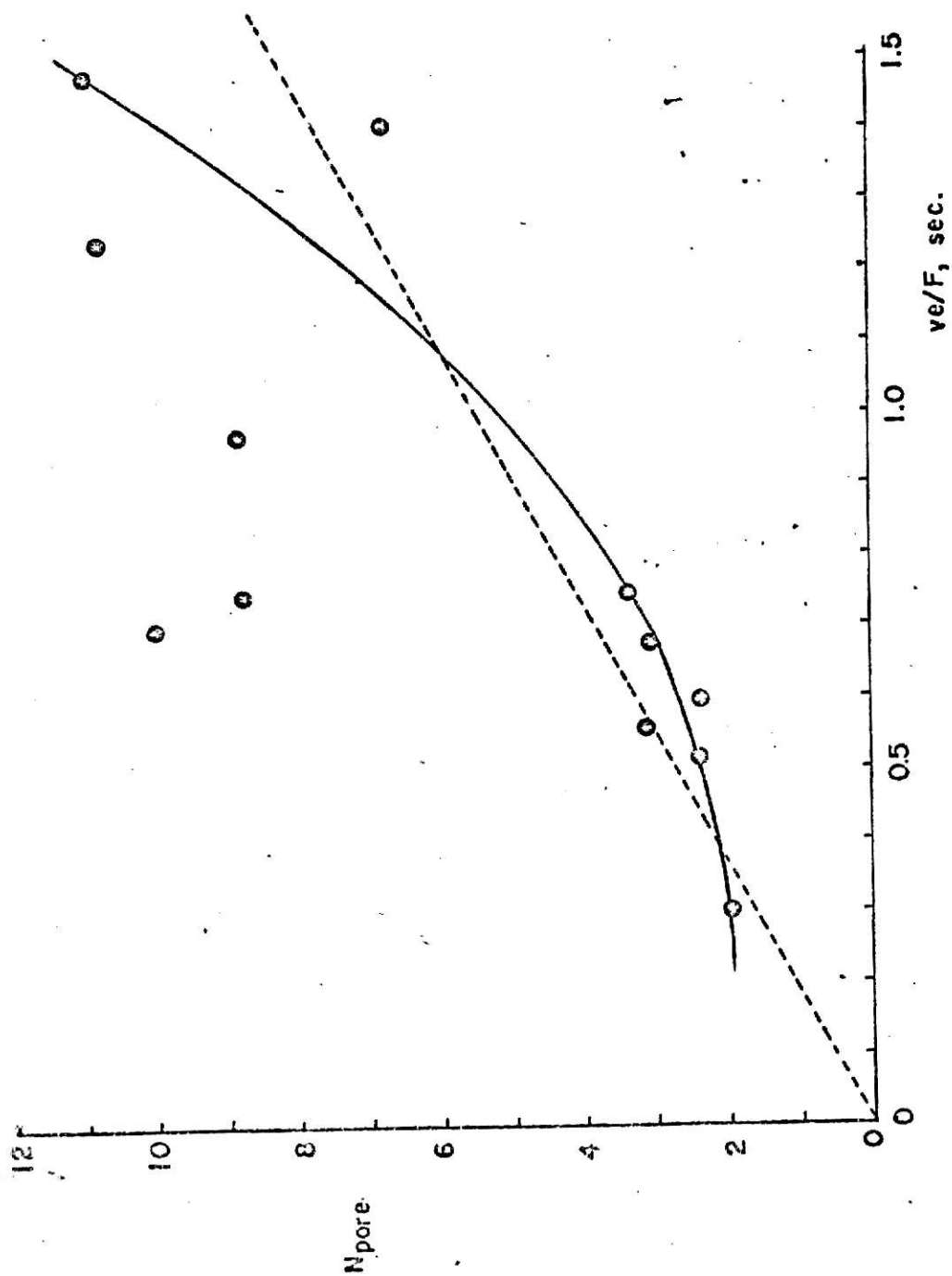


FIG. (III-9), NUMBER OF MASS TRANSFER UNITS VERSUS RESIDENCE TIME FOR PORE DIFFUSION MODEL

N_{pore} values obtained from this straight line did not fit the experimental breakthrough data as well as those obtained from the solid curve.

To determine whether the number of mass transfer units obtained from the modeling study were realistic or not, N_{pore} values were calculated from equation (III-4). This equation combined with equation (I-15) can be written as

$$N_{\text{pore}} = \frac{60(1 - e)}{d_p} \frac{D_{\text{pore}}}{D_f} \frac{1}{Pe} \text{-----(III-5)}$$

where Pe is Peclet number for flow: $Pe = d_p F / (D_f S)$

The D_{pore}/D_f value can be calculated using Wheeler's analytical solution, equation (I-13). With the values $D_f = 0.1 \text{ cm}^2/\text{sec}$, $T = 303.2 \text{ }^\circ\text{K}$, $x_p = 0.612$, $\bar{r}_p = 10 \text{ A}^\circ$, and $M = 29$, the ratio D_{pore}/D_f is 0.0322. From this value and the other known values, N_{pore} values were calculated and the results are shown in Table (III-6). As the results show, the N_{pore} values calculated in this way do not match exactly with those of modeling study, but they are fairly close and in the same range. Therefore it can be said that the N_{pore} values estimated by the model equation are reasonable.

The model equation containing the average D_{pore} value and the N_{pore} values obtained from the smooth curve of Figure (III-9) was used to back calculate the breakthrough curves and the break-times. The complete results are shown in Table (III-4) and Table (III-5) and comparisons of the model equations with the experimental breakthrough curves are shown

Table (III-4). Parameters obtained from Model Equation
for Pore Diffusion Model

Run No.	ve/F sec	Effective Dist- ribution Ratio Depore	Number of Mass Transfer Units N _{pore}
APC-14	0.677	60,746	3.081
APC-18	0.595	55,543	2.373
APC-19	0.592	54,146	2.384
APC-20	0.515	55,441	2.355
APC-21	0.303	53,650	1.985
APC-22	0.747	63,739	3.349
APC-26	0.556	54,009	3.188
APC-29	1.471	52,624	10.990
APC-30	0.966	56,130	8.827
APC-31	0.691	44,064	10.040
APC-32	0.745	48,199	8.768
APC-38	1.239	50,385	10.769
APC-39	1.401	54,321	6.782

Table (III-5). Calculated Break-time and Estimation Error based on the Smoothed Parameters for Pore Diffusion Model.

Run No.	Smoothed Model Parameters		Break- time		Error* %
	Depore	N _{pore}	Calculated sec	Experimental sec	
APC-14	53,210	3.00	23,306	23,400	- 0.40
APC-18	53,210	2.68	19,149	18,300	+ 4.64
APC-19	53,210	2.68	19,052	16,800	+ 8.25
APC-20	53,210	2.40	15,310	15,300	+ 0.07
APC-21	53,210	2.00	7,585	7,200	+ 5.35
APC-22	53,210	3.26	26,835	28,800	- 6.82
APC-26	53,210	2.55	17,298	18,000	- 3.90
APC-29	53,210	10.95	70,702	66,600	+ 6.16
APC-30	53,210	4.85	40,177	44,280	- 9.27
APC-31	53,210	3.04	23,959	22,500	+ 6.48
APC-32	53,210	3.25	26,723	28,080	- 4.83
APC-38	53,210	7.90	57,089	53,100	+ 7.51
APC-39	53,210	10.00	66,652	62,400	+ 6.81

$$* \text{ Error \%} = \frac{t_{x=0.05}(\text{Modeling}) - t_{x=0.05}(\text{Experimental})}{t_{x=0.05}(\text{Experimental})} \times 100$$

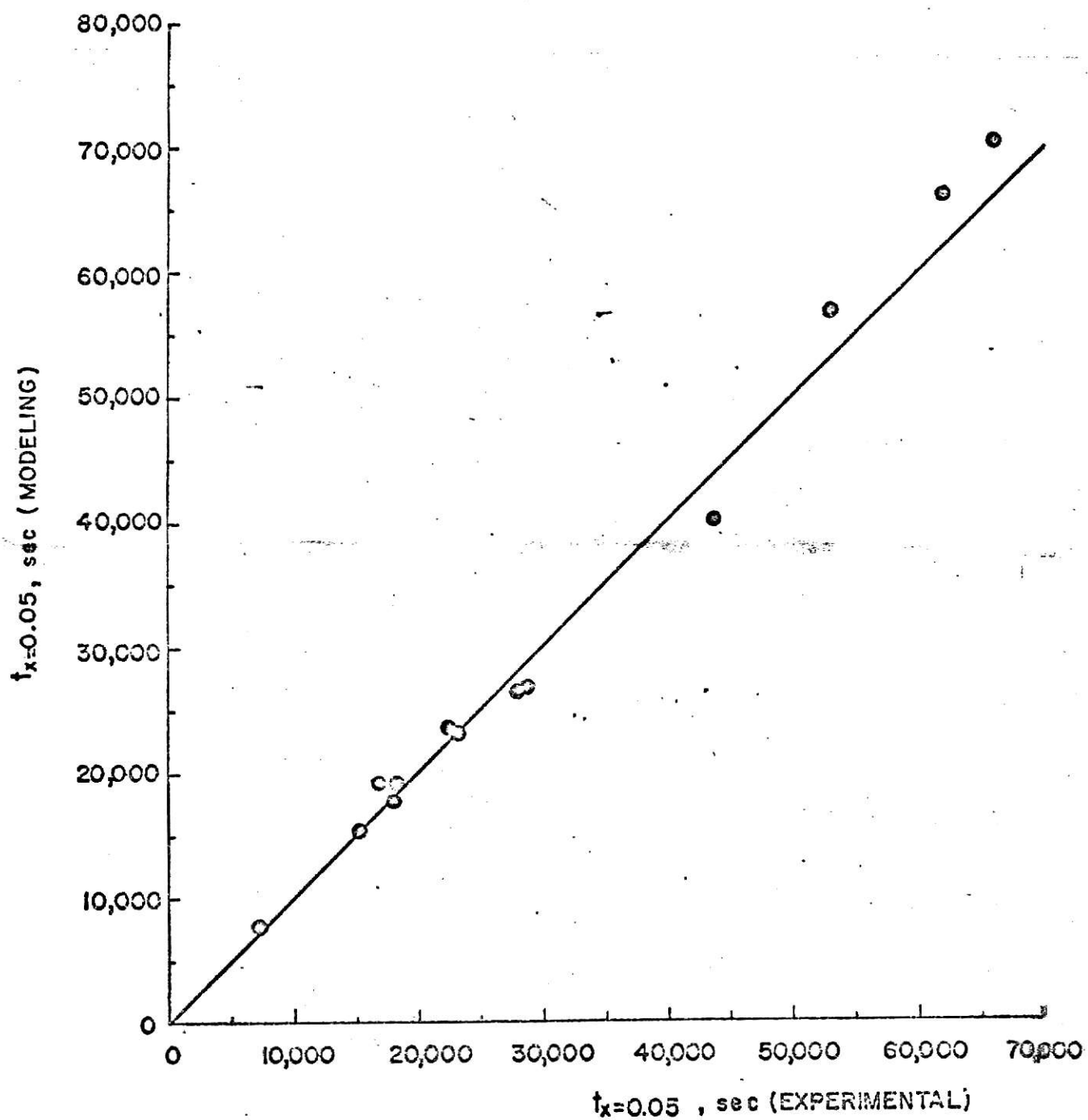


FIG.(III-10). COMPARISON OF PORE DIFFUSION MODELING
BREAK-TIME WITH EXPERIMENTAL VALUES

on Figures (A-1) to (A-13) in appendix. The sample calculation of break-time is also shown in appendix (A-4). As shown in Table (III-5), the break-times can be estimated within $\pm 10\%$ accuracy and the model breakthrough curves fit the experimental data fairly well in the range of 20 to 60 % of effluent concentration. In Figure (III-10), the calculated break-times are compared with the experimental values.

Table (III-6). Comparison of Calculated N_{pore} Values with Modeling Values.

Run No.	e	d_p mm	Pe	Calculated N_{pore}	Modeling N_{pore}
APC-14	0.649	1.41	11.61	3.59	3.00
APC-18	0.649	1.41	16.54	2.95	2.68
APC-19	0.649	1.41	22.63	2.94	2.68
APC-20	0.649	1.41	22.63	2.41	2.40
APC-21	0.649	1.41	22.63	1.61	2.00
APC-22	0.649	1.41	16.54	3.66	3.26
APC-26	0.525	1.41	54.54	2.42	2.55
APC-29	0.520	1.41	22.63	13.29	10.95
APC-30	0.520	1.41	34.47	8.73	4.85
APC-31	0.520	1.41	48.20	6.24	3.04
APC-32	0.520	1.41	41.36	7.27	3.25
APC-38	0.465	2.00	32.80	7.20	7.90
APC-39	0.474	1.68	27.55	10.04	10.00

(c) External Diffusion Model.

The external diffusion equation for favorable equilibrium with a constant separation factor is

$$\frac{1}{1-R} \ln X - \frac{R}{1-R} \ln(1-X) = N_f(Z-1) + \alpha_f \quad \text{------(I-69)}$$

For this system, R is 0.28 and α_f is - 1.13 (see Figure (A-16) in appendix). The equation then becomes

$$1.389 \ln X - 0.389 \ln(1-X) + 1.13 = N_f \left(\frac{t}{D_{ef} v e/F} - 1 \right) \quad \text{------(III-5)}$$

where

$$N_f = \frac{k_f a_p v}{F} \quad \text{------(III-6)}$$

The number of mass transfer units, N_f , and the effective distribution ratio, D_{ef} , were determined in the same way as for the previous model equations. The D_{ef} value was found to be constant at 47,607 with standard deviation of 4,279.5 and is shown on Figure (III-11). Values of N_f are plotted against ve/F on Figure (III-12). Then from the model equation using these smoothed values, the break-times were calculated and the model breakthrough curves constructed. These results are shown in Tables (III-7) and (III-8), and Figures (A-1) through (A-13) in appendix. And the comparison of calculated and experimentally obtained break-time data are shown on Figure (III-13). As the

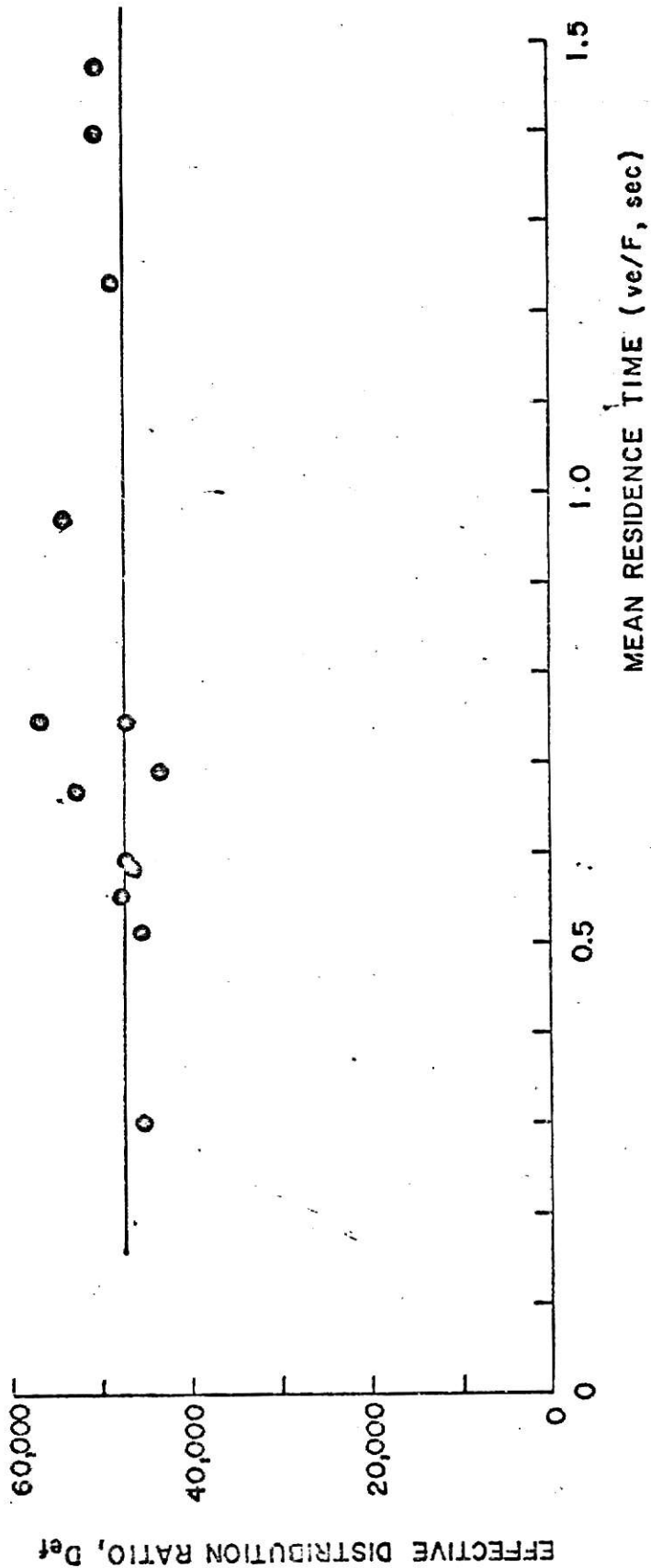


FIG. (III-III). RELATIONSHIP BETWEEN MEAN RESIDENCE TIME AND EFFECTIVE DISTRIBUTION RATIO FOR EXTERNAL DIFFUSION MODEL
AVERAGE VALUE OF $D_{eff} = 47,607$

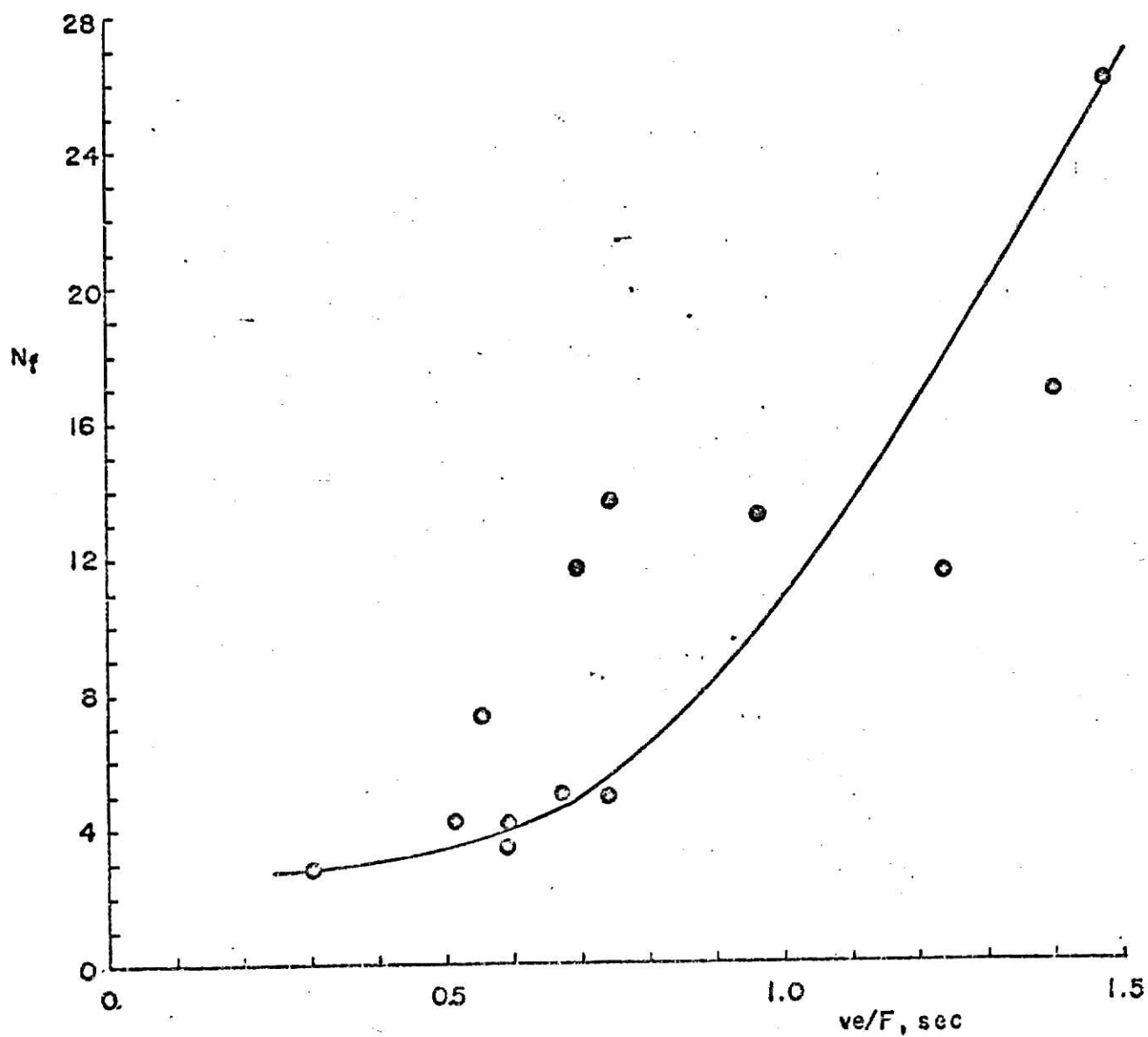


FIG.(III-12). NUMBER OF MASS TRANSFER UNITS VERSUS MEAN RESIDENCE TIME FOR EXTERNAL DIFFUSION MODEL

Table (III-7). Parameters obtained from External Diffusion Model Equation.

Run No.	ve/F sec	Effective Dist- ribution Ratio D_{ef}	Number of Mass Transfer Units N_f
APC-14	0.677	53,000	5.026
APC-18	0.595	47,457	4.164
APC-19	0.592	46,644	3.363
APC-20	0.515	45,252	4.081
APC-21	0.303	44,281	2.685
APC-22	0.747	57,431	4.807
APC-26	0.556	47,915	7.466
APC-29	1.471	50,954	26.261
APC-30	0.966	54,125	13.320
APC-31	0.691	42,703	11.806
APC-32	0.745	46,454	13.846
APC-38	1.239	48,960	11.331
APC-39	1.401	51,341	16.796

Table (III-8). Calculated Break-time and Estimation Error based on the Smoothed Parameters for External Diffusion Model.

Run No.	Smoothed Model Parameters		Break-time		Error* %
	Def	N _f	Calculated sec	Experimental sec	
APC-14	47,607	4.6	24,080	23,400	+ 2.91
APC-18	47,607	3.9	19,877	18,300	+ 8.61
APC-19	47,607	3.9	19,775	16,800	+ 11.79
APC-20	47,607	3.4	16,130	15,300	+ 5.43
APC-21	47,607	2.6	7,971	7,200	+ 13.48
APC-22	47,607	5.6	28,175	28,800	- 2.17
APC-26	47,607	3.7	18,148	18,000	+ 0.82
APC-29	47,607	26.0	66,897	66,600	+ 0.45
APC-30	47,607	9.9	40,585	44,280	- 8.34
APC-31	47,607	4.9	25,087	22,500	+ 11.50
APC-32	47,607	5.6	28,098	28,080	+ 0.06
APC-38	47,607	18.0	55,173	53,100	+ 3.90
APC-39	47,607	23.3	63,368	62,400	+ 1.55

$$* \text{ Error \%} = \frac{t_{x=0.05}(\text{Modeling}) - t_{x=0.05}(\text{Experimental})}{t_{x=0.05}(\text{Experimental})} \times 100$$

results show, the break-time can be calculated within $\pm 10\%$ accuracy and the breakthrough curves fit the experimental data fairly well in the range of 20 to 60 % of effluent concentration.

As was done for the pore diffusion model, the reality of the N_f values were tested by using equation (III-6) combined with equation (I-17). The resulting equation is

$$N_f = \frac{10.9(1 - e)H}{d_p} \left(\frac{D_f \rho_f}{\mu} \right)^{0.16} \left(\frac{1}{Pe} \right)^{0.51} \text{ ----(III-7)}$$

here H is the height of the fixed-bed. The N_f values calculated by this equation are shown in Table (III-9) compared with the modeling values. The agreement is not good, but since they are in the same range, the modeling N_f values can be called reasonable.

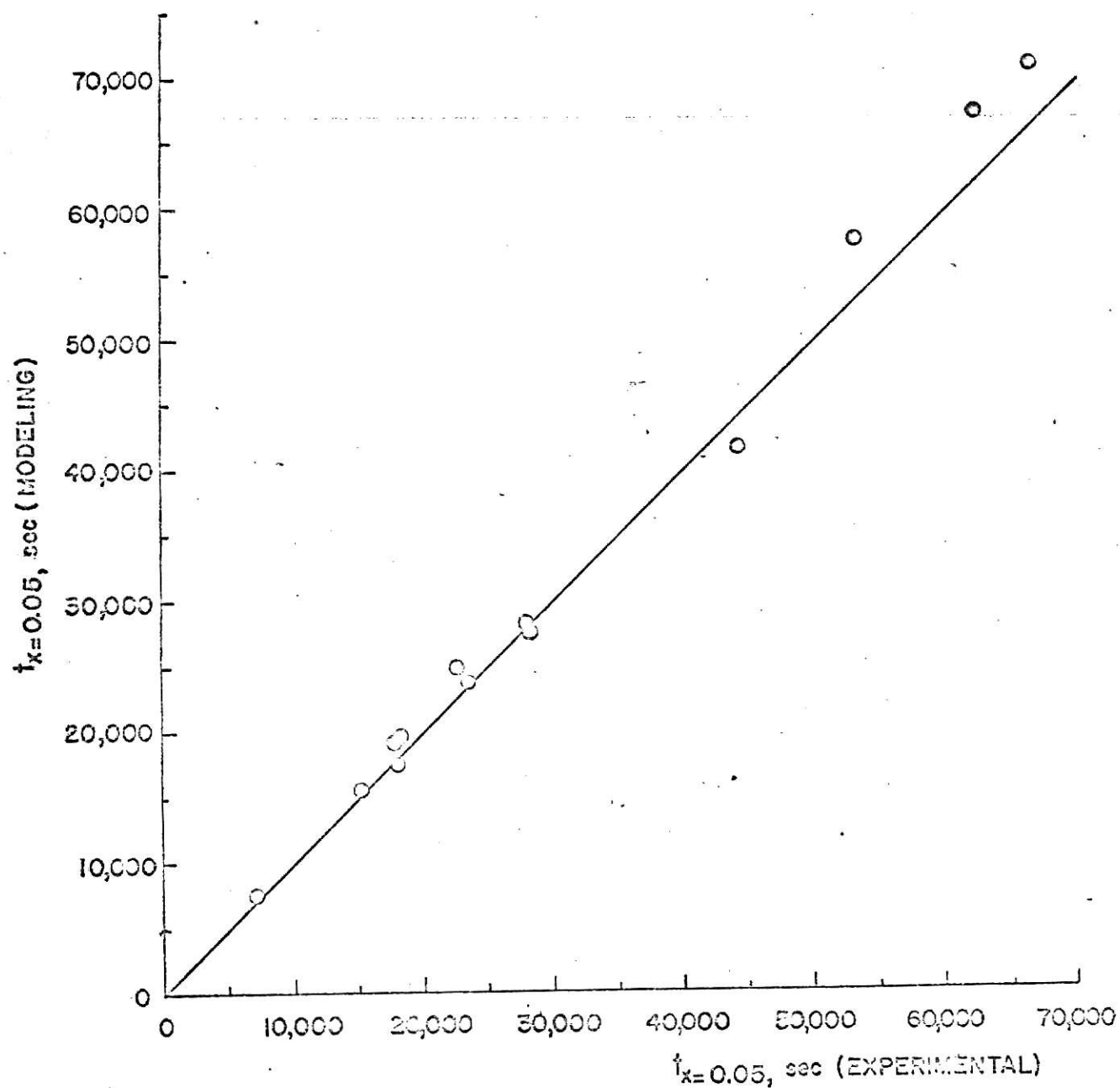


FIG.(III-13). COMPARISON OF EXTERNAL DIFFUSION MODELING BREAK-TIMES WITH EXPERIMENTAL VALUES

Table (III-9). Results of Calculated N_f values compared with the Modeling N_f .

Run No.	H cm	e	d_p mm	P_e	Calculated N_f	Modeling N_f
APC-14	8.66	0.649	1.41	11.61	6.35	4.6
APC-18	10.16	0.649	1.41	16.54	6.22	3.9
APC-19	13.82	0.649	1.41	22.63	7.22	3.9
APC-20	11.33	0.649	1.41	22.63	5.92	3.4
APC-21	7.56	0.649	1.41	22.63	3.95	2.6
APC-22	12.59	0.649	1.41	16.54	7.71	5.6
APC-26	20.32	0.525	1.41	54.54	9.17	3.7
APC-29	45.72	0.520	1.41	22.63	32.65	26
APC-30	45.72	0.520	1.41	34.47	26.34	9.9
APC-31	45.72	0.520	1.41	48.20	22.20	4.9
APC-32	45.72	0.520	1.41	41.36	24.00	5.6
APC-38	45.72	0.465	2.00	32.80	21.22	18
APC-39	45.72	0.474	1.68	27.55	27.15	23.3

(d) Reaction Kinetics Model.

As stated in chapter I, the reaction kinetics model equation for favorable equilibrium and a constant separation factor can be expressed as

$$X = \frac{1}{1 + e^{-u}} \text{------(I-73)}$$

with

$$u = (1 - R) N_R (Z - 1)$$

Where

$$Z = \frac{t}{D_{er} v e / F}$$

$$N_R = \frac{k_F v}{F} \text{------(III-8)}$$

Again R is 0.28. The D_{er} and N_R values were determined in the same way as stated before. D_{er} is constant at 51,520 with standard deviation of 4,405 as shown on Figure (III-14) and N_R values are plotted versus ve/F on Figure (III-15).

With these smoothed parameters, the breakthrough equation was determined and the break-times for various tests calculated as shown in Table (III-10) and Table (III-11). The model breakthrough curves are shown on Figures (A-1) to (A-13) in appendix, and the sample calculation of break-time is shown in appendix (A-4). This model equation reproduces the break-times within $\pm 10\%$ accuracy and fits the breakthrough curves in the 20 to 60 % of the effluent concentration range. In Figure (III-16), the comparison between calculated and experimental break-time data is displayed.

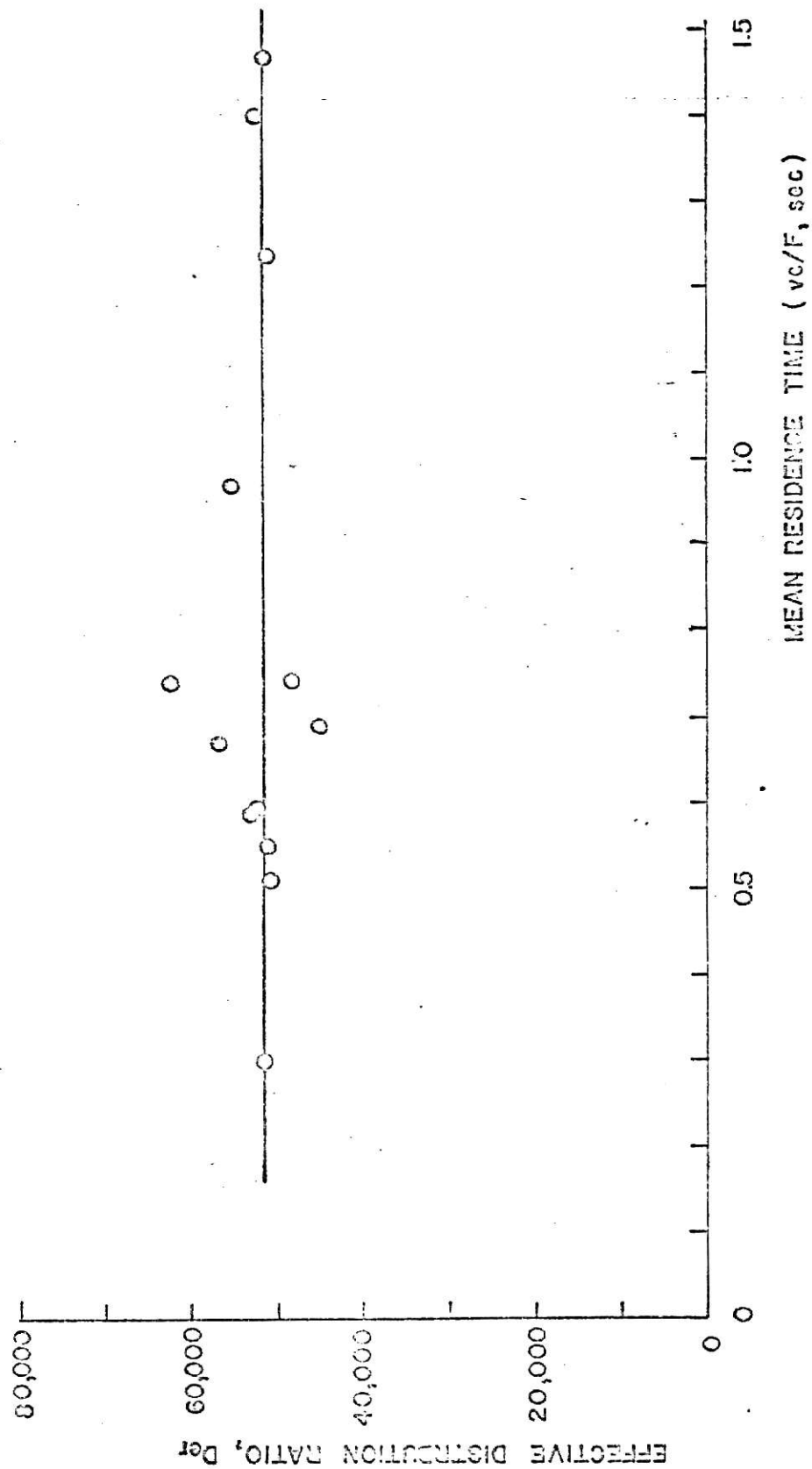


FIG.(III-14). RELATION BETWEEN MEAN RESIDENCE TIME AND EFFECTIVE
DISTRIBUTION RATIO FOR REACTION KINETICS MODEL
AVERAGE VALUE OF $D_{cr} = 51,520$

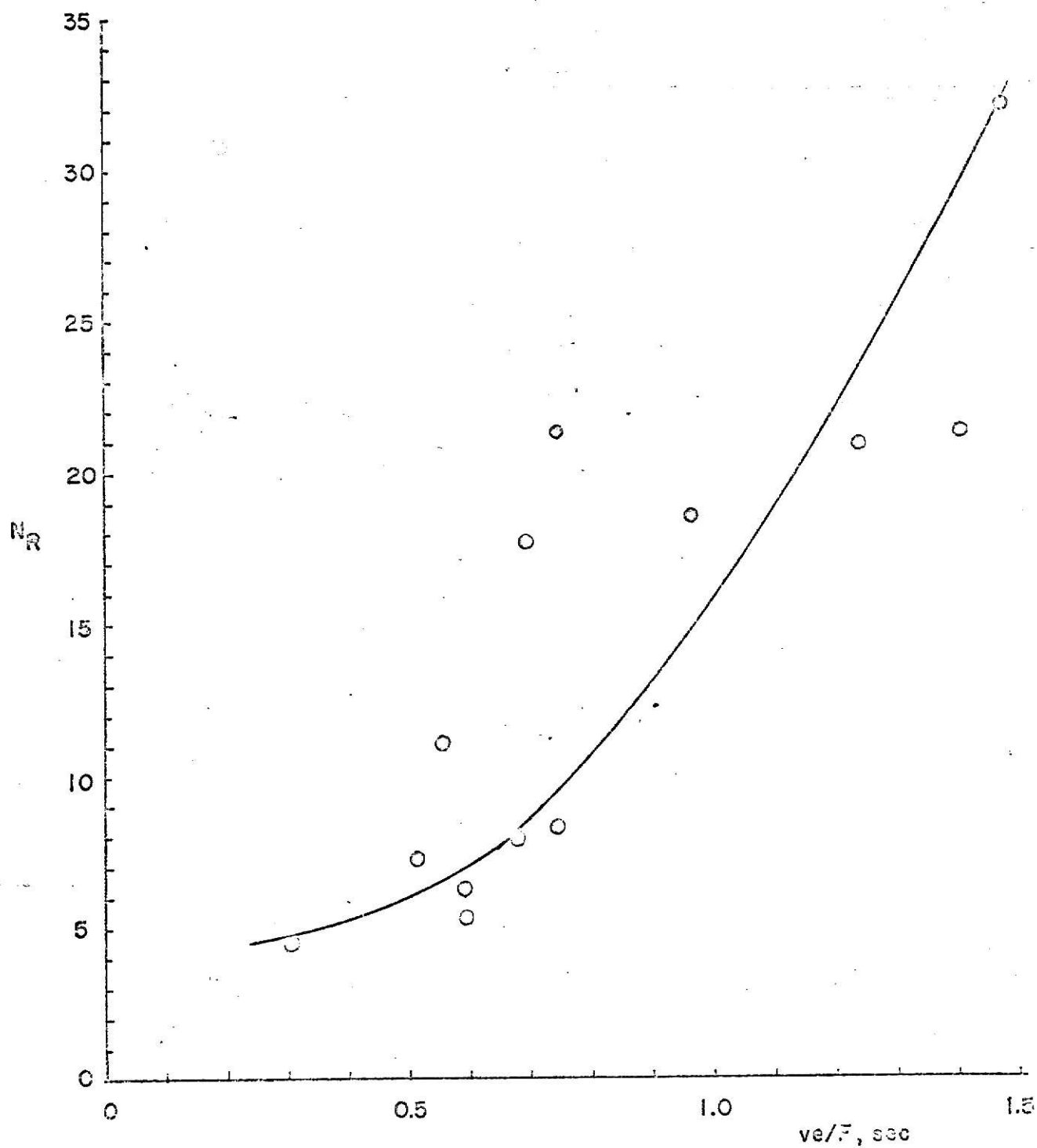


FIG.(III-15). NUMBER OF MASS TRANSFER UNITS VERSUS RESIDENCE TIME FOR REACTION KINETICS MODEL

Table (III-10). Parameters obtained from Reaction Kinetics Model Equation.

Run No.	v_e/F sec	Effective Dist- ribution Ratio D_{er}	Number of Mass Transfer Units N_R
APC-14	0.677	57,607	7.85
APC-18	0.595	52,437	6.28
APC-19	0.592	52,703	5.35
APC-20	0.515	50,097	7.35
APC-21	0.303	51,485	4.59
APC-22	0.747	62,651	8.33
APC-26	0.556	50,719	11.11
APC-29	1.471	51,801	32.07
APC-30	0.966	55,901	18.52
APC-31	0.691	44,284	17.71
APC-32	0.745	47,919	21.33
APC-38	1.239	50,847	20.83
APC-39	1.401	52,677	21.35

Table (III-11). Calculated Break-time and Estimation Error based on the Smoothed Parameters for Reaction Kinetics Model.

Run No.	Smoothed Model Parameters		Break-time		Error* %
	Der	N _R	Calculated sec	Experimental sec	
APC-14	51,520	8.1	24,115	23,400	+ 3.06
APC-18	51,520	7.0	19,708	18,300	+ 7.69
APC-19	51,520	7.0	19,586	16,800	+ 11.28
APC-20	51,520	6.2	15,749	15,300	+ 2.93
APC-21	51,520	4.8	7,480	7,200	+ 3.89
APC-22	51,520	9.4	28,247	28,800	- 1.92
APC-26	51,520	6.6	17,796	18,000	- 1.13
APC-29	51,520	32.0	69,868	66,600	+ 4.92
APC-30	51,520	14.8	41,360	44,280	- 6.59
APC-31	51,520	8.4	25,006	22,500	+ 11.14
APC-32	51,520	9.4	28,176	28,080	+ 0.34
APC-38	51,520	23.6	57,070	53,100	+ 7.48
APC-39	51,520	29.2	65,998	62,400	+ 5.77

*

$$\text{Error \%} = \frac{t_{x=0.05}(\text{Modeling}) - t_{x=0.05}(\text{Experimental})}{t_{x=0.05}(\text{Experimental})} \times 100$$

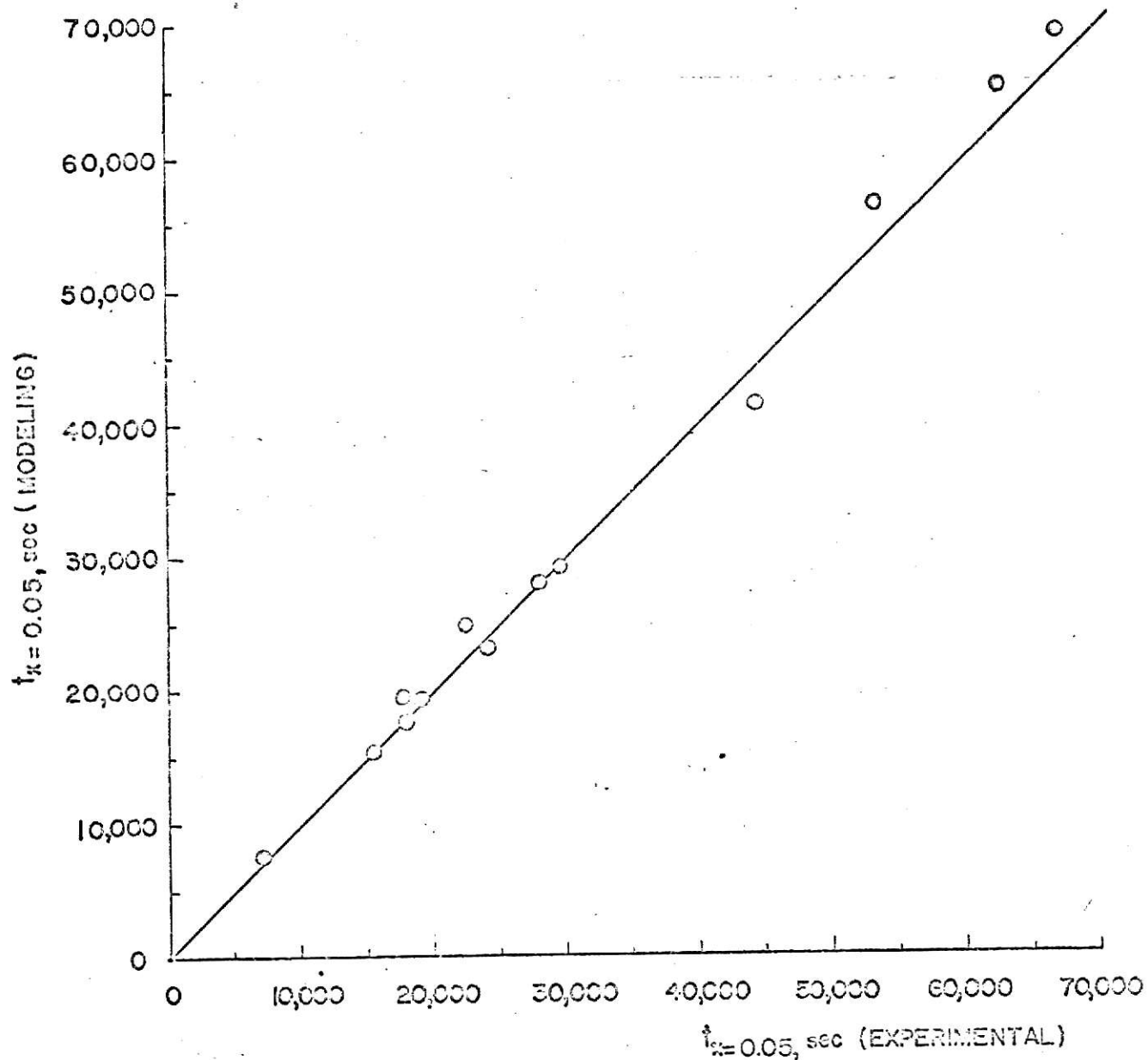


FIG. (III-13). COMPARISON OF REACTION KINETICS MODEL BREAK-TIME DATA WITH EXPERIMENTAL VALUES

All four models fit the breakthrough curve in the range of 20 to 60 % of influent concentration, but the solid diffusion model is the best choice to fit from 0 to 60 % of influent concentration. Because of the unfitness of the model equations in the range of 0 to 20 % of the breakthrough curve, the break-times were calculated by extending the mid-point gradient to the 5 % influent concentration point. By this way, the break-times were predicted equally well by all four models.

The number of mass transfer units for pore diffusion and external diffusion model appeared to be reasonable. For the other two models, it was not possible to test, because the diffusivities can not be estimated. The effective distribution ratio is not in the range expected, but it is constant.

To construct a completely matched breakthrough curve with a model equation, probably more complicated combined diffusion mechanisms should be applied or, as Hiester et al. (19) have stated, local values of the number of mass transfer units should be estimated at each concentration. But to avoid this complexity, it is reasonable to accept the model equations as they are. The breakthrough behavior of these models are shown on Figure (III-17) as a function of $N(Z - 1)$ to show the general shapes of the model breakthrough curves.

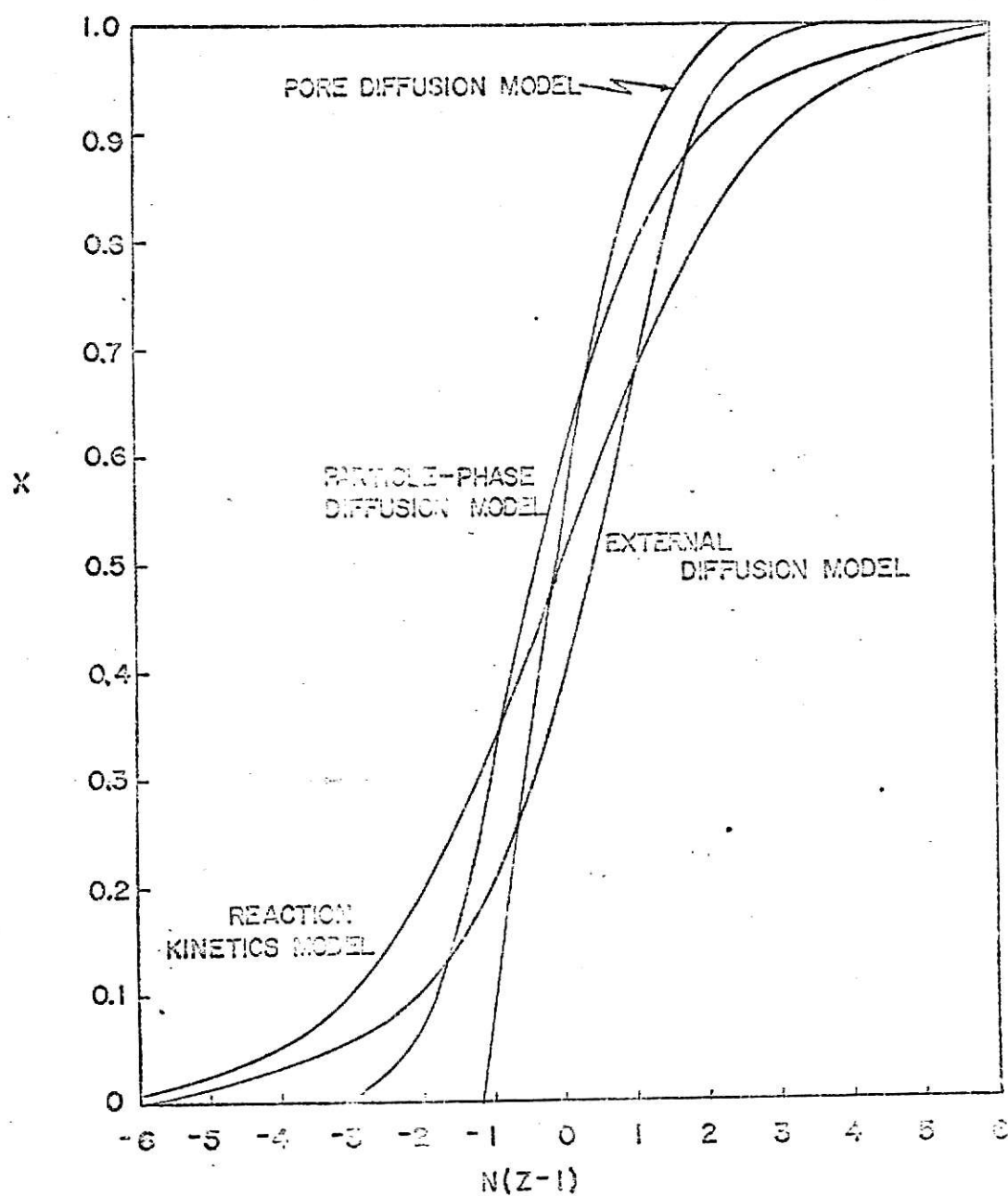


FIG.(III-17). BREAKTHROUGH BEHAVIOR FOR FAVORABLE EQUILIBRIUM WITH CONSTANT SEPARATION FACTOR

III-3. Charcoal Capacity.

(a) Capacity from experimental breakthrough curve.

It is generally accepted that the capacity of a fixed-bed fed with a given influent concentration can be calculated from the breakthrough curve (see appendix A-3). When the effluent concentration reaches the influent concentration, it is considered that the adsorbent is in equilibrium with the influent stream and thus the bed is saturated. This capacity is also expected to be a point on the adsorption isotherm. No simplifying assumptions regarding the rate controlling steps or flow patterns are necessary to obtain this equilibrium data.

The results of the fixed-bed tests made with Pittsburgh PCB charcoal and acetaldehyde are summarized in Tables (III-12) and (III-13). The breakthrough curves obtained experimentally are shown on Figures (A-1) through (A-13) in appendix. All tests were made at 30 °C using an influent concentration of 28 ppm of acetaldehyde in air by volume. As Table (III-12) shows, three different sizes of charcoal were used although only one test each was performed for 10 and 12 mesh charcoal. The average capacity for 14 mesh charcoal is 0.00793 gm of acetaldehyde per gm of charcoal with the standard deviation of 0.000964 and this capacity seems to decrease with the increasing size of charcoal (0.0061 gm/(gm charcoal) for 12 mesh and 0.0058 gm/(gm charcoal) for 10 mesh), even though the difference may not be statistically significant.

Table (III-12). Charcoal Capacities upon Different Conditions with Acetaldehyde Adsorbed on Pittsburgh PCB Charcoal.

Run No.	Bed Dia. mm	Bed Height cm	Bed Weight gm	Bed Volume cm ³	Charcoal Size mesh*	Flow Rate cc/sec.	Superficial Velocity cm/sec.	Charcoal Capacity gm/gm
APC-14	16	8.66	5.2	17.412	14	16.67	8.4	0.00812
APC-18	16	10.16	6.1	20.428	14	23.75	12	0.00858
APC-19	16	13.82	8.3	27.787	14	32.5	16.4	0.00751
APC-20	16	11.33	6.8	22.780	14	32.5	16.4	0.00884
APC-21	16	7.56	4.54	15.200	14	32.5	16.4	0.00759
APC-22	16	12.59	7.56	25.314	14	23.75	12	0.00872
APC-26	16	20.32	16.5	40.856	14	78.33	39.5	0.00977
APC-29	16	45.72	37.5	91.925	14	32.5	16.4	0.00722
APC-30	16	45.72	37.5	91.925	14	49.5	25.0	0.00740
APC-31	16	45.72	37.5	91.925	14	69.22	35.0	0.00650
APC-32	16	45.72	37.5	91.925	14	59.4	30.0	0.00700
APC-38	25	45.72	102	224.427	10	79.35	16.4	0.00580
APC-39	19	45.72	58	129.629	12	45.83	16.4	0.00610

* U.S. standard.

Table (III-13). Data obtained and calculated from the Experimental Breakthrough Curves.

Run No.	Break-time $t_x=0.05$, sec.	Mid-point Time $t_x=0.5$, sec.	Exhaustion Time $t_x=0.95$, sec.	Mid-point Slope $(dx/dt)_x=0.5 \times 10^5$	Mean Residence Time v_e/F sec.
APC-14	23,400	39,000	150,000	3.623	0.677
APC-18	18,300	31,200	120,000	3.623	0.595
APC-19	16,800	31,200	93,000	3.086	0.592
APC-20	15,300	25,800	114,000	5.128	0.515
APC-21	7,200	15,600	63,000	5.291	0.303
APC-22	28,800	46,800	150,000	3.203	0.747
APC-26	18,000	28,200	120,000	7.092	0.556
APC-29	66,600	76,200	669,000	7.576	1.471
APC-30	44,280	54,000	510,000	6.173	0.966
APC-31	22,500	30,600	294,000	10.418	0.691
APC-32	28,080	35,700	420,000	10.753	0.745
APC-38	53,100	63,000	312,000	5.952	1.239
APC-39	62,400	73,800	297,600	5.208	1.401

(b) Capacity from equilibrium tests.

Equilibrium data points have been obtained using the "Static Equilibrium Test Method" described in chapter II. The results of these tests with 3,000 cc flasks are shown in Table (III-14). The test 0 was a blank and was conducted without any charcoal in the flask to examine the concentration change in the flask. As the results of this test show, the concentration of acetaldehyde decreases with time. Since acetaldehyde is highly reactive and easily oxidized to acetic acid and reduced to ethanol (51), this phenomenon is presumed to be the air oxidation of acetaldehyde in the flask. In support of this, it should be recalled that an air oxidation hypothesis appeared reasonable in explaining the observed behavior of acetaldehyde in the diffusion tube.

When all of the static equilibrium data were plotted as an isotherm, there was no apparent trend. Therefore a detailed error analysis was made (see appendix A-5) so that the reasonable data should be chosen out of these results. The result of this error analysis shows all of the scatter is not due to random errors.

When tests 1 through 4 are examined, the concentrations after 20 days and 25 days are almost constant and after 20 days, the concentration of test 0 shows a value reasonably close to the original concentration (59 ppm to 61 ppm), therefore it is reasonable to take data after 20 days to plot the isotherm curve. The data after 25 days or longer time period may not be as

Table (III-14). Results of Static Equilibrium Tests.

Test No.	Initial Conc. ppm	Charcoal Weight gm	After 9 days ppm cap.	After 20 days ppm cap.	After 25 days ppm cap.	After 31 days ppm cap.	After 45 days ppm cap.	After 54 days ppm cap.
0	61	0	60.5	59	58			
1	64	0.0296	24.5	24	24.5			
2	61	0.0368	21.5	20	19.5			
3	63	0.0338	22.5	21.5	21.5			
4	58	0.0388	17.5	15.5	16			
5	61	0.0159	0.00555	35	0.00582		21	
6	61	0.0206		28.5	0.00839		15	
7	63	0.0753		5.5	0.00406		3	
8	63	0.1291		3	0.00247		2	

Table (III-14). Continued

Test No.	Initial Conc. ppm	Charcoal Weight gm	After 9 days		After 20 days		After 25 days		After 31 days		After 45 days		After 54 days	
			ppm	cap.	ppm	cap.	ppm	cap.	ppm	cap.	ppm	cap.	ppm	cap.
9	65	0.2703			1.5						1			
10	53	0.0239							24				20	
11	53	0.0365								0.00645				0.0072
12	54	0.0168							20				16	
13	54	0.0122								0.00481				0.0053
14	54	0.0092							25.5				22	
										0.00902				0.0102
									26.3				24.5	
										0.01207				0.0130
									29.5				29	
										0.01416				0.0140

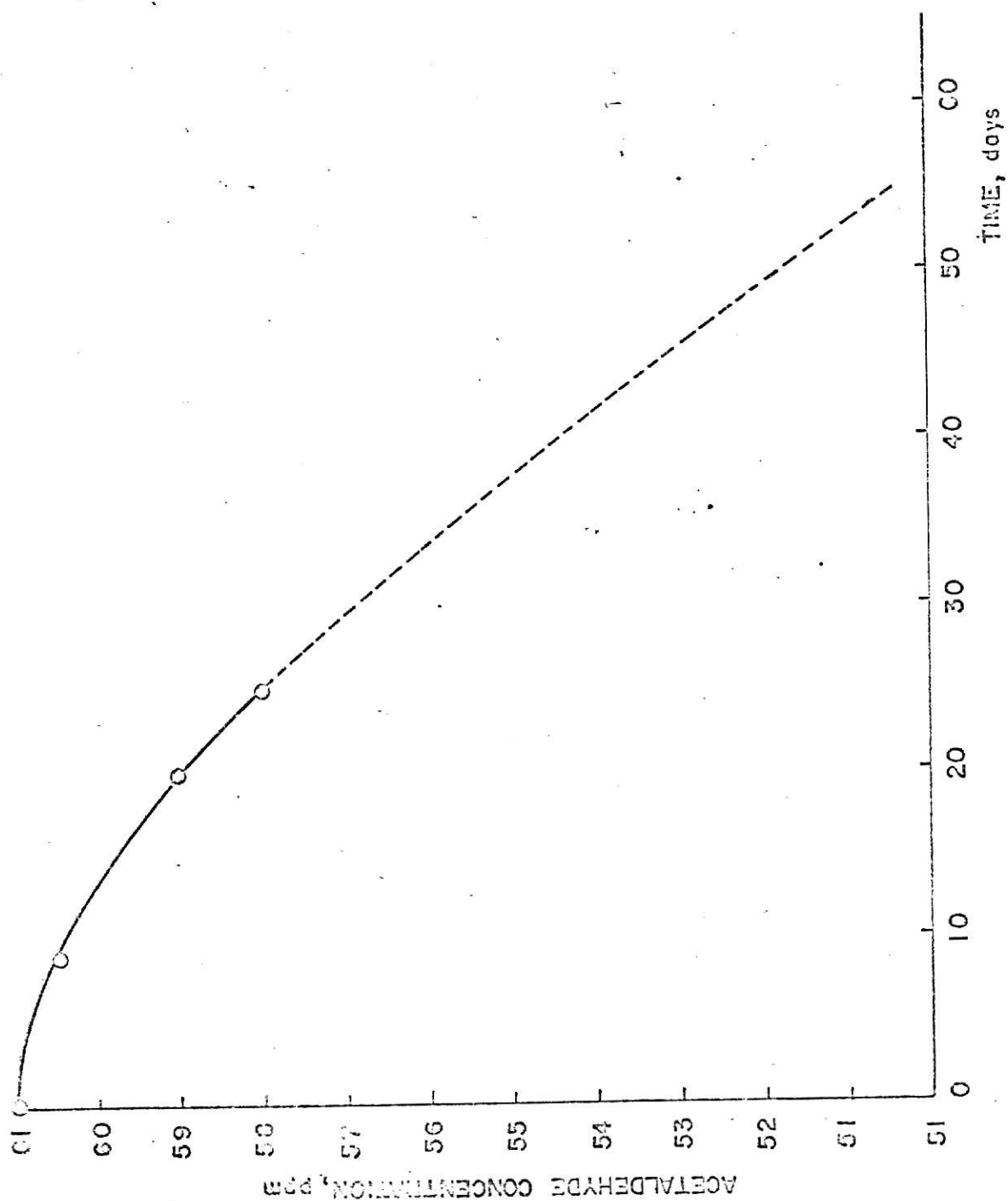


FIG.(III-13). CONCENTRATION CHANGE OF ACETALDEHYDE IN AIR WITH TIME

reliable, because the concentration decrease by chemical reaction becomes larger as it appears from Figure (III-18), that the rate of reaction increases with time. Therefore, the tests of 20 days duration (test 1 to 9) were selected to plot a isotherm curve in the range of 0 to 40 ppm of acetaldehyde in air. This plot is shown on Figure (III-19).

The capacity of charcoal from this plot is 0.00775 gm per gm charcoal at 28 ppm of acetaldehyde concentration. This value is slightly lower than the average capacity found for the fixed-bed tests (0.00793 gm/(gm charcoal)), but is well within one standard deviation. Since this discrepancy is so small and without statistical significance, this value can be accepted properly as the static equilibrium capacity.

Attempts were made to fit the isotherm data to the Langmuir equation. The Langmuir isotherm equation (I-4) can be written as

$$\frac{C}{q} = \frac{C}{q_m} + \frac{1}{q_m K_L} \text{-----(III-9)}$$

Where q is the solid-phase adsorbate concentration, q_m is the maximum solid-phase adsorbate concentration, C is the fluid-phase adsorbate concentration, and K_L is the Langmuir equation constant. Examination of equation (III-9) indicates that a plot of C/q versus C should be a straight line to fit the isotherm data to the Langmuir isotherm equation. Such a plot is

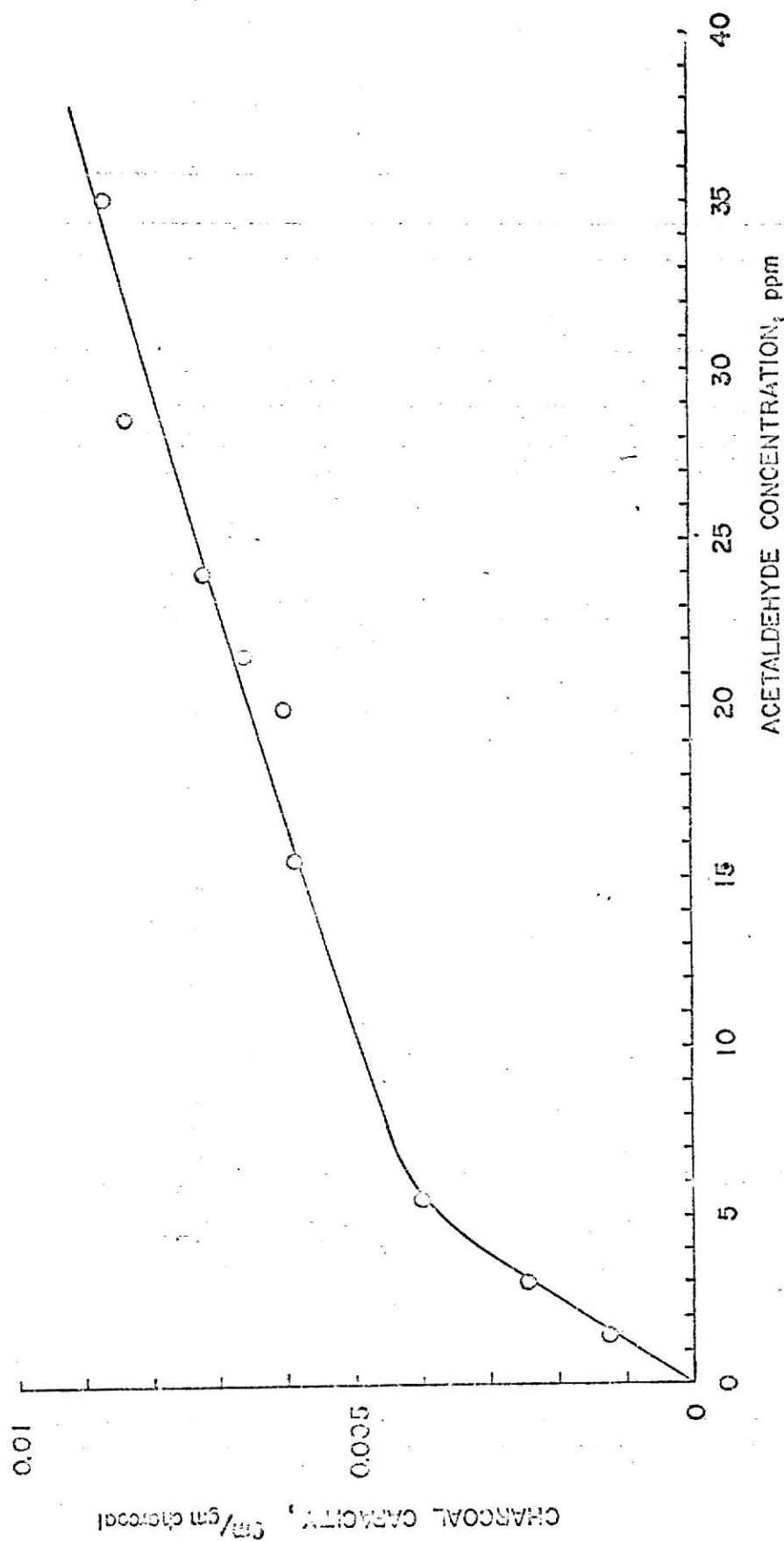


FIG.(III-19). STATIC EQUILIBRIUM DATA FOR ACETALDEHYDE ON
PITTSBURGH PCB CHARCOAL/L AT 30 °C

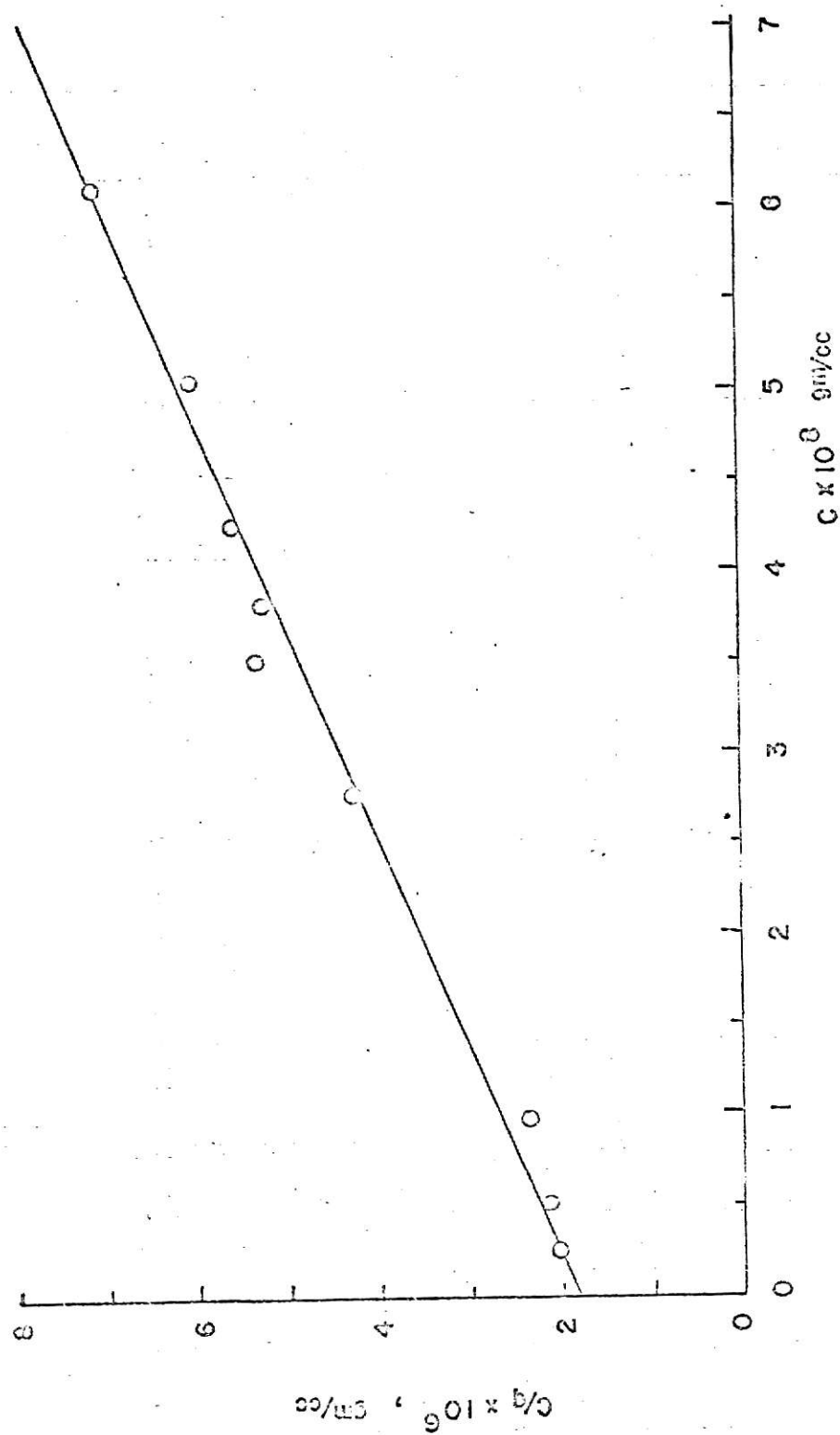


FIG.(III-20). EQUILIBRIUM DATA FOR ACETALDEHYDE ON PITTSBURGH
PCB CHARCOAL IN LINEAR FORM

shown on Figure (III-20) where it is seen that these data fit the Langmuir equation fairly well. From this plot, K_L can be calculated from the slope, $1/q_m$, and the interception $1/(q_m K_L)$. With the known values of K_L and C_o , the separation factor R , can be calculated from the equation

$$R = \frac{1}{1 + K_L C_o} \text{ ----- (III-10)}$$

For this system, R is found to be 0.28. This R value is between 0 to 1, therefore the isotherm is favorable. This R value was used in the modeling equations.

(c) Capacity from Modeling Study.

Since the model equations predict only the lower half of the experimental breakthrough data, the capacities calculated from these model equations are much lower than the actual capacity. The capacities based on the modeling breakthrough curves are only 20 to 30 % of the actual capacity. Therefore, the modeling equations are useful only for predicting break-time and lower half of the breakthrough curve.

CHAPTER IV

CONCLUSIONS AND APPLICATIONS TO DESIGN

The dependence of breakthrough curve behavior upon bed length, superficial velocity, and charcoal particle size was examined. It was found that the lower half of the breakthrough curves do not strongly depend on these variables. Thus the constant pattern limit was applied for the modeling study. Four model equations (solid diffusion, pore diffusion, external diffusion, and reaction kinetics model) containing two parameters (the number of mass transfer units and the distribution ratio) were fitted to breakthrough curves. Parameters from these model equations were plotted versus ve/F . Smoothed parameters were read from the curves and used to back calculate the first half of the breakthrough curves and the break-times. The results showed that the calculated break-times were within $\pm 10\%$ of the experimental data and the breakthrough curves could be reproduced in the range of 20 to 60 % of the experimental breakthrough curves. Among the model equations, the particle-phase diffusion model fits the experimental breakthrough curve best (0 to 60 % of the effluent concentration) and the N_p values show less scatter than any other models.

Charcoal capacities were determined based on the experimental breakthrough curves and the experimentally determined equilibrium isotherm data. The equilibrium isotherm result of 0.00775 gm/(gm charcoal) deviates from the experimental breakthrough result of 0.00793 gm/(gm charcoal) by less than

one standard deviation.

Since the fixed-bed operating time should be considered up to the break-time for actual adsorption system design, an adsorption system can be designed from the break-time data. Thus, for design purposes, it is only necessary to predict the lower part of the breakthrough curve. However, in order to do this, it is necessary to have a model equation which represents the lower part of the breakthrough curve whose parameters can be determined from readily available data. Of the four models tested, only N_{pore} can be estimated reasonably well from the published data as shown in Table (III-6). Presently, the distribution ratio can not be estimated from pertinent data as is suggested by the defining equation.

As a ultimate goal of this work in the future, the estimation of the parameters for these models from the published data should be accomplished for the effective use of these model equations for design purposes.

NOMENCLATURE

- A : Cross sectional area of the diffusion tube, cm^2
 a : Amount of adsorbate accumulation on adsorbent, gm
 a_p : Outer-surface interfacial area of the adsorbent particles per unit volume of packed-bed, cm^2/cc
 a_s : Saturation amount of adsorbate accumulation on adsorbent, gm
 b_L, b_{L1}, b_{L2} : Langmuir equation constants
 B : Logarithmic mean of Y and $(1 - Y)$
 C : Concentration of adsorbate in the fluid phase, gm/cc
 C_e : Effluent concentration of adsorbate in the fluid phase, gm/cc
 C_o : Total concentration of adsorbate in fluid-phase, gm/cc
 D_m : Molecular diffusion coefficient of the vapour into the nitrogen gas, cm^2/sec
 D : Distribution ratio
 $D_{ep}, D_{epore}, D_{ef}, D_{er}$: Effective distribution ratio
 D_f, D_p, D_{pore} : Diffusivity
 d_p : Effective spherical diameter of granular adsorbent, cm
 e : External void fraction
 F : Volumetric flow rate, cc/sec
 g : Constant
 H : Bed height, cm
 k, k' : Constants
 k_p, k_{pore}, k_f : Mass transfer coefficient
 k_i : Rate coefficient of surface adsorption

K_L : Langmuir equation constant
 L : Length of diffusion path, cm
 M : Mean molecular weight of fluid
 n : Freundlich equation constant
 N_p, N_{pore}, N_f, N_R : Number of mass transfer units
 p, p_1, p_2 : Equilibrium partial pressure, atm.
 p_0 : Upper limit of fluid phase pressure, atm.
 P : Total pressure, atm.
 Pe : Peclet number for flow
 q : Concentration of adsorbate in the particle phase, gm/gm
 q_0 : Total concentration of adsorbate in solid phase, gm/gm
 q_m : Maximum concentration of adsorbate in solid phase, gm/gm
 R : Separation factor
 r, r_i : Internal particle radius, cm
 r_d : Rate of diffusion of vapour out of diffusion tube, gm/sec
 \bar{r}_p : Average pore radius, cm
 r_s : Particle radius up to outer-surface, cm
 R_g : Gas law constant, liter·atm/(mole·°K)
 S : Cross sectional area of fixed-bed, cm²
 T : Absolute temperature, °K
 t : time, sec
 V : volume of fluid entering bed, cc
 v : Volume of bed, cc
 $V - v_e$: Amount of fluid that has flowed through bed volume v
 v_a : Volume of adsorbate adsorbed at pressure p , cc

- v_{a1}, v_{a2} : The volume of gas 1 and gas 2 at equilibrium pressure p_1 and p_2 respectively, cc
- v_{m1}, v_{m2} : The volume of gas necessary to cover the entire surface with unimolecular adsorbed layer of gas 1 or 2, cc
- v_o : Volume adsorbed at the upper limit of fluid phase pressure p_o , cc
- W : The weight of fixed-bed, gm
- X : Dimensionless fluid-phase concentration
- X^* : Dimensionless fluid-phase concentration in equilibrium with the outer surface of the solid
- X_o : Initial dimensionless fluid-phase concentration
- x_p : Internal porosity of the particle
- X_r : Dimensionless fluid-phase concentration in the pore at any internal radius r
- Y : Dimensionless solid-phase concentration
- Y^* : Dimensionless concentration that is in equilibrium with the instantaneous fluid-phase concentration outside the particle
- Y_o : Initial dimensionless solid-phase concentration
- Y_r : Dimensionless solid-phase concentration at any internal radius r
- y : The amount of gas or vapour adsorbed per gram of solid, gm/gm
- Z : The dimensionless through-put parameter

Greek letters

α_p, α_f : Constants for particle-phase or external diffusion
model equations

ρ_b : Bulk density of solid particles in bed

ρ_f : Fluid-phase density

μ : Viscosity

ψ : Correction factor

Subscripts

f : External diffusion

p : Particle-phase diffusion

pore : Pore diffusion

R : Reaction kinetics

ACKNOWLEDGMENTS

I wish to express my appreciation to Dr. Benjamin G. Kyle for his advice and encouragement during all stages of this work. Financial support was provided by Environmental Protection Agency Research Assistantship and is deeply appreciated.

In addition, my thanks go to my graduate committee members, Dr. Liang T. Fan, Dr. Richard G. Akins, and Dr. Dean N. Eckhoff for reading this thesis and giving valuable suggestions. Finally, I express my thanks to my wife, Inja, for her help during the past years.

BIBLIOGRAPHY

1. Altshuller, A. P., and Cohen, I. R., "Application of Diffusion Cells to the Production of Known Concentrations of Gaseous Hydrocarbons," *Analytical Chemistry*, 32, 802(1960)
2. Barneby, H. L., "Activated Charcoal in the Petrochemical Industry," *Chem. Eng. Progr.*, 67(11) (1971)
3. Bird, R. B., Stewart, W. E., and Lightfoot, E. N., "Transport Phenomena," John Wiley & Sons (1960)
4. Bohart, G. S., and Adams, E. Q., Jr., "Some Aspects of the Behavior of Charcoal with respect to Chlorine," *J. Am. Chem. Soc.*, 42, 523(1920)
5. Brunauer, S., "The adsorption of Gases and Vapors," Vol. I. Physical Adsorption, Princeton Univ. Press (1943)
6. Chaplin, R., "Adsorption of Nitrogen at Low Pressure by Activated Charcoal," *Phil. Mag.* (7) 2, 1198(1926)
7. Clapham, T. M., Junker, T. J., and Tobias, G. S., "Activated Carbon Odorant Removal from Air Quantified," paper No. 2145, ASHRAE Annual Meeting, Kansas City, Mo., June 1970
8. DeVault, D., "The Theory of Chromatography," *Am. Chem. Soc.*, 65, 532(1943)
9. Edeskuty, F. J., and Amundson, N. R., "Mathematics of Adsorption. IV. Effect of Intraparticle Diffusion in Agitated Static Systems," *J. Phys. Chem.*, 56, 148(1952)
10. Emmett, P. H., Brunauer, S., and Love, K., "The Measurement of Surface Areas of Soils and Soil Colloids by the Use of Low Temperature van der Waals Adsorption Isotherms," *Soil Sci.* 45, 57(1938)
11. Flood, E. A., "The Solid-Gas Interface," Vol. I Edward Arnold (1967)
12. Fuller, R. D., "Adsorption" in Chapter 9 of Gas Purification Process for Air Pollution Control, edited by G. Nonhebel. London Newnes-Butterworths (1972)

13. Glueckauf, E., and Coates, J. I., "Theory of Chromatography. Part IV. The Influence of Incomplete Equilibrium on the Front Boundary of Chromatograms and on the Effectiveness of Separation," Chem. Soc. of London J., 1315(1947)
14. Glueckauf, E., "Theory of Chromatography. Part 10- Formulae for Diffusion into Spheres and their Application to Chromatography," Trans. Faraday Soc. 51, 1540(1955)
15. Gregg, S. J., and Sing, K. S. W., "Adsorption, Surface Area, and Porosity," Academic Press (1967)
16. Hall, K. R., Eagleton, L. C., Acrivos, A., and Vermeulen, T., "Pore- and Solid-Diffusion Kinetics in Fixed-Bed Adsorption under Constant Pattern Conditions," Ind. & Eng. Chem. Fund. 5, 212(1966)
17. Helfferich, F., "Ion Exchange," McGraw Hill (1962)
18. Hiester, N. K., Radding, S. B., Nelson, R. L., Jr., and Vermeulen, T., "Interpretation and Correlation of Ion Exchange Column Performance under Nonlinear Equilibrium," A.I.Ch.E. J. 2, 404(1956)
19. Hiester, N. K., Vermeulen, T., Klein, G., "Adsorption and Ion Exchange," Section 16 of John H. Perry's Chemical Engineers' Handbook 4th edition, McGraw Hill (1963)
20. Hougen, O. A., and Marshall, W. R., Jr., "Adsorption from a Fluid Stream Flowing through a Stationary Granular Bed," Chem. Eng. Progr., 43, 197(1947)
21. Klotz, I. M., "The Adsorption Wave," Chem. Rev., 32, 241(1946)
22. Lambert, B., and Peel, D. H. P., "Gas-Solid Equilibria. V. Pressure-Concentration Equilibria between Silica Gel and (1) Oxygen (2) Nitrogen (3) Mixtures of Oxygen and Nitrogen Determined Isothermally at 0 °," Proc. Roy. Soc. (London) A 144, 205(1934)
23. Langmuir, I., "Adsorption of Gas by Solids," J. Am. Chem. Soc., 38, 2267(1916)
24. ———, "The Evaporation, Condensation and Reflection of Molecules and the Mechanism of Adsorption," Phys. Rev. (ser. 2), 8, 149(1916)
25. ———, "The adsorption of Gases on Plane Surface of Glass, Mica, and Platinum," J. Am. Chem. Soc., 40, 1316(1918)

26. Lightfoot, E. N., Sanchez-Palma, R. J., and Edwards, D. O., "Chromatography and Allied Fixed-Bed Separation Processes," in Chapter 2 of New Chemical Engineering Separation Techniques edited by H. M. Schoen, Interscience Publishers, New York, London (1962)
27. Markham, E. C., and Benton, F., "The Adsorption of Gas Mixtures by Silica," J. Am. Chem. Soc., 53, 497(1931)
28. Michaels, A. S., "Simplified Method of Interpreting Kinetic Data in Fixed-Bed Ion Exchange," Ind. Eng. Chem., 44, 1922(1952)
29. Peters, K., and Weil, K., "Adsorption Experiments with Heavy Noble Gases," Z. Physik. Chem., Abt. A, 148, 1(1930)
30. Polanyi, M., "Adsorption from the Point of View of the Third Law of Thermodynamics," Verh. dtsh. phys. Ges., 16, 1012(1914)
31. ———, "Adsorption of Gases(Vapours) by a Solid Non-Volatile Adsorbent," Ibid., 18, 55(1916)
32. ———, "Adsorption and the Origin of Adsorption Forces," Z. Elektrochem., 26, 370(1920)
33. ———, "Fundamentals of the Potential Theory of Adsorption," Ibid., 35, 431(1929)
34. Rosen, J. B., "Kinetics of a Fixed-Bed System for Solid Diffusion into Spherical Particles," J. Chem. Phys., 20, 387(1952)
35. Idem., "General Numerical Solution for Solid Diffusion in Fixed Beds," Ind. Eng. Chem., 46, 1590(1954)
36. Ross, S., and Olivier, J. P., "On Physical Adsorption," Interscience (1964)
37. Sillen, L. G., "Filtration through a Sorbent Layer. I. An Attempt at a Simple Mathematical Treatment," Arkiv. Kemi, Mineral Geol., A22, No. 15, 22(1946)
38. Thomas, H. C., "Chromatography: A Problem in Kinetics," Ann. N.Y. Acad. Sci., 49, 161(1948)
39. ———, "Heterogeneous Ion Exchange in a Flowing System," J. Am. Chem Soc., 66, 1664(1944)
40. ———, "Solid Diffusion in Chromatography," J. Chem. Phys., 19, 1213(1951)

41. Vermeulen, T., "Separation by Adsorption Method," in Vol. II of Advances in Chemical Engineering, edited by T. B. Drew and J. W. Hoopes, Jr., Academic Press, New York (1958)
42. Vermeulen, T., and Klein, G., "Recent Background Developments for Adsorption Column Design," A.I.Ch.E. Symposium Series 62, 65(1971)
43. Walter, J. E., "Multiple Adsorption from Solutions," J. Chem. Phys., 13, 229(1945)
44. Wheeler, A., "Reaction Rates and Selectivity in Catalyst Pores," Advances in Catalysis, 2, 250(1951) Academic Press
45. Wicke, E., "Empirical and Theoretical Investigation of the Sorption Velocity of Gases on Porous Substances. I," Kolloid-Z., 86, 167(1939)
46. Wiessman, H., and Neumann, W., "Gas Sorption by Soil Components and Soils. I," Z. Pflanzenernähr., Düngung Bodenk., 40, 49(1935)
47. Wilke, C. R., and Hougen, O. A., "Mass Transfer in the Flow of Gases through Granular Solids Extended to Low Modified Reynolds Numbers," Trans. Am. Inst. Chem. Engrs., 41, 445(1945)
48. Wilson, J. N., "A Theory of Chromatography," Am. Chem. Soc., 62, 1583(1940)
49. Young, D. H., and Crowell, A. D., "Physical Adsorption of Gases," Butterworths (1962)
50. Zel'dovich, Ya., "Theory of the Freundlich Adsorption Isotherm," Acta Physicochim. U.R.S.S. 1, 961(1934)
51. "Aldehydes," Union Carbide Chemicals Company, 1960

APPENDIX

A-1. Verification of Constant $(\partial Zv/\partial v)_x$ for Constant-pattern Limit.

For constant-pattern limit, all parts of the exchange zone move through the column at a constant rate. This statement can be expressed as

$$\left(\frac{\partial t}{\partial v}\right)_x = \text{const.} \text{------(A-1)}$$

By the definition of through-put parameter, Z

$$Z = \frac{t}{D \text{ ev}/F} \text{------(A-2)}$$

or

$$t = \frac{Z D \text{ ev}}{F} \text{------(A-3)}$$

For constant De/F , by substituting equation (A-3) into equation (A-1).

$$\frac{De}{F} \left(\frac{\partial Zv}{\partial v}\right)_x = \text{const.}$$

or

$$\left(\frac{\partial Zv}{\partial v}\right)_x = \text{const.}$$

A-2. Experimental Breakthrough Curves and Modeling Breakthrough Curves.

The experimental breakthrough curves were constructed and are shown on Fig.(A-1) through (A-13). Also the four modeling breakthrough curves (solid phase diffusion, pore diffusion, external diffusion, and reaction kinetics model) are shown on the same figures to compare with the experimental results.

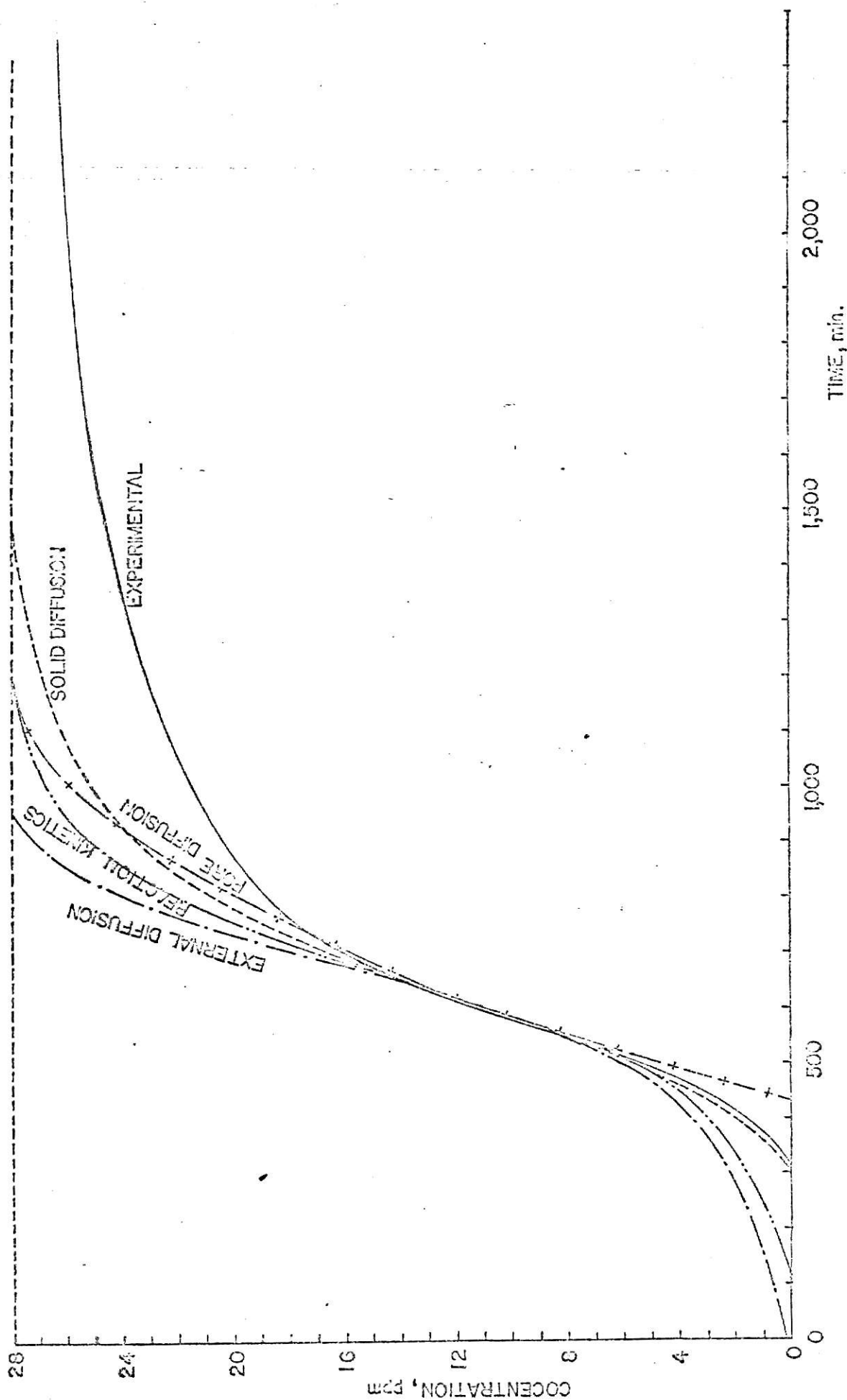


FIG. (A-1). APC-14, FIXED-BED TEST WITH 14 MESH CHARCOAL, 8.66 cm DEEP BED, AND 16.07 cc/sec FLOW RATE COMPARED WITH MODEL BREAKTHROUGH CURVES

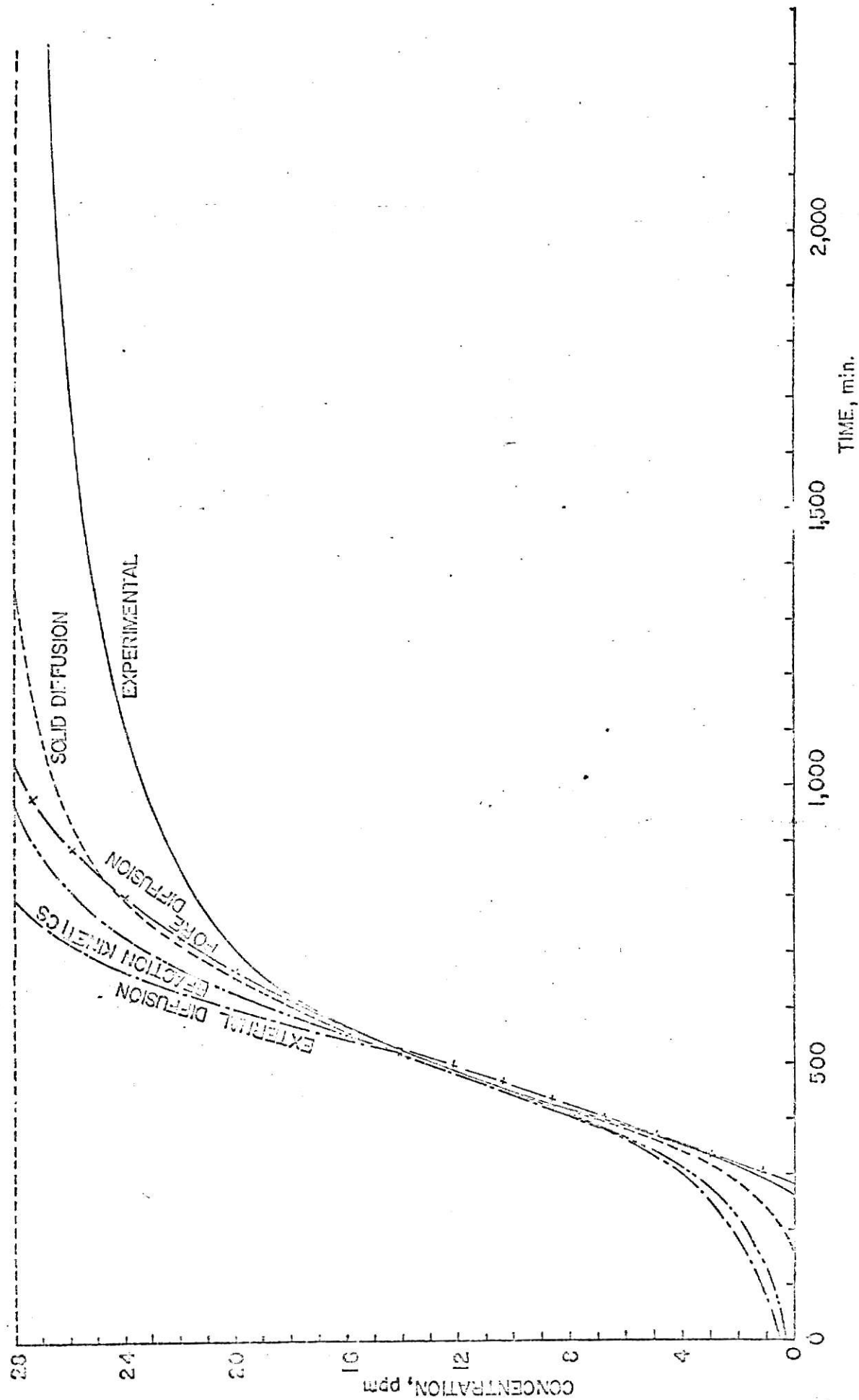


FIG. (A-2). APC-13, FIXED-BED TEST WITH 14 MESH CHARCOAL, 10.16 cm DEEP BED, AND 23.75 cc/g_{sec} FLOW RATE COMPARED WITH MODEL BREAKTHROUGH CURVES

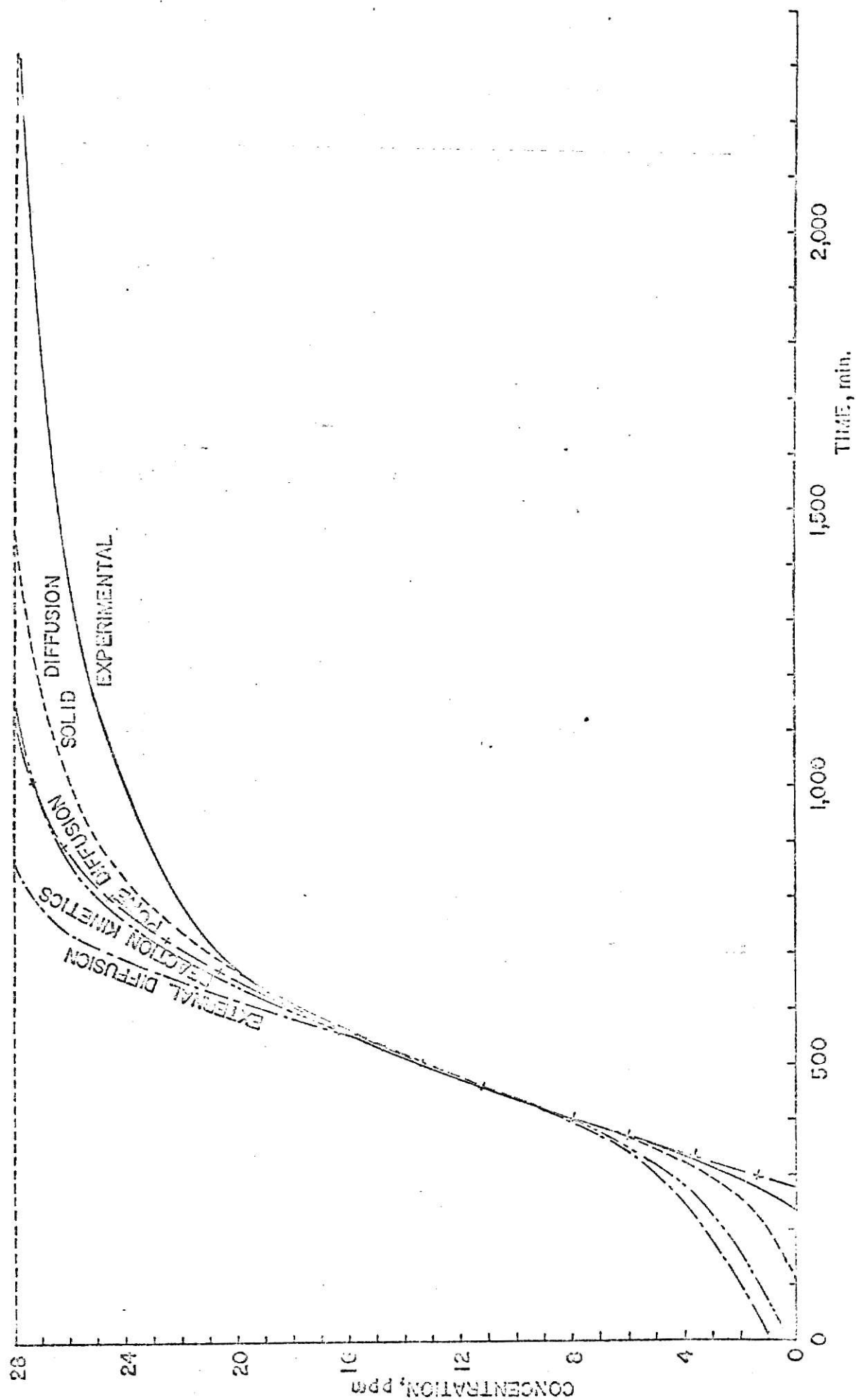


FIG.(A-3). APC-19, FIXED-BED TEST WITH 14 MESH CHARCOAL, 13.82 cm DEEP BED AND 32.5 cc/sec FLOW RATE COMPARED WITH MODEL BREAKTHROUGH CURVES

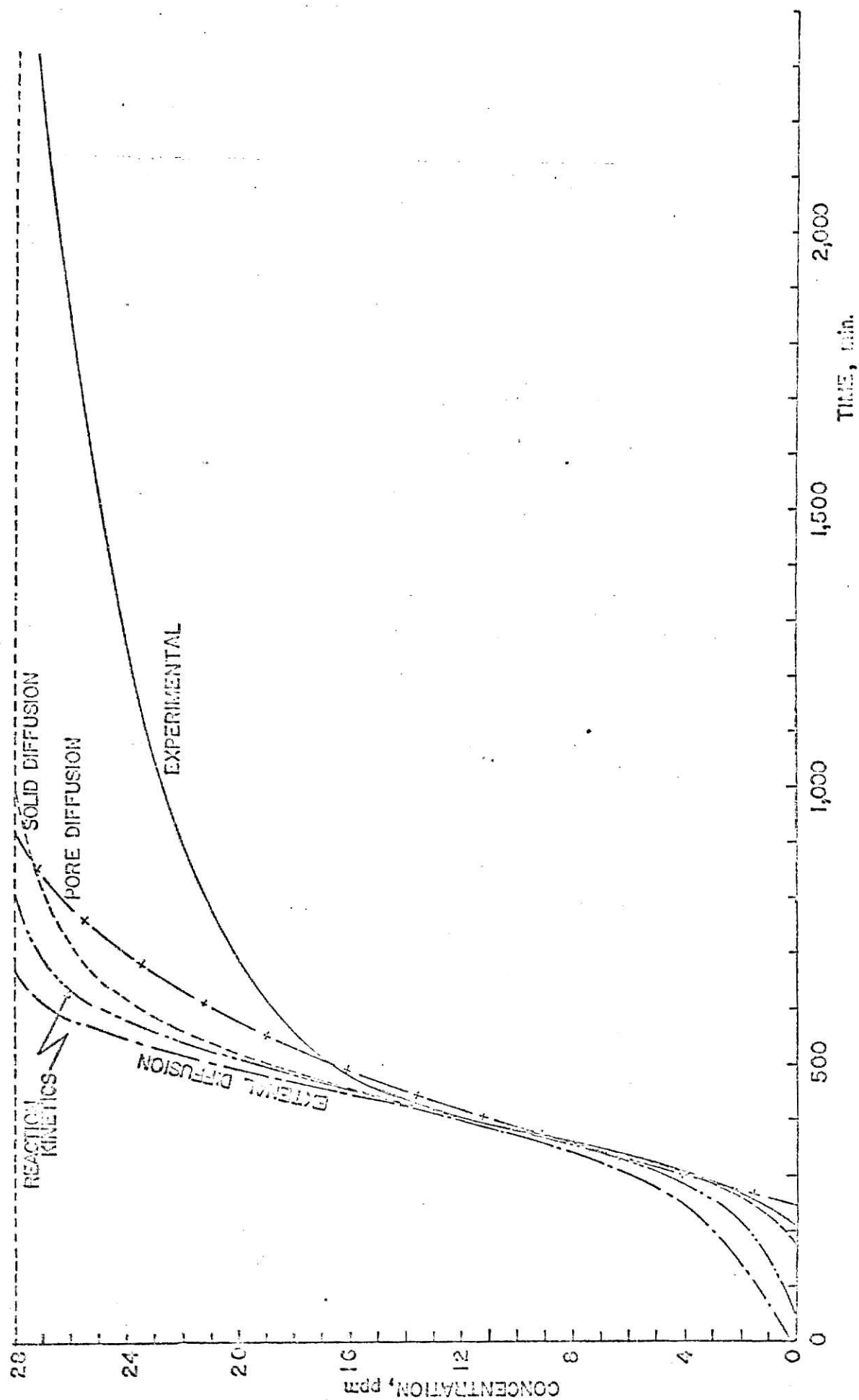


FIG.(A-4). APC-20, FIXED-BED TEST WITH 14 MESH CHARCOAL, 11.33 cm DEEP BED AND 32.5 cc/sec FLOW RATE COMPARED WITH MODEL BREAKTHROUGH CURVES

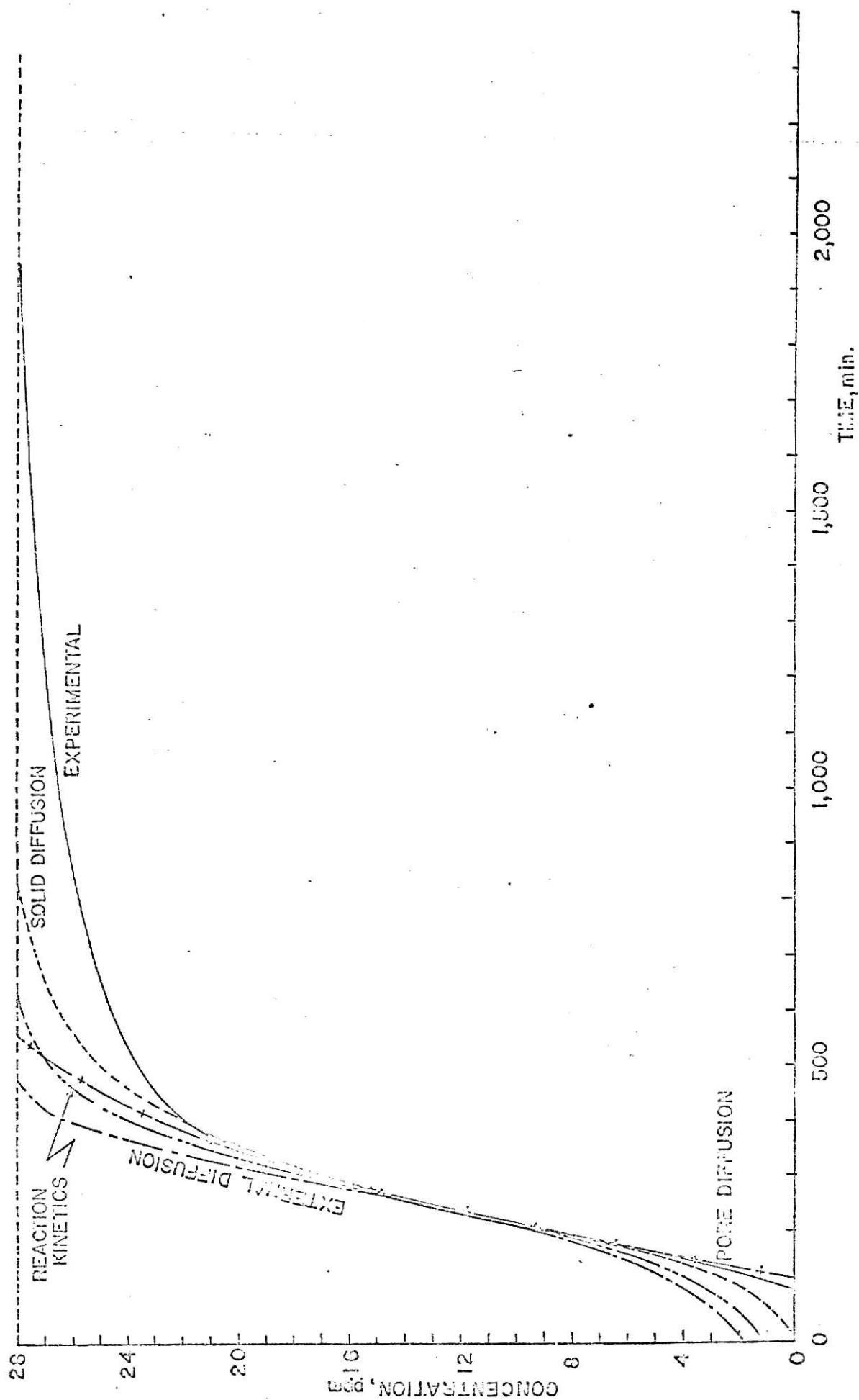


FIG.(A-5). APC-21, FIXED-BED TEST WITH 14 MESH CHARCOAL, 7.56 cm DEEP BED, AND 32.5 cc/sec FLOW RATE COMPARED WITH MODEL BREAKTHROUGH CURVES

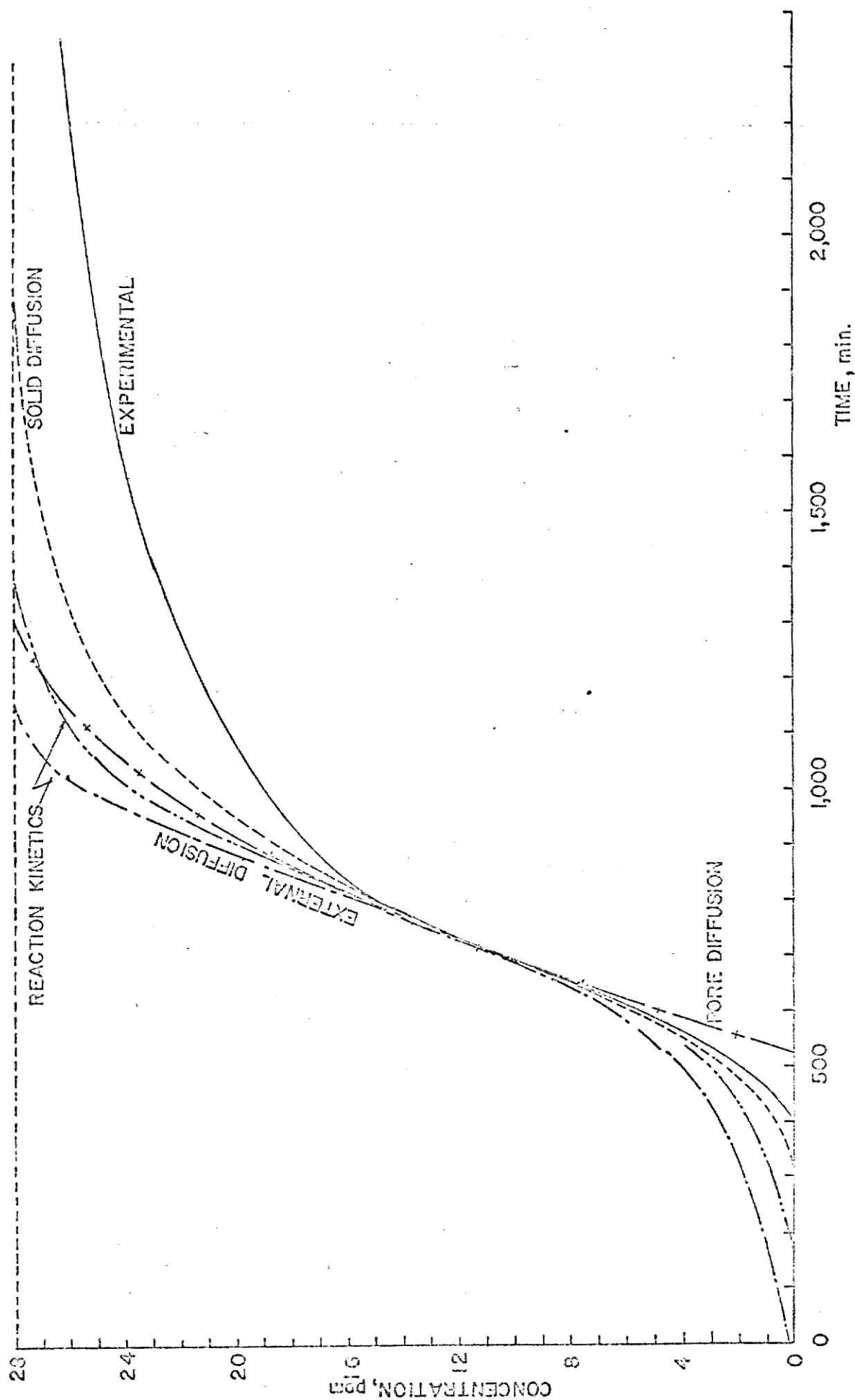


FIG.(A-6). APC-22, FIXED-BED TEST WITH 14 MESH CHARCOAL, 12.59 cm DEEP BED, AND 23.75 cc/sec FLOW RATE COMPARED WITH MODEL BREAKTHROUGH CURVES

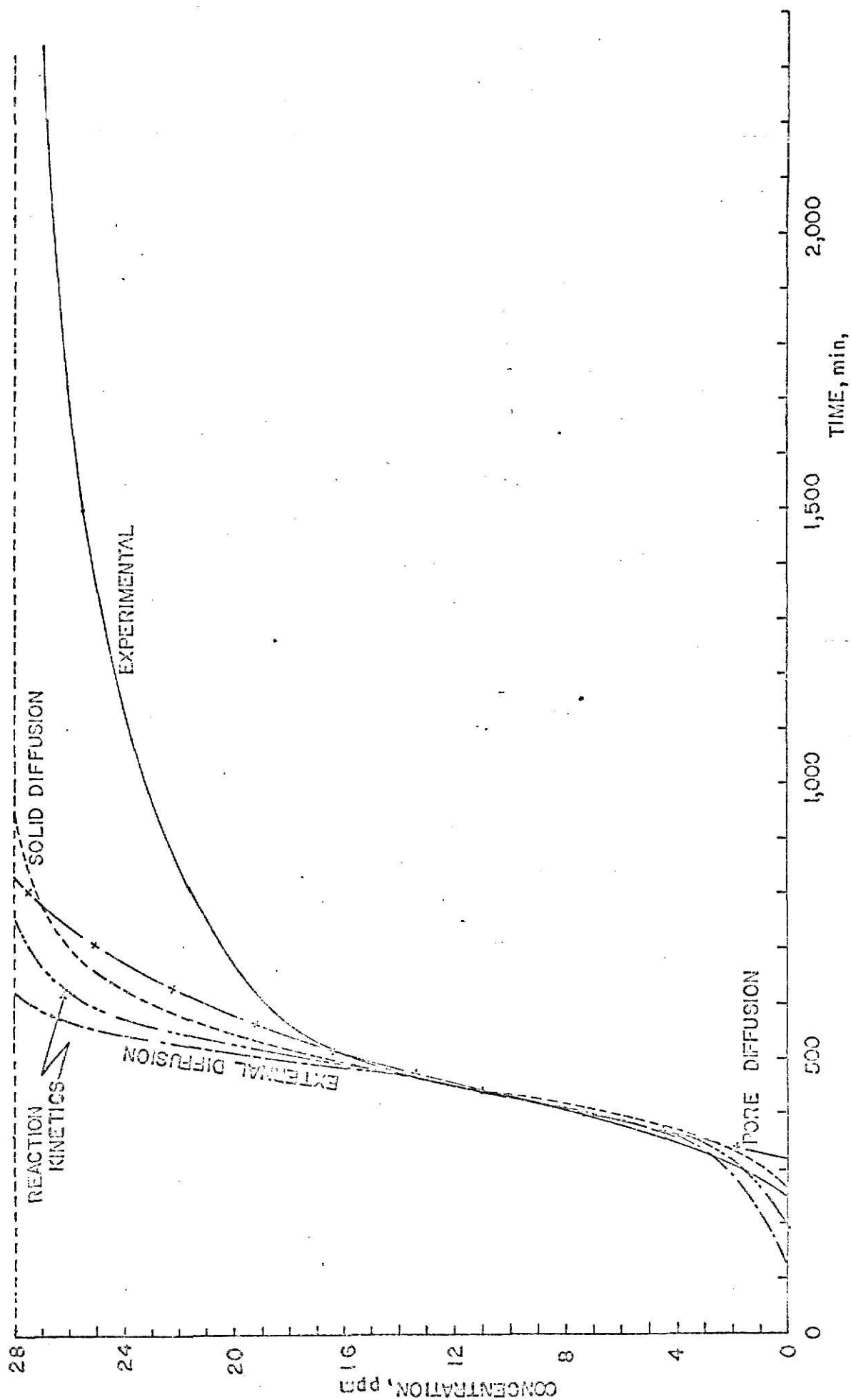


FIG.(A-7). APC-26, FIXED-BED TEST WITH 14 MESH CHARCOAL, 20.32 cm DEEP BED, AND 73.33 cc/sec FLOW RATE COMPARED WITH MODEL BREAKTHROUGH CURVES

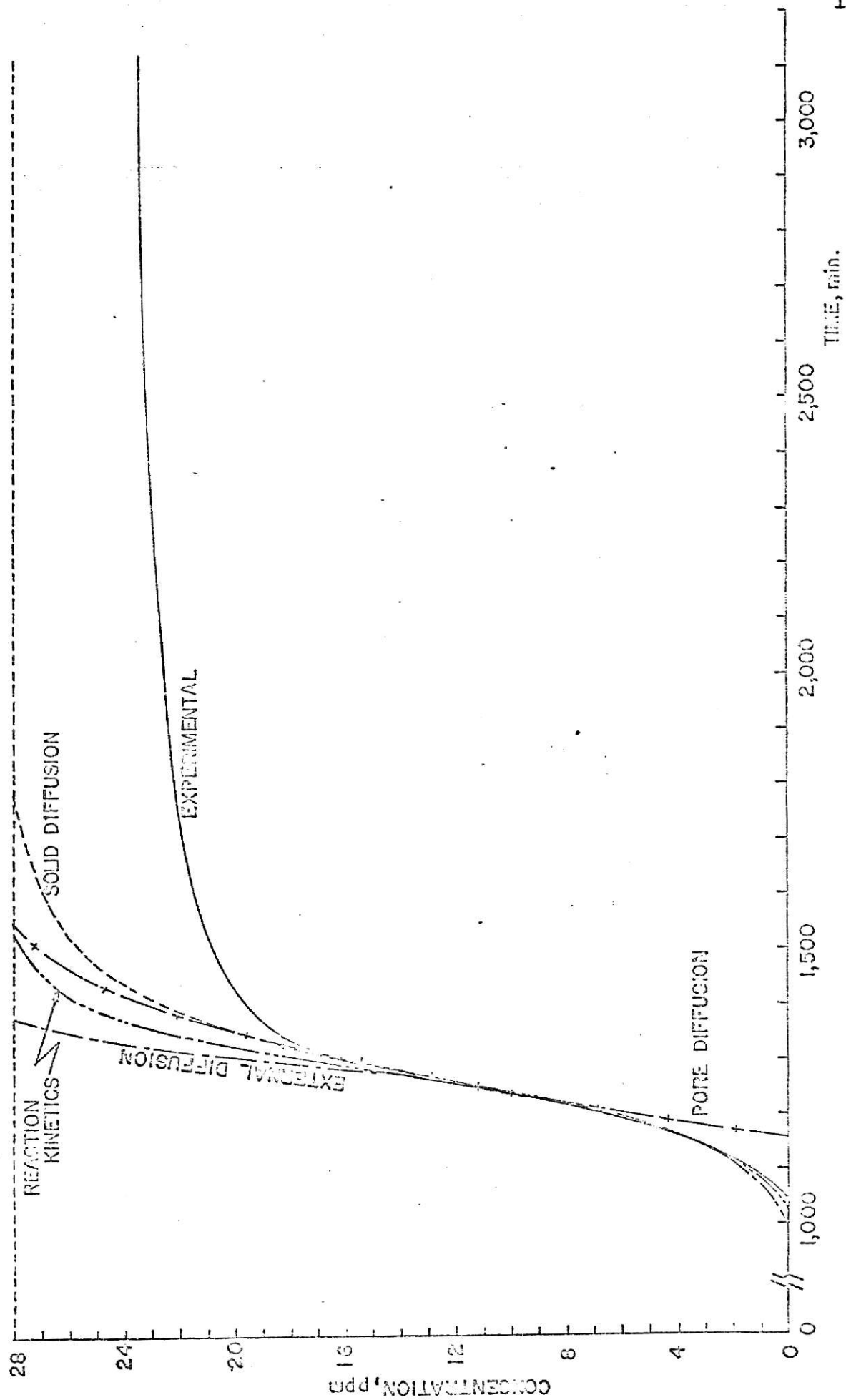


FIG.(A-6). APC-29, FIXED-BED TEST WITH 14 MESH CHARCOAL, 45.72 cc DEEP BED AND 32.5 cc. cc
FLOW RATE COMPARED WITH MODEL BREAKTHROUGH CURVES

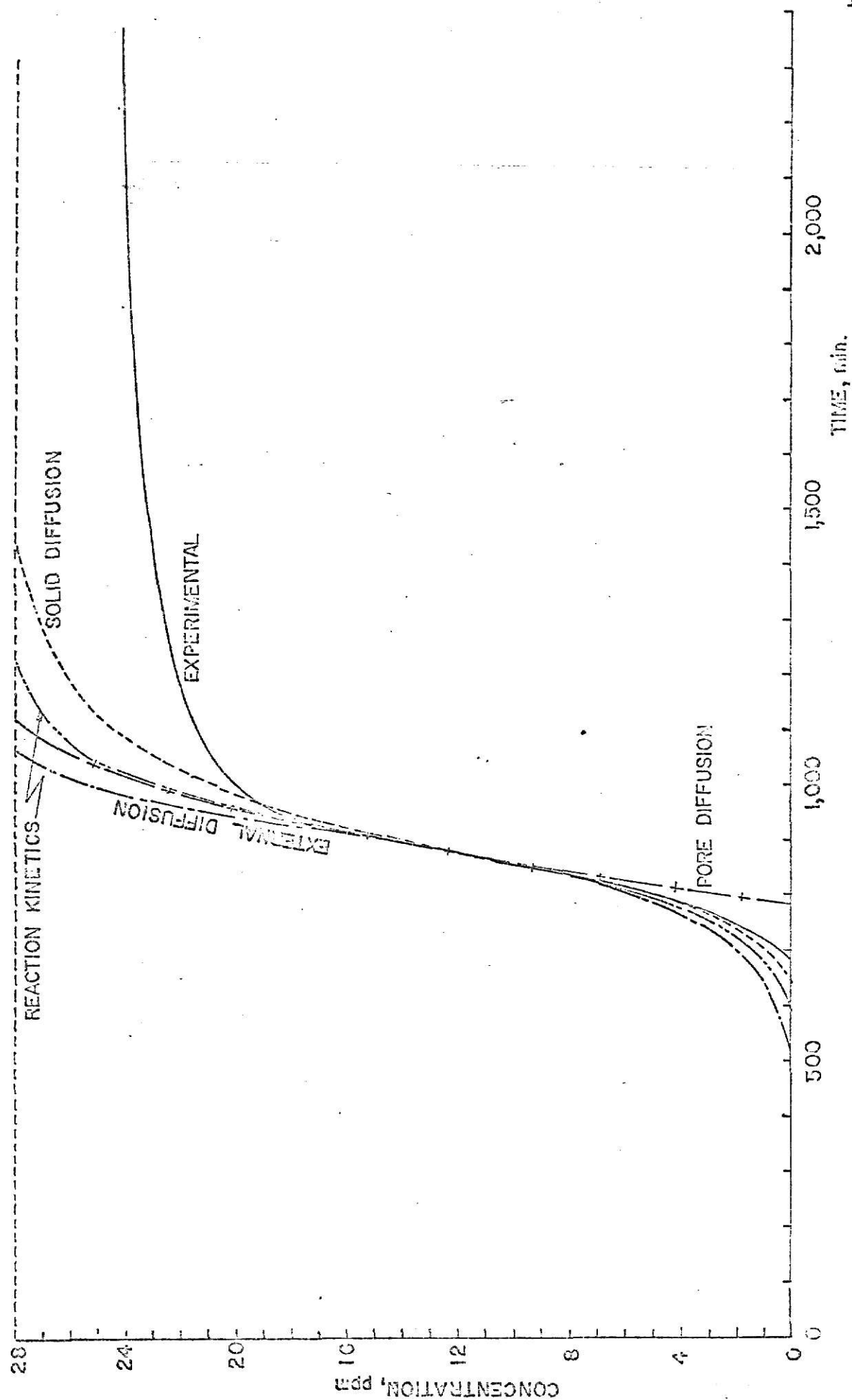


FIG.(A-9). APC-30, FIXED-BED TEST WITH 14 MESH CHARCOAL, 42.72 cm DEEP BED, AND 49.5 cm^3/sec FLOW RATE COMPARED WITH MODEL BREAKTHROUGH CURVES

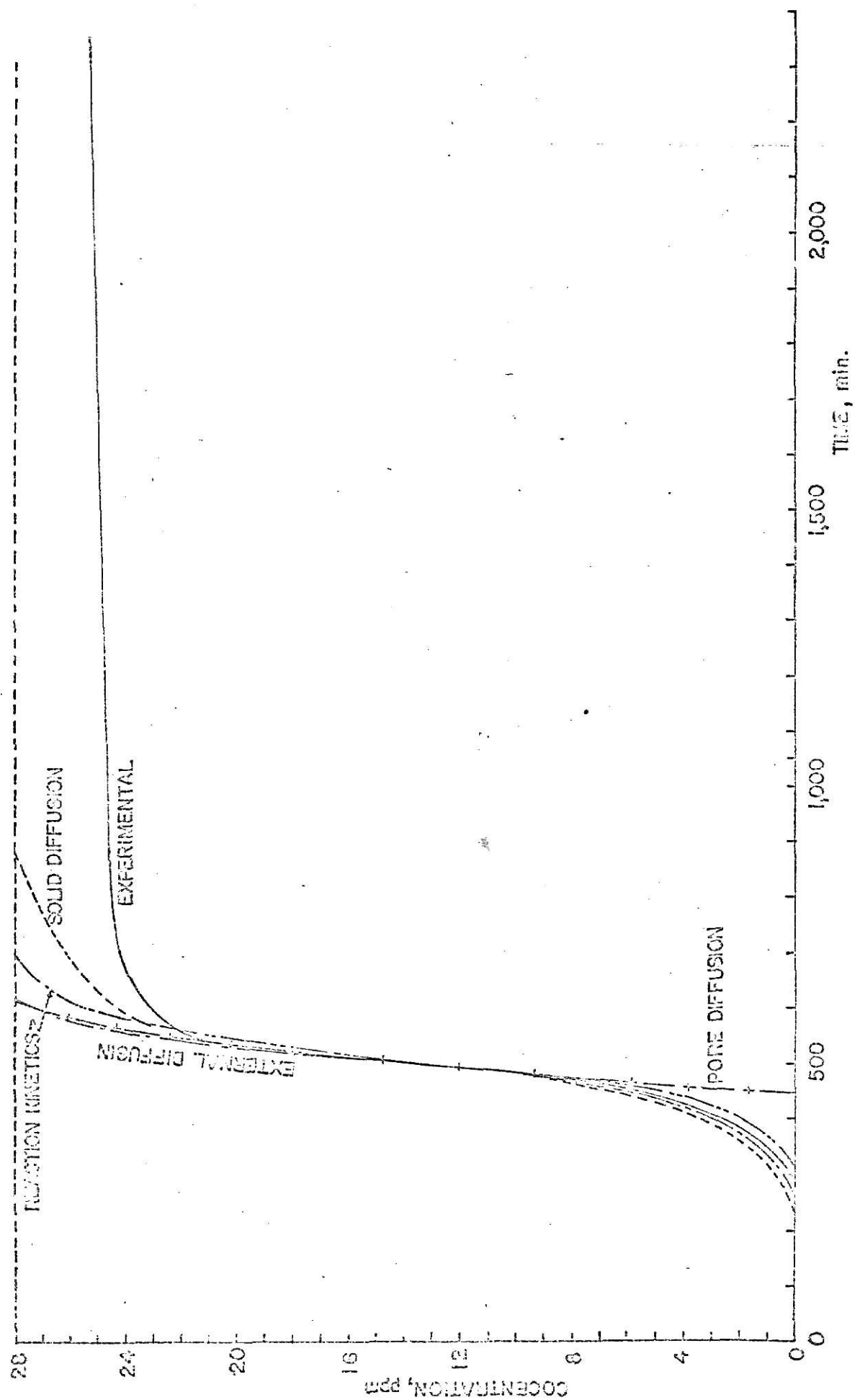


FIG.(A-10). APC-31, FIXED-BED TEST WITH 14 MESH CHARCOAL, 45.72 cm DEEP BED AND 6022 $^{\circ}\text{C}/\text{sec}$ FLOW RATE COMPARED WITH MODEL BREAKTHROUGH CURVES

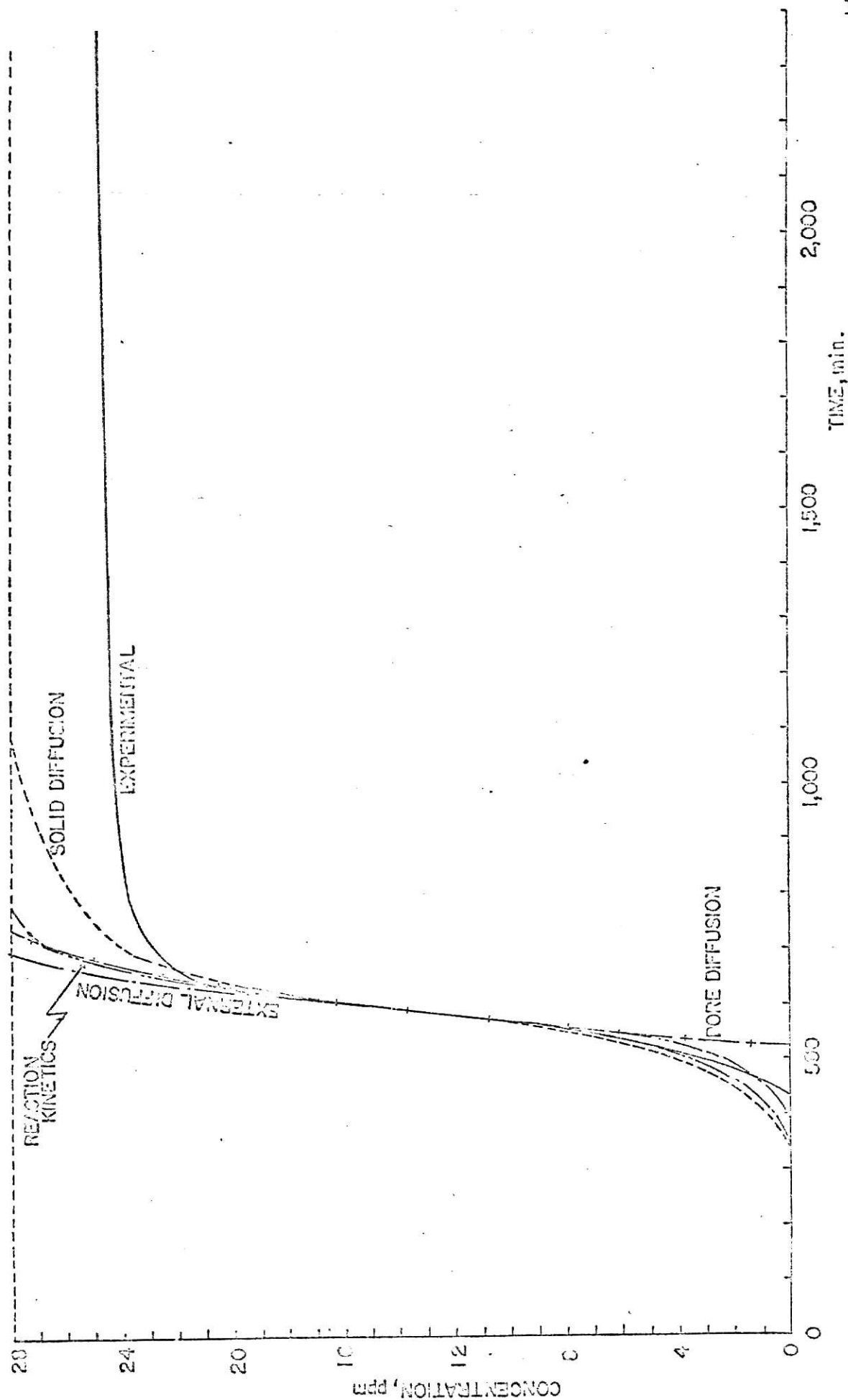


FIG. (A-11). APC-32, FIXED-BED TEST WITH 14 MESH CHARCOAL, 45.72 cm DEEP BED AND 59.4 cc/sec
FLOW RATE COMPARED WITH MODEL BREAKTHROUGH CURVES

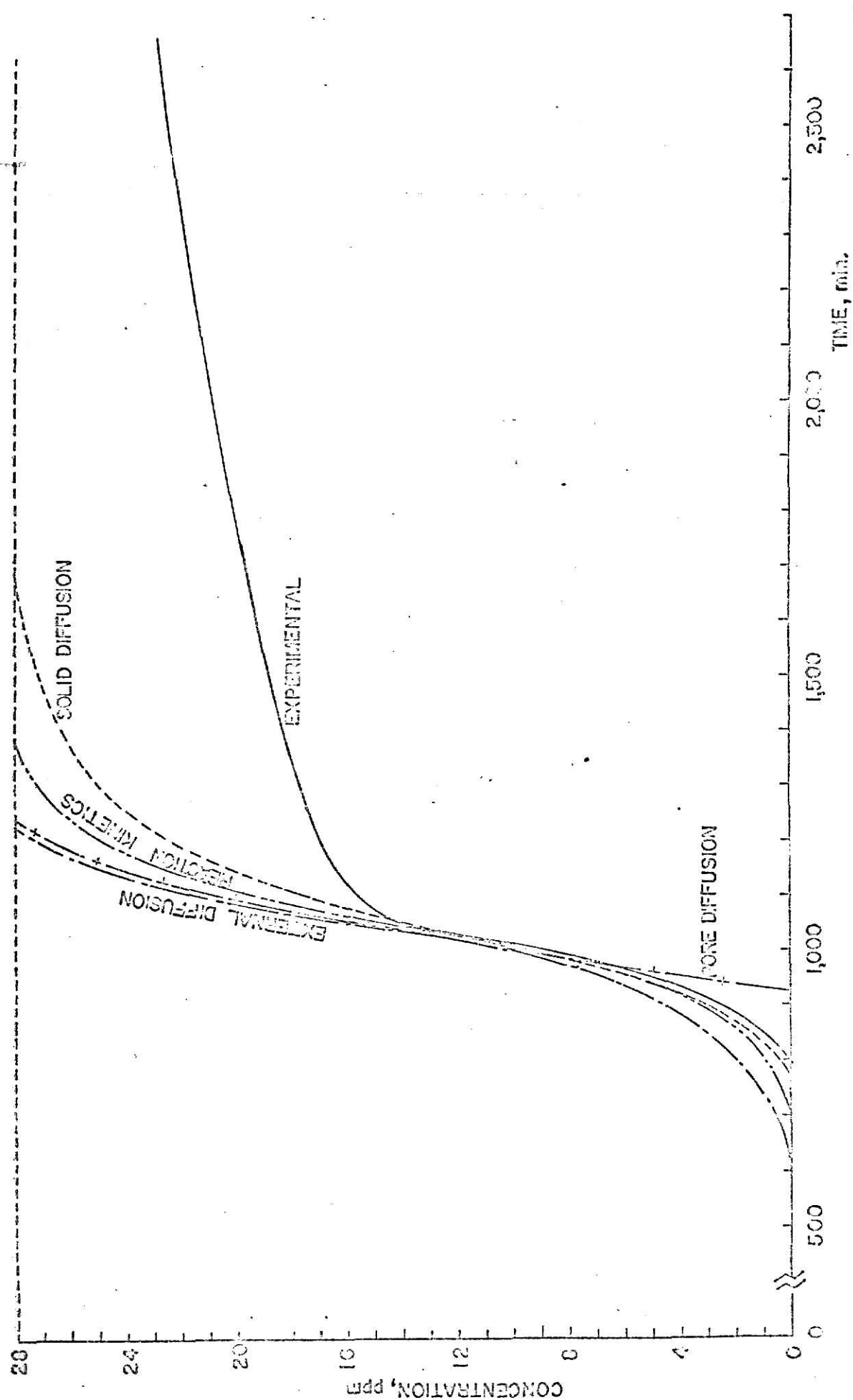


FIG.(A-12). APC-30, FIXED-BED TEST WITH 10 MESH CHARCOAL, 45.7% IN DEEP BED AND 79.35 %/sec

FLOW RATE COMPARED WITH MODEL BREAKTHROUGH CURVES

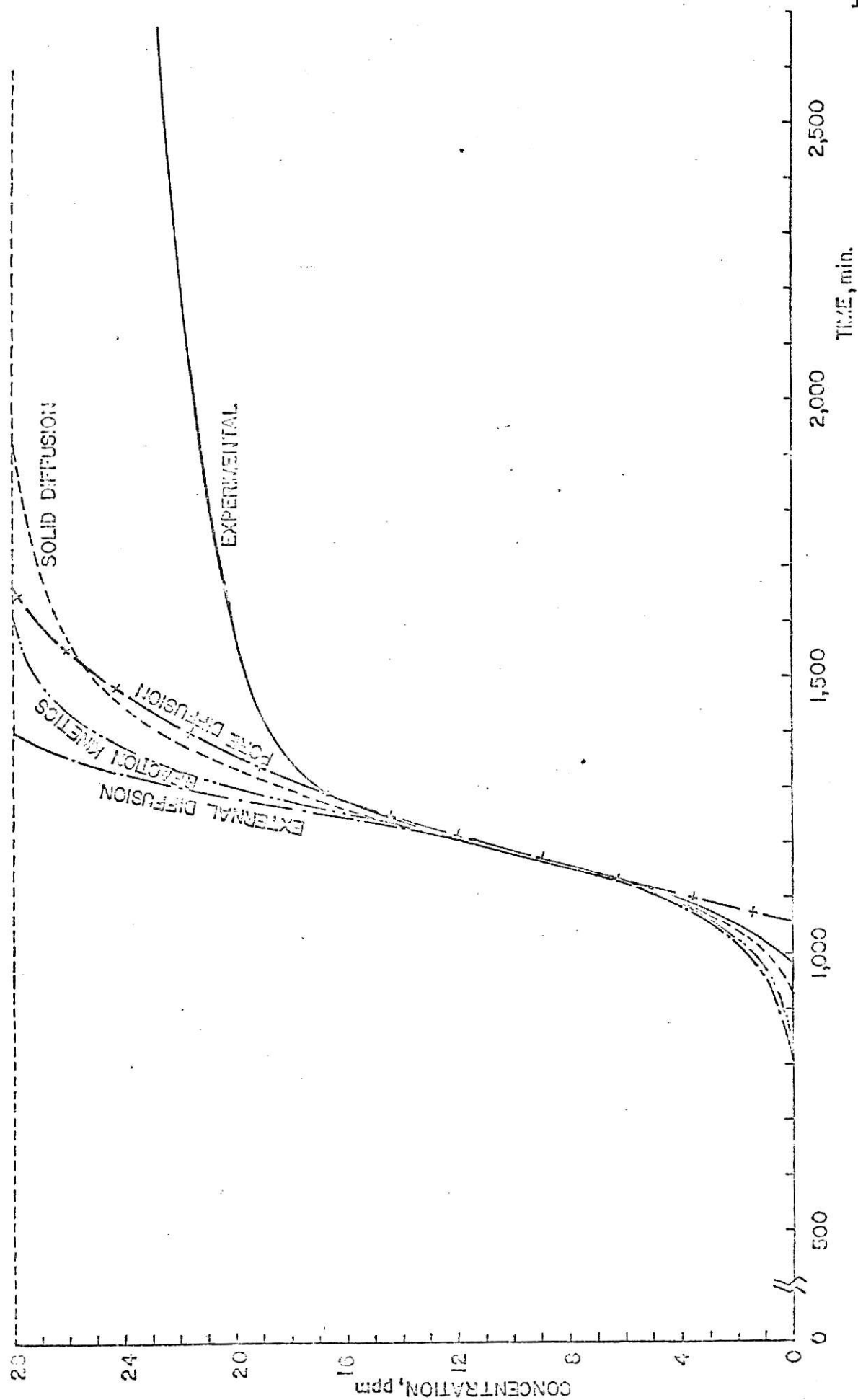


FIG.(A-13). APC-39, FIXED-BED TEST WITH 12 MESH CHARCOAL, 45.72 cm DEEP BED, AND 4593 cm^3/sec FLOW RATE COMPARED WITH MODEL. BREAKTHROUGH CURVES

A-3. Calculation of Bed Capacity from the Breakthrough Curve.

A stream of concentration C_0 enters a fixed-bed at a flow rate $F(\text{cc/sec})$. At any time $t(\text{sec})$, the effluent concentration is $C(\text{ppm})$. A material balance during the time dt can be written as

$$\begin{array}{ccccc} C_0 F dt & - & C F dt & = & da \\ \text{in} & & \text{out} & & \text{accumulation} \end{array} \text{-----} (A-4)$$

At time zero, the amount of adsorbate in the bed, a , is zero, hence integration of the material balance equation gives

$$a = F \int_0^t (C_0 - C) dt \text{-----} (A-5)$$

When the bed is saturated with respect to the influent gas, the amount of adsorbate in the bed is

$$a_s = F \int_0^{\infty} (C_0 - C) dt \text{-----} (A-6)$$

The integral in equation (A-6) can be evaluated by graphical integration of the breakthrough curve and is represented the shaded area in the Fig.(A-14).

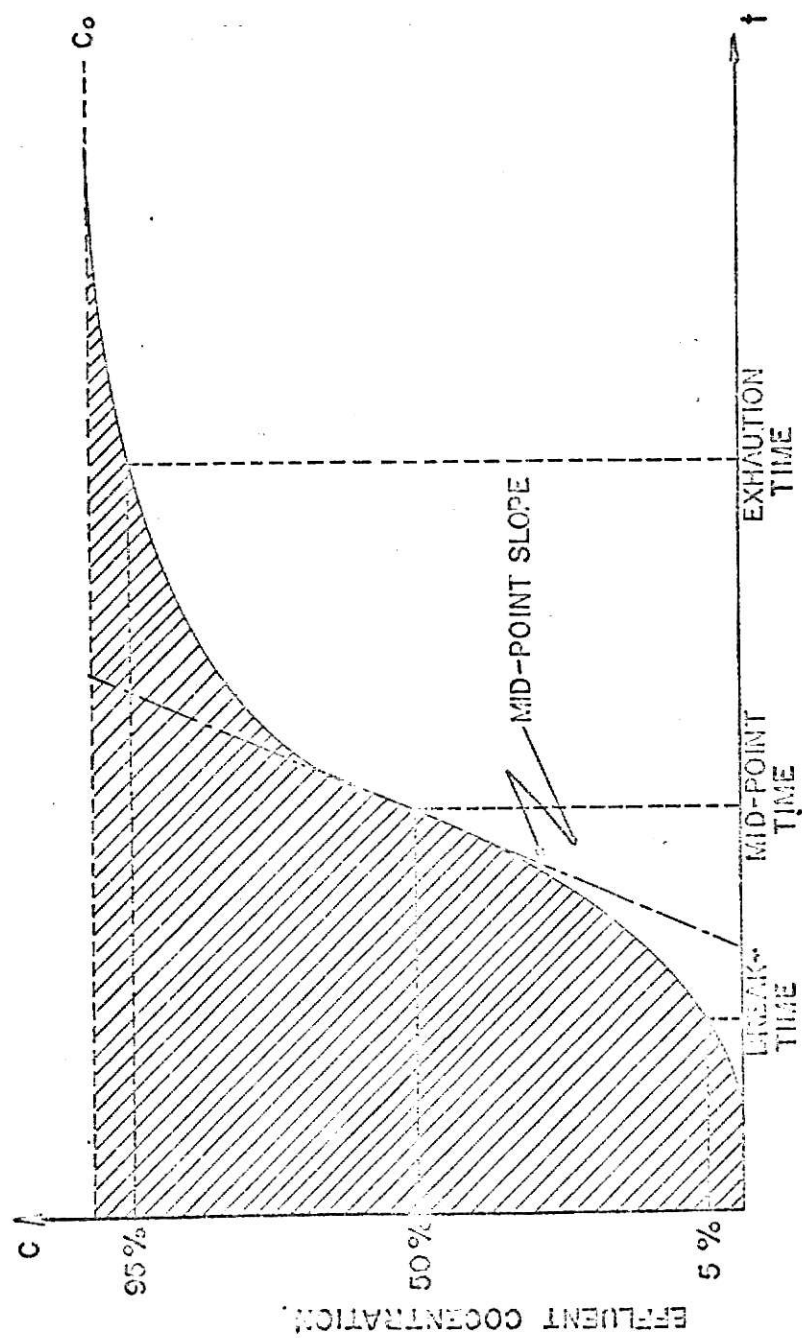


FIG. (A-14). BREAKTHROUGH CURVE FOR BED CAPACITY
CALCULATION

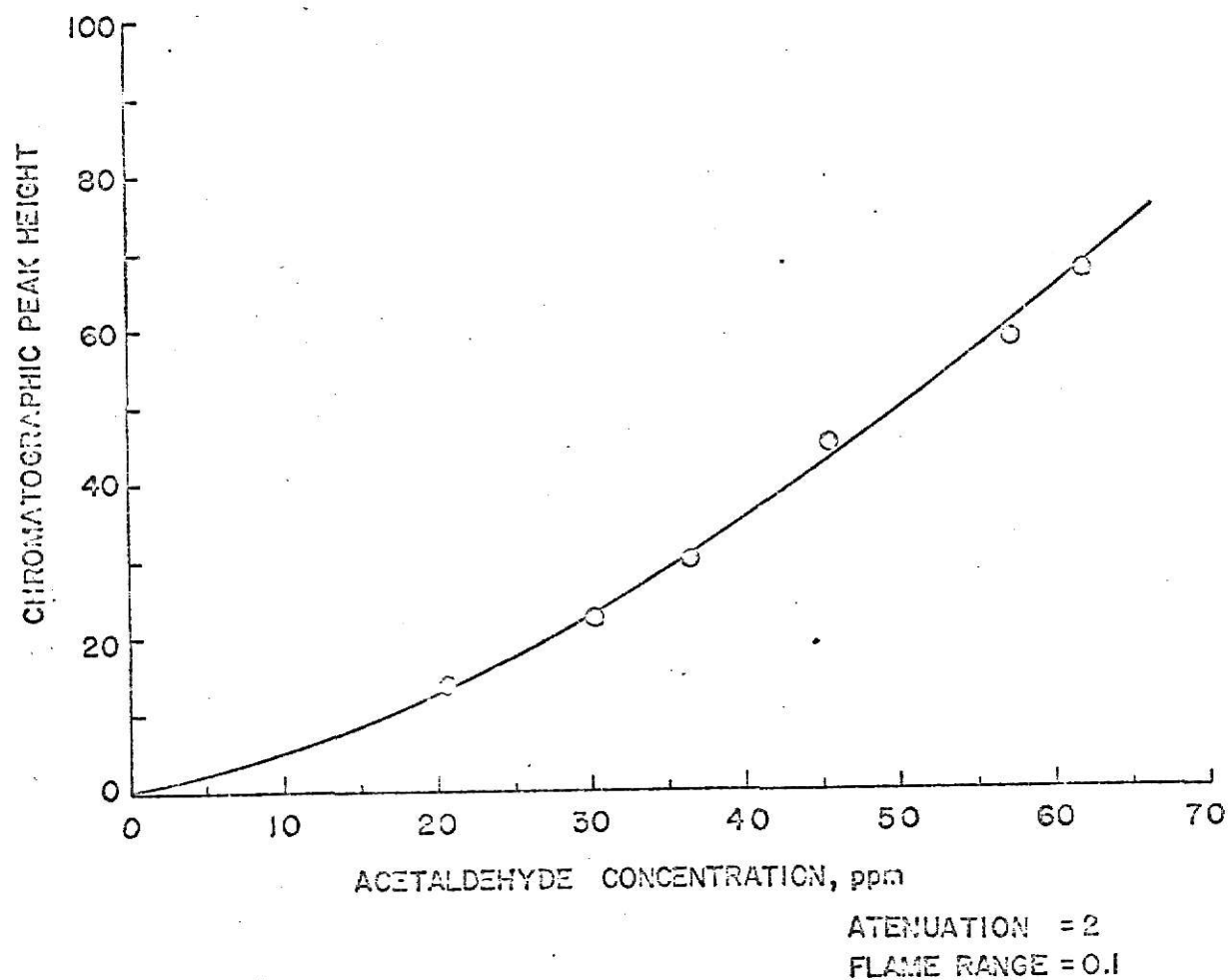


FIG.(A-15). CHROMATOGRAPHIC CALIBRATION CURVE
ACETALDEHYDE

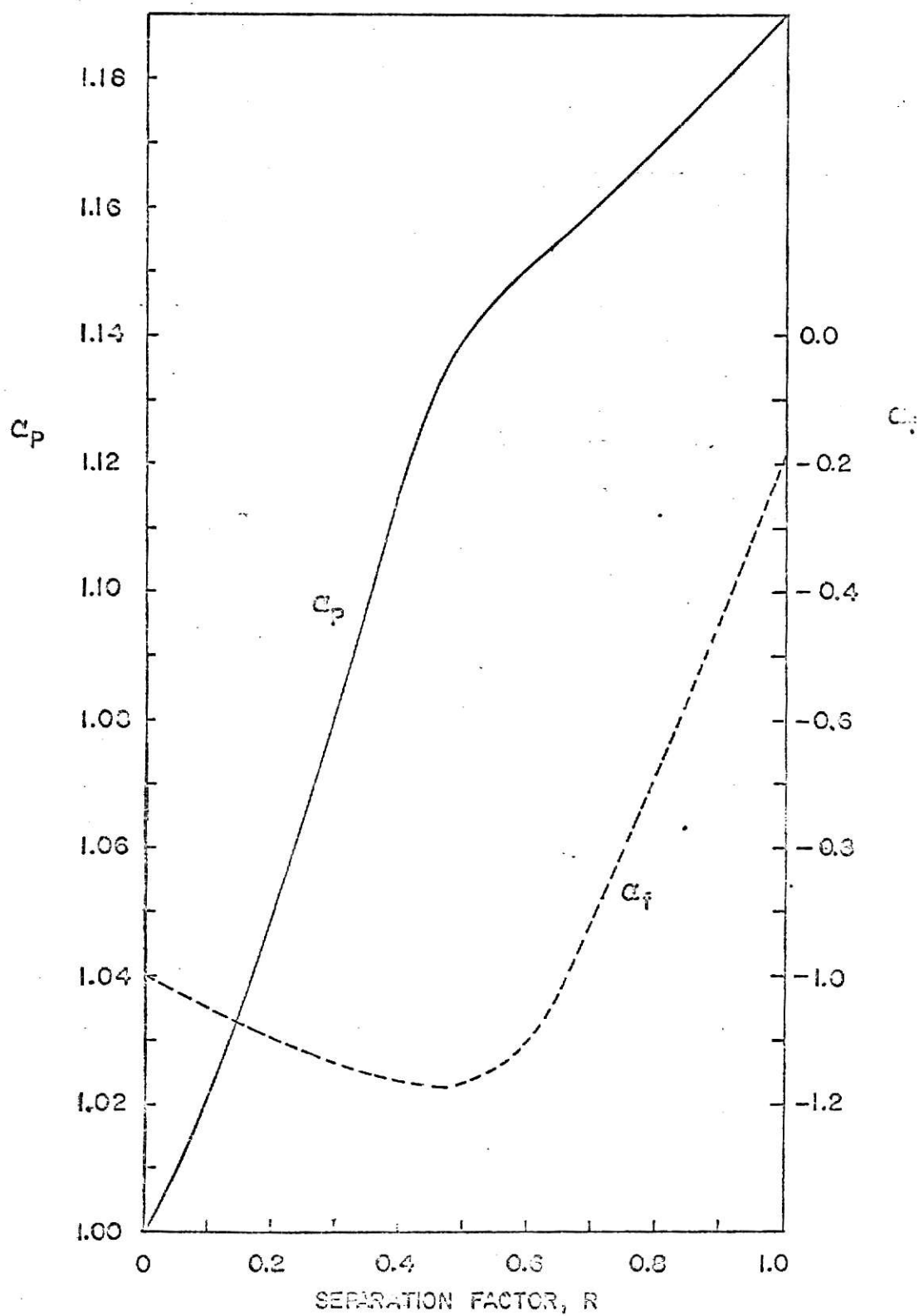


FIG.(A-16). α_p AND α_f VALUES FOR PARTICLE-PHASE AND EXTERNAL DIFFUSION MODEL EQUATIONS

A-4. The Sample Calculations of Modeling Break-Time.

As an example, APC-18 was chosen to calculate the break-time by using modeling equations. For APC-18, residence time, ve/F is 0.595 sec and the break-time ($t_{x=0.05}$) obtained from experimental breakthrough curve is 18,300 sec.

1. Particle-phase Diffusion Model.

From Fig.(III-6), modeling N_p is 4.4 and effective distribution ratio D_{ep} is 57,865, thus $D_{ep} ve/F$ is 34,430. Then the particle-phase diffusion equation (III-2) becomes

$$0.389 \ln X - 1.389 \ln(1 - X) - 1.076 = 4.4 \left(\frac{t}{34,430} - 1 \right) \quad \text{----- (A-7)}$$

At $X=0.5$, $t_{x=0.5}$ from above equation is 31,434 sec.

To obtain $(dX/dt)_{x=0.5}$, differentiate equation (A-7) at $t_{x=0.5}$ then

$$\left(\frac{dX}{dt} \right)_{x=0.5} = 3.594 \times 10^{-5}$$

This is the mid-point slope, and by using this value, break-time is calculated from the equation

$$t_{x=0.05} = t_{x=0.5} - \frac{0.45}{(dX/dt)_{x=0.5}} \quad \text{----- (A-8)}$$

The $t_{x=0.05}$ value calculated from the equation (A-8) is 18,911 sec which has + 3.34 % error compared to the experimental value.

2. Pore Diffusion Model.

Modeling N_{pore} value of 2.68 can be obtained from Fig.(III-8) for 0.595 of ve/F and D_{epore} is 53,210, therefore $D_{\text{epore}} ve/F$ is 31,660. With these values, the pore diffusion equation (I-67) becomes

$$X = 0.557 \left[2.68 \left(\frac{t}{31,660} - 1 \right) + 1.15 \right] - 0.0774 \left[2.68 \left(\frac{t}{31,660} - 1 \right) + 1.15 \right]^2 \quad \text{----- (A-9)}$$

From above equation, two values of t can be calculated for $X = 0.05$. The two values are 19,149 sec and 113,805 sec. Among these two values, the smaller one should be picked as a modeling break-time. The reason is clear from Fig.(A-17). This modeling break-time value of 19,149 sec has + 8.25 % error compared to the experimental break-time.

3. External Diffusion Model.

Modeling N_f value obtained from Fig.(III-12) is 3.9 and experimentally determined effective distribution ratio D_{ef} is 47,607, then $D_{\text{ef}} ve/F$ is 28,326. By substituting these values in the external diffusion model equation (III-5)

$$1.389 \ln X - 0.389 \ln(1 - X) + 1.13 = 3.9 \left(\frac{t}{28,326} - 1 \right) \quad \text{----- (A-10)}$$

At $X=0.5$, the calculated value $t_{X=0.5}$ is 31,499 sec.

And by differentiation of equation (A-10) at $t_{X=0.5}$

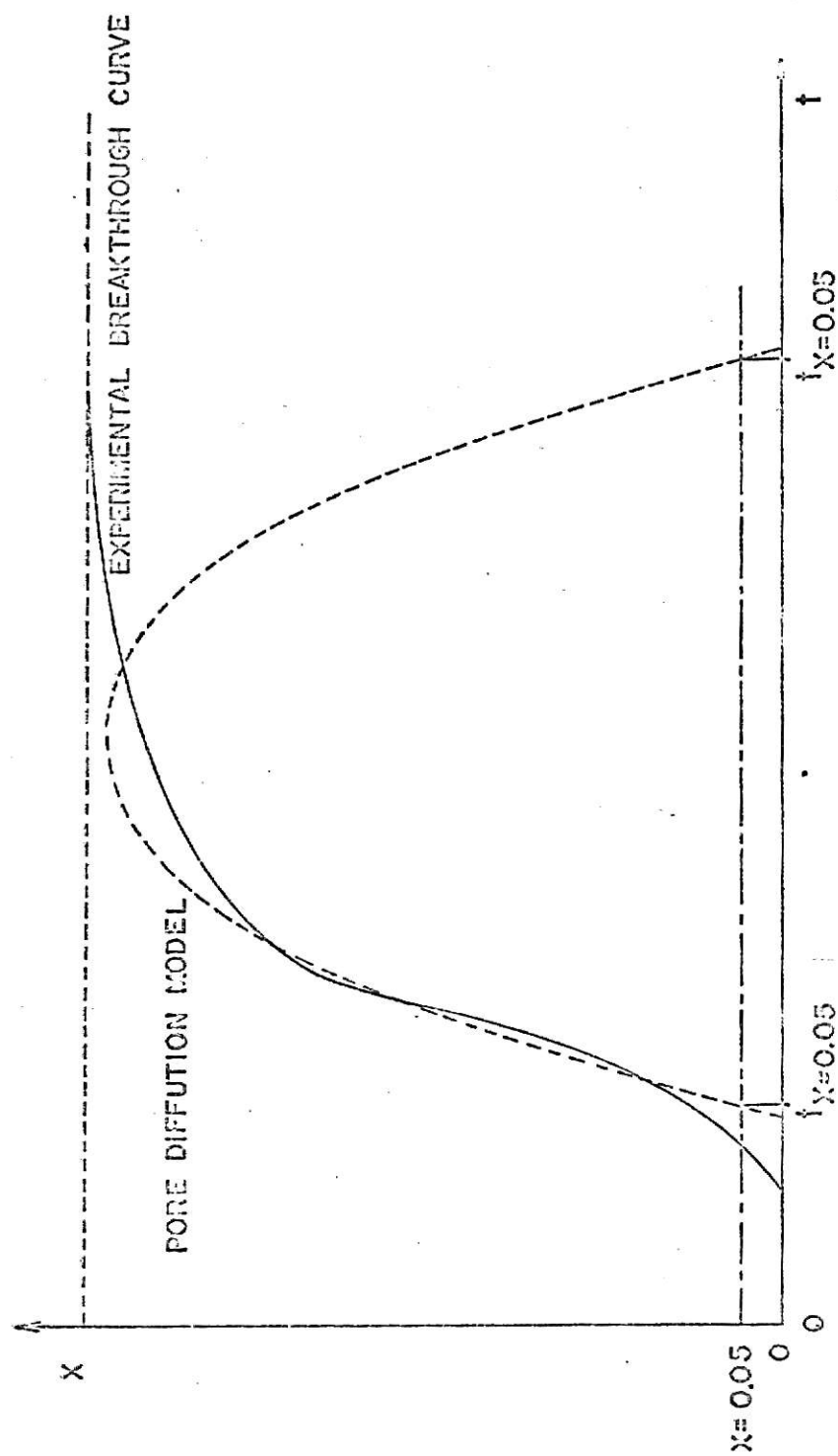


FIG.(A-17). BREAK-TIME CALCULATION FROM PORE DIFFUSION MODEL
BREAKTHROUGH CURVE

$$\left(\frac{dX}{dt}\right)_{x=0.5} = 3.872 \times 10^{-5}$$

By using this mid-point slope and equation (A-8), $t_{x=0.5}$ is 19,877 sec which is 8.62 % bigger than the experimental value.

4. Reaction Kinetics Model.

Modeling N_R is 7.0 from Fig.(III-15) for 0.595 of ve/F and experimentally determined effective distribution ratio D_{er} is 51,520, thus $D_{er} ve/F$ is 30,654. From these values, the reaction kinetics model equation (I-73) becomes

$$X = \frac{1}{1 + e^{-u}} \text{ -----(I-73)}$$

with $u = 5.04(t/30,654 - 1)$ -----(A-11)

At $X=0.5$, the calculated value of $t_{x=0.5}$ is 30,654 sec.

To obtain $(dX/dt)_{x=0.5}$, differentiate the equation (I-73) at $t_{x=0.5}$, then

$$\left(\frac{dX}{dt}\right)_{x=0.5} = 4.110 \times 10^{-5}$$

By using this mid-point slope and equation(A-8), break-time is 19,708 sec which has + 7.69 % error compared to the experimental break-time.

A-5. Static Equilibrium Measurement Error Analysis.

Capacity of flask : 3,000cc

Molecular weight of acetaldehyde : 44 gm/gmole

Initial acetaldehyde concentration in the flask : C_0 ppmThe weight of charcoal in the flask : W gmFluid-phase acetaldehyde concentration at equilibrium with charcoal : C ppmSolid-phase acetaldehyde concentration at equilibrium : q^* gm/gm

The gmole of gas mixture in the flask :

$$\frac{3,000 \text{ cc}}{22,400 \text{ cc/gmole}} = 0.134 \text{ gmole}$$

The gmole of acetaldehyde in the flask at equilibrium :

$$0.134 \times 10^{-6} \times C$$

The gmole of acetaldehyde in the flask initially :

$$0.134 \times 10^{-6} \times C_0$$

The gmole of acetaldehyde on W gm of charcoal

$$\frac{q^* W}{M}$$

From mass balance

$$0.134 \times 10^{-6} \times C_0 = 0.134 \times 10^{-6} \times C + \frac{q^* W}{44}$$

or

$$0.134 \times 10^{-6} (C_0 - C) = \frac{q^* W}{44}$$

and

$$q^* = \frac{0.134 \times 10^{-6} (C_0 - C) \times 44}{W} = \frac{5.896 \times 10^{-6}}{W} (C_0 - C)$$

----- (A-12)

Since

$$dq^* = \frac{\partial q^*}{\partial W} dW + \frac{\partial q^*}{\partial C_o} dC_o + \frac{\partial q^*}{\partial C} dC \quad \text{----- (A-13)}$$

for

$$C_o = 64 \text{ ppm} \quad dC_o = \pm 1$$

$$C = 24.5 \text{ ppm} \quad dC = \pm 1$$

$$W = 0.0296 \text{ gm} \quad dW = \pm 0.0002$$

from equation (A-12)

$$\frac{\partial q^*}{\partial W} = - \frac{5.896 \times 10^{-6} (C_o - C)}{W^2} = - 0.2658$$

$$\frac{\partial q^*}{\partial W} dW = \pm 5.316 \times 10^{-6}$$

$$\frac{\partial q^*}{\partial C_o} = \frac{5.896 \times 10^{-6}}{W} = 2.00 \times 10^{-4}$$

$$\frac{\partial q^*}{\partial C_o} dC_o = 2 \times 10^{-4} = \frac{\partial q^*}{\partial C} dC$$

and

$$dq^* = 4 \times 10^{-4} + 0.5316 \times 10^{-4} = 4.5316 \times 10^{-4}$$

$$q^* = \frac{5.896 \times 10^{-6} (64 - 24.5)}{0.0296} = 7.868 \times 10^{-3}$$

Then

$$\frac{dq^*}{q^*} = \frac{4.5316 \times 10^{-4}}{7.8680 \times 10^{-3}} = 0.0576$$

Therefore the error is $\pm 5.76 \%$.

ADSORPTION OF ACETALDEHYDE VAPOUR IN LOW CONCENTRATION
IN AIR WITH FIXED-BEDS OF CHARCOAL

by

HEUNGWOO CHUN

B. S., University of Southern California, 1969

B. S., Seoul National University, 1965

AN ABSTRACT OF MASTER'S THESIS

submitted in partial fulfillment of the
requirement for the degree

MASTER OF SCIENCE

Department of Chemical Engineering

KANSAS STATE UNIVERSITY

Manhattan, Kansas

1974

As a main objective of this work, the behavior of fixed-beds of Pittsburgh PCB activated charcoal fed with low concentrations of acetaldehyde in air was determined. Breakthrough curves were obtained for various flow rates through the fixed-bed of charcoal and various sizes of charcoal beds with an influent concentration of 28 parts per million of acetaldehyde in air under the isothermal condition of 30 °C.

Appropriate model equations were chosen and tested against the breakthrough data. Four kinds of such model equations were applied to calculate the break-times and also construct the lower part of the breakthrough curves. The four models were particle-phase diffusion model, pore diffusion model, external diffusion model, and reaction kinetics model. All these models calculate the break-times accurate enough ($\pm 10\%$) for design purposes. These model equations have two parameters: the number of mass transfer units and the distribution ratio. These parameters do not coincide with the theoretical values, but the model equations with experimentally determined parameters fit the experimental breakthrough curve and calculate the break-times well.

The average charcoal capacity obtained by graphical integration of the breakthrough curves was 0.00793 gram per gram charcoal. This capacity was verified by the static equilibrium test capacity of 0.00775 gram per gram charcoal which deviates from the experimental breakthrough result by less than one standard deviation. The capacity calculated from the model

equations do not fit for this capacity. But model equations predict the break-times well and can be used to predict the capacity at the break point which is the capacity needed for design.